November 2016

Bacteriophage-Based Colorimetric Detection of Escherichia Coli in Drinking Water

Juhong Chen
University of Massachusetts - Amherst

BACTERIOPHAGE-BASED COLORIMETRIC DETECTION OF *ESCHERICHIA COLI* IN DRINKING WATER

A Dissertation Presented

By

JUHONG CHEN

Submitted to the Graduate School of the

University of Massachusetts Amherst in partial fulfillment

of the requirements for the degree of

DOCTOR OF PHILOSOPHY

September 2016

Food Science

BACTERIOPHAGE-BASED COLORIMETRIC DETECTION OF *ESCHERICHIA COLI* IN DRINKING WATER

A Dissertation Presented

By

JUHONG CHEN

Approved as to style and content by:

_____
Sam R. Nugen, Co-Chair

_____
Vincent M. Rotello, Co-Chair

_____
Julie M. Goddard, Member

_____
Eric A. Decker, Department Head

Food Science

DEDICATION

TO MY BELOVED PARENTS

ACKNOWLEDGMENTS

First, I would like to express my deepest sincere and gratitude to my advisor, Prof. Sam R. Nugen, for his thoughtful guidance, tremendous patience, and constant encouragement towards me throughout my entire doctoral studies. He opened the science gate to me and led me on the scientific road. Most importantly, he gave me absolute freedom to test my hypothesis when some curiosities came to my mind. Next, I would like to acknowledge my co-advisor, Prof. Vincent M. Rotello, for his influential guidance. He taught me how to look for the whole picture of a project and tell an attractive story in my manuscript. It has been my great honor to work with both of them.

I would also like to extend my gratitude to my committee member, to Prof. Julie M. Goddard, for her valuable advice and constructive comments towards my presenting skills and this thesis work.

My special thanks to all the past and present BIOENG members: Fei, Angelyca, Mindy, Charmaine, Sam, Ziyuan, Danhui, Troy, Earl, Jeff, Theo, Rachael, Joey, Kang, Fang, Luis, Dana, Maxine, Stephanie, Jason, Anna, Paul, Anne, Vivian, Andrea. I really enjoyed the friendly and collaborative environment. I am also grateful to my collaborates: Prof. He, Shintaro, Panxue, Ziwen, Brad, Cola, Prof. Watkins, Prof. Carter, Yinyong, Yiliang. In particular, I am thankful to Cindy for her help on numerous orders.

At last but not least, I wish to give my sincerest and hearty thanks to my parents and my family for their endless love and bless. Without your support, I would never have got the chance to go so far to pursue academics. Thanks all the people who have helped me in my life.

ABSTRACT

BACTERIOPHAGE-BASED COLORIMETRIC DETECTION OF *ESCHERICHIA COLI* IN DRINKING WATER

SEPTEMBER 2016

JUHONG CHEN,

B.S., EAST CHINA UNIVERSITY OF SCIENCE AND TECHNOLOGY

Ph.D., UNIVERSITY OF MASSACHUSETTS AMHERST

Directed by: Professor Sam R. Nugen and Vincent M. Rotello

One of the major safety causes in drinking water is from the bacteria contamination, especially in developing countries and resource-limited settings. Although many of these *Escherichia coli* (*E. coli*) strains in drinking water are nonpathogenic, they sever as the indicator for bacterial contamination. And, the more widely used method to detect *E. coli* in drinking water is to determine the activity of β-galactosidase (β-gal), which is released by *E. coli*. Rapid, sensitive and inexpensive detection of *E. coli* in drinking water can reduce the risk of food-borne bacteria infection and stop the disease widely spreading.

In this degree research, phage-based colorimetric methods were developed to detect viable *Escherichia coli* (*E. coli*) concentration in drinking water. During the phage infection cycle, phages can specifically recognize target *E. coli* cells and release intracellular β-gal enzyme. Using our proposed novel biosensor strategies, the β-gal enzymatic activity as the indictor for the presence of *E. coli* in drinking water was

measured. Firstly, T7 phage covalently conjugated to magnetic beads were used to capture, separate, and purity *E. coli* cells from drinking water. The released β-gal was determined using commercial colorimetric substrates. Due to the specific chemical and physical properties of nanomaterials, T7 phage were immobilized on magnetic nanoparticle to improve the capture efficiency of bacteria separation. Next, a novel enzyme-induced metallization multi-colorimetric assay was developed to monitor and measure β-gal activity, which was further employed for high-resolution colorimetric phage-enabled detection of *E. coli*. In order to improve the limit of detection and decrease the effect of the β-gal vary of in different *E. coli* strains, engineered phage ($T7_{lacZ}$) carrying *lacZ* gene was furthermore built to force overexpression of β-gal in *E. coli* cells during phage infection. The uses of $T7_{lacZ}$ phage have been demonstrated to become a rapid, sensitive, and reliable colorimetric detection of viable *E. coli*.

TABLE OF CONTENTS

Page

ACKNOWLEDGMENTS ..... **v**

ABSTRACT ..... **vi**

LIST OF TABLES ..... **xii**

LIST OF FIGURES ..... **xiii**

CHAPTER

1. INTRODUCTION **1**

2. LITERATURE REVIEW **3**

2.1 Introduction 3

2.2 Fabrication of Nanoscale Probes 4

2.3 Antibody-Based Detection of Bacteria Cell 5

2.3.1 Plasmonic Noble Metal Nanoprobes 6

2.3.2 Magnetic Nanoprobes 10

2.4 Aptamer-Based Detection of Bacteria Cell 12

2.4.1 Fluorescent Nanoprobes 13

2.4.2 SERS-Based Nanoprobes 17

2.5 Bacteriophage-Based Detection of Bacteria Cell 19

2.5.1 Phage Lysis Assays-Based Detection 20

2.5.2 Engineered Phage replication assays 22

2.5.3 Phage-Nanomaterial Hybrids 24

2.6 Electrostatic Interaction-Based Sensing of Bacteria Cell 25

2.6.1 Selective Detection of Bacteria Cell 26

2.6.2 Array-Based Sensing of Bacteria 28

2.7 Other recognition element-based detection of bacteria 29

2.8 Conclusions 30

3. DETECTION OF *ESCHERICHIA COLI* IN DRINKING WATER USING T7 BACTERIOPHAGE-CONJUGATED MAGNETIC PROBE 32

3.1 Introduction 32

3.2 Experimental Section 35

3.2.1 Chemicals and Materials 35

3.2.2 Instrumentation. 36

3.2.3 Preparation of T7 Bacteriophage-Conjugated Magnetic Beads (Phage-MBs) 36

3.2.4 Bacteria Culture 37

3.2.5 Colorimetric Detection of E. coli BL21 Using T7 Phage-Conjugated Magnetic Probes 37

3.2.6 Detection of E. coli in Drinking Water 38

3.2.7 Statistical Analysis 39

3.3 Results and Discussion 39

3.3.1 Covalent Immobilization of T7 phage on Magnetic Beads and Separation of *E. coli* BL21 39

3.3.2 Optimization of Detection Conditions 41

3.3.3 Analytical Performance of *E. coli* BL21 Using T7 Bacteriophage-conjugated Magnetic Beads 44

3.3.4 Detection of Bacteria in Drinking Water with a Pre-enrich Step 47

3.4 Conclusions 49

4. BACTERIOPHAGE-BASED NANOPROBES FOR RAPID BACTERIA SEPARATION 51

4.1 Introduction 51

4.2 Experimental Section 53

4.2.1 Synthesis of Oleic Acid Protected FeCo MNPs 53

4.2.2 Preparation of Silica-Coated FeCo Core/Shell MNPs 54

4.2.3 Immobilization of Streptavidin on Silica-Coated FeCo MNPs 55

4.2.4 Quantification of Biotin Capacity of Streptavidin Coated Nanoparticles 55

4.2.5 Preparation of Biotinlyted T7 Bacteriophage 56

4.2.6 Preparation of Antibody or Phage Magnetic Nanoprobes 56
4.2.7 Estimation of the Capture Efficiency of Phage or Antibody Probes on Bacterial Separation 57
4.3 Results and Discussion 57
4.3.1 Preparation and Characterization of FeCo MNPs.....57
4.3.2 Immobilization of Streptavidin on FeCo MNPs 59
4.3.3 Determination of Biotin Binding Capacity of Nanoparticles 61
4.3.5 Biofunctionalization of Nanoparticles with Phages or Antibodies 63
4.3.6 Comparison of the Capture Efficiency between Antibody and Phage-Conjugated magnetic Nanoprobes 64
4.4 Conclusions.....67
5. COLORIMETRIC DETECTION OF *ESCHERICHIA COLI* BASED ON THE ENZYME-INDUCED METALLIZATION OF GOLD NANORODS 69
5.1 Introduction.....69
5.2 Experimental Section 71
5.2.1 Chemicals and Materials.....71
5.2.2 Synthesis and Coating of AuNRs. 72
5.2.3 AuNRs-Based Colorimetric Monitoring of β–gal Concentration.....72
5.3 Results and Discussion 74
5.3.1 Sensing Mechanism of Enzyme-Induced Colorimetric Assay 74
5.3.2 Characteristics and Control Experiments for Enzyme-Induced Colorimetric Assay 75
5.3.3 Optimization of Experimental Conditions for Silver Deposition Reaction.....78
5.3.4 Analytical Performance for Colorimetric Detection of β-gal Concentration.....81
5.3.5 Application for AuNR-Based Colorimetric Detection of E. coli.....85
5.4 Conclusions.....87
6. $T7_{LACZ}$ ENGINEERED BACTERIOPHAGE FOR SIMPLE COLORIMETRIC DETECTION OF VIABLE *ESCHERICHIA COLI* 88

6.1 Introduction 88
6.2 Experimental Section 90
6.2.1 Bacterial strains, bacteriophage, and chemicals 90
6.2.2 Construction and purification of engineered bacteriophage 91
6.2.3 Bacteria culture 92
6.2.4 Comparison of one-step *E. coli* detection using $T7_{lacZ}$ and $T7_{control}$ phage 92
6.2.5 Two-step detection of *E. coli* cells using $T7_{lacZ}$ phage 92
6.2.6 Sensing of antibiotic drugs 93
6.2.7 Statistical analysis 93
6.3 Results 93
6.3.1 Construction of enzymatic reporter-produced bacteriophage 93
6.3.2 Characterization of enzymatically active engineered bacteriophage 95
6.3.3 One-step detection of *E. coli* cells using engineered $T7_{lacZ}$ and $T7_{control}$ bacteriophage 96
6.3.5 Two-step detection of *E. coli* cells using $T7_{lacZ}$ engineered bacteriophage 99
6.3.6 High-throughput sensing of antibiotics 103
6.4 Discussion 105
7. CONCLUSIONS 108
APPENDIX: PUBLICATION 111
BIBLIOGRAPHY 112

LIST OF TABLES

Table Page

3.1 Summary and comparison of techniques for detection of *E. coli* stains. 34

LIST OF FIGURES

Figure Page

2.1 Schematic representation showing the fabrication of recognition elements on nanomterials as bacteria-selective nanoprobes to detect and sense bacteria cells. 4

2.2 (a) Schematic representation of the synthesis of anti-*E. coli* antibodies-conjugated AuNRs nanoprobes. (b) TEM images of the specific interaction of anti-*E. coli* antibodies-conjugated AuNRs with *E. coli* bacteria cells with different coverage. (c) UV-vis absorbance spectra of anti-*E. coli* antibodies-conjugated AuNRs with various concentrations of *E. coli* bacteria cells (from 10 to 10^6 CFU·mL^{-1}). 8

2.3 (a) Schematic representation of colorimetric detection of *E. coli* bacteria cells using anti-*E. coli* antibody-conjugated gold nanorods. (b) Photograph of colorimetric change after adding *E. coli* bacteria cells. (c) TEM images of aggregation of anti-*E. coli* antibody-conjugated AuNRs on the surface of *E. coli* bacteria cells with various concentrations (i. control; ii. 10^2; iii. 8 x 10^4; and iv. 10^7 CFU·mL^{-1}) (d) Plot of two photon scattering intensity change against bacteria concentrations. 10

2.4 Magnetic separation of bound bacteria on the magnetic nanoprobes from unbound bacteria in the supernatant. (Where, $CFU_{original}$ is the total number of bacteria cells present in the initial sample, $CFU_{supernatant}$ is the number of bacteria cells which remained unbound to the magnetic nanoprobes, and CFU_{MNPs} is the number of bacteria cells bound to magnetic nanoprobes.) 12

2.5 (a) Schematic illustration of graphene oxide sensing platform for the detection *S. typhimurium* (Bacteria cell concentration can be detected by turning on the fluorescence signal after the aptamer is bind to target bacteria cells). (b) Schematic representation of the PDMS/paper hybrid microfluidic chips for one step pathogenic bacteria detection. (c) Illustration of the pathogenic bacteria detection principle inside the microfluidic channels. 15

2.6 (a) Schematic illustration of single enhancement by cocktail aptamers for bacteria cells detection. (b) Fluorescence intensity of bacteria cell suspensions obtained after the fluorescence nanoprobes labeled with single, double, and triple aptamers. 17

2.7 (a) Schematic illustration of the aptamer-conjugated nanoprobes for simultaneous detection of *S. aureus* and *S. typhimurium* based on SERS reporter molecules on AuNPs. (b) The Raman spectra of reporter molecules indicating the present of *S. aureus* and *S. typhimurium* in detection solution. 19

2.8 Schematic illustrations of bacteriophage replication assays. 21

2.9 (a) Schematic representation of bacteria detection using engineered T7 phages labeled with quantum dots via streptavidin-biotin interaction. (b) Western blot analysis of T7biotin and T7control phage particles. 24

2.10 TEM images of (a) FeCo MNPs, (b) negatively stained T7 phage particles, (c) positively stained biotinylated phage bound to streptavidin-coated FeCo MNPs, (e) antibody-conjugated MNPs attached on the surface of bacteria cells, (f) phage-modified magnetic nanoprobes attached on the surface of bacteria cells. (g) Comparison the capture efficiency between antibody- and phage-conjugated magnetic nanoprobes. 25

2.11 (a) Schematic illustration of selective detection of bacteria cells based on the switchable interaction of positively charged AuNPs and negatively charged enzyme. (b) Photograph and (c) absorbance intensity at the wavelength of 595 nm of the detection of bacteria cells with different concentrations. (d) Inkjet printing scheme for the fabrication of test strips. (e) Photograph of inkjet printed test strip for the Gram positive and Gram negative bacteria detection. 27

2.12 (a) Schematic illustration of the signal pattern generation using array-based sensing. (b) Schematic representation of the detection of bacteria strains using turning-on fluorescence array sensors. (c) Canonical score plot for the fluorescence array patterns calculated using LDA. 29

3.1 Schematic representation of detection of *Escherichia coli* in drinking water using T7 bacteriophage-conjugated magnetic probe. Three steps were involved: (i) Separation of *E. coli* from drinking water using T7 bacteriophage-conjugated magnetic probe to; (ii) T7 bacteriophage infection of *Escherichia coli* and the consequent release of *β*-gal. (iii) *β*-gal catalyzed CPRG hydrolysis to produce colorimetric readout. 35

3.2 SEM images of (a) and (b) carboxylic acid coated magnetic beads, (c) and (d) T7 bacteriophage-conjugated magnetic beads, (e) *E. coli* BL21 cells and (f) *E. coli* BL21 cells attached to T7 bacteriophage-conjugated magnetic beads through tail fiber. 41

3.3 Colorimetric response of released *β*-gal from *E. coli* BL21. (a) Detection of *β*-gal activity from *E. coli* BL21 cells (0, 10^5, 10^6 and 10^7 CFU·mL^{-1}) after incubated with phage or phage free buffer for 0, 1 and 2 hours. (b) Detection of *β*-gal activity from *E. coli* BL21 cells (0, 10^5, 10^6 and 10^7 CFU·mL^{-1}) after incubated with CPRG solution (0, 2, 4, 6, 8, 10 and 12 mM) at 25 °C and 37 °C. Error bars represent the standard deviation of a minimum of three replicates. 42

3.4 (a) Photographs of bacteria detection at different concentrations before and after magnetic separation. (b) Photograph of colorimetric response and (c) absorbance upon different bacteria concentrations. Error bars represent the standard deviation of a minimum of three replicates. 45

3.5 Schematic illustration of the RGB values to analyze *β*-gal activity released from different concentrations of *E. coli* BL21 cells. (a) Image of colorimetric response of *β*-gal activity released from different concentration. (b) Red, green and blue channels from original image (a) to different concentration processed using ImageJ. (c) Values of red, green and blue channels obtained from original image (a) to different concentration of *E. coli* BL 21 cells. Error bars represent the standard deviation of a minimum of three replicates. 46

3.6 (a) Photographs and (b) absorbance of specificity of the T7 phage-conjugated magnetic probes against *E. coli*, *S. enterica*, *S. aureus*, *P. aeruginosa*, *S. enterica* + *E. coli*, *S aureus* + *E. coli*, *P. aeruginosa* + *E. coli* and mixture$^{\#}$ at concentration of 10^6 CFU·mL^{-1} (mixture$^{\#}$ represents a mixture of *E. coli*, *S. enterica*, *S. aureus* and *P. aeruginosa*). 47

3.7 Detection of E. coli in drinking water using T7 bacteriophage-conjugated magnetic probe. (a) Photographs and (b) absorbance of detecting bacteria concentrations after 5-8 hours of pre-enrichment. (c) Detection of E. coli at 10 CFU·mL-1 after 5 hours of pre-enrichment for 10 times (the solid line represents the average of absorbance of the control (0 CFU·mL-1) while the dashed lines represent the standard deviation. 49

4.1 (a) Transmission Electron Microscopy (TEM) image of oleic acid protected FeCo MNPs, and b) magnetization curve of FeCo MNPs at room temperature. 58

4.2 The XPS spectra of FeCo MNPs (black line) and silica coated FeCo MNPs (red line). 59

4.3 Functionalization magnetic nanoparticles. (A) A silica shell was synthesized from tetraethylorthosilicate (TEOS) which was then functionalized with streptavidin (SA) using carbonyldiimidazole (CDI). (b) Transmission electron micrographs of silica-coated FeCo MNPs. c) TEM images of streptavidin coated on MNPs (insets: streptavidin coated on MNPs at high magnification). 60

4.4 (a) Schematic showing the mechanism to measure the biotin binding capacity and (b) biotin binding capacity of streptavidin-coated nanoparticles. 62

4.5 TEM images of (a) negative uranyl acetate staining of biotin T7 phage and (b) positive uranyl acetate staining of biotin T7 phage attached to streptavidin-coated FeCo MNPs. 63

4.6 Magnetic separation of bound bacteria on the magnetic nanoprobes from unbound bacteria in the supernatant (not drawn to scale)..... 65

4.7 TEM images of nanoprobes bound to *E. coli* K12: a) antibody-conjugated nanoparticles, b) phage-conjugated nanoparticles, e) antibody-conjugated microbeads and f) phage-conjugated microbeads, (c) and (f) comparison the capture efficiency between the two magnetic nanoprobes: phage magnetic nanoprobes (solid round line) and antibody magnetic nanoprobes (hollow round line), and phage magnetic microprobes (solid square line) and antibody magnetic microprobes (hollow square line)..... 66

5.1 Sensing mechanism of enzyme-induced AuNR-based colorimetric assay for the monitoring and measuring of β-gal concentration. Three steps were involved: (i) β-gal converted PAPG into PAP serving as weak reducing agent, (ii) PAP reduced silver ions to metallic silver, and (iii) the AuNRs were coated with metallic silver, resulting in various colorful detection solutions. 74

5.2 The UV-vis absorbance spectra of the AuNRs-CTAB in MQ water (black), AuNRs-PSS in MQ water (red), AuNRs-CTAB in PB (green), and AuNRs-PSS in PB (blue). 76

5.3 TEM images of AuNRs (a) before and (b) after silver deposition (their corresponding EDX elemental mapping images of silver and gold were displayed on the right of their TEM images). Control experiments of the enzyme-inducted metallization colorimetric detection. (c) UV-vis absorption spectra and (d) table of reagents added to each tube of (i) $AgNO_3$ + PAPG + AuNRs, (ii) $AgNO_3$ + *β*-gal + AuNRs, (iii) *β*-gal + PAPG + AuNRs, (iv) $AgNO_3$ + *β*-gal + PAPG, (v) $AgNO_3$ + *β*-gal + PAPG + AuNRs, and (vi) $AgNO_3$ + AuNRs + PAP. 77

5.4 The experimental conditions for silver deposition reaction. The effects of silver-depositing AuNRs (a-b) $AgNO_3$ concentration, (c-d) PAPG concentration, (e-f) PB concentration, and (g-h) pH. Error bars represent the standard deviation of three replicates. 80

5.5 The colorimetric detection of *β*-gal concentration using enzyme-induced metallization of gold nanorods. (a) UV-vis absorption spectra, (b) the blue shift in the longitudinal LSPR peak (insert: linear range, the solid and dash lines indicates the average and ± 3 standard deviation of $\Delta\lambda_{max}$ of control samples), and (c) photographs of colorimetric assay toward various concentrations of *β*-gal. 83

5.6 The colorimetric detection of *β*-gal concentration using the ONPG-based conventional colorimetric method. (a) UV-vis absorption spectra, (b) the absorbance intensity at the wavelength of 405 nm (insert: linear range, the solid and dash lines indicates the average and ± 3 standard deviation of absorbance intensity of control samples), and (c) photographs of colorimetric assay toward various concentrations of *β*-gal. 84

5.7 The specificity of this proposed method for *β*-gal against common competing proteins (5 nM): ChT, GOx, PhosB, Lip, Mayo, and BSA. (a) UV-vis absorption spectra of the colorimetric assay toward various protein competitors. (b) The blue shift in the longitudinal LSPR peak of the specificity of *β*-gal against various protein competitors (insert: the corresponding photographs). Error bars represent the standard deviation of three replicates. 85

5.8 (a) Schematic illustration of the enzyme-induced metallization colorimetric assay for the detection of *E. coli* cells: (i) phage infection of *E. coli* cells to release *β*-gal, and (ii) the signal generation based on enzyme-induced silver metallization on the surface of AuNRs. (b) UV-vis absorption spectra of the colorimetric assay toward various *E. coli* BL21 concentrations. (c) The blue shift in the longitudinal LSPR peak towards various *E. coli*

BL21 concentrations (insert: the corresponding photographs). Error bars represent the standard deviation of three replicates. Significant values (t-test) were marked by an asterisk (*, $0.01 < p < 0.05$) and two asterisks (**, $p < 0.01$), respectively..... 86

6.1 1Schematic illustration of E. coli detection using enzymatically active β-galactosidase-overexpressed via engineered bacteriophage. Initial infection of E. coli cells results in rapid propagation of phages and overexpression of β-gal. Upon phage-induced cell lysis, both phages and β-gal are released, leading to subsequent infections and catalysis of chlorophenol red-β-D-galactopyranoside to produce a colorimetric signal. 90

6.2 Genomes of engineered bacteriophage used for *E. coli* detection. (a) Genome of *lacZ* inserted construction. (b) Genome of T7Select415-1 shows 10B capsid protein and cloning site. (c) Genome of *β*-gal-overexpressing $T7_{lacZ}$ phage created by cloning *lacZ* inserted construction into T7Select415-1 genome. (d) Genome of non-*β*-gal-overexpressing $T7_{control}$ phage created by cloning *S·Tag* into T7Select415-1 genome. 94

6.3 Comparison of overexpressed *β*-gal activity with different treatment types. (a) UV-vis absorption spectra of different treatment types and (b) plot of absorbance intensities (574 nm) towards different treatment types of (i) *E. coli* BL21 + CPRG + $T7_{control}$, (ii) *E. coli* BL21 + CPRG + $T7_{lacZ}$, (iii) *E. coli* BL21 + $T7_{lacZ}$, (iv) CPRG + $T7_{lacZ}$, (v) *E. coli* BL21 + CPRG, (vi) $T7_{lacZ}$, (vii) CPRG, and (viii) *E. coli* BL21. (Error bars represent one standard deviation of three independent experiments)..... 96

6.4 Comparison of one-step *E. coli* detection using $T7_{lacZ}$ and $T7_{control}$ engineered bacteriophage. Contour plots of absorbance intensities (574 nm) of colorimetric response as 2D function of *E. coli* BL21 concentration and total detection time using (a) $T7_{lacZ}$ phage and (b) $T7_{control}$ phage. Contour plots of photograph of colorimetric response as 2D function of *E. coli* BL21 concentration and total detection time using (c) $T7_{lacZ}$ phage and (d) $T7_{control}$ phage. (The absorbance intensity data shown here represents the average of three independent experiments)..... 97

6.5 Comparison of one-step *E. coli* detection using engineered $T7_{control}$ and $T7_{lacZ}$ bacteriophage. Plots of absorbance intensities (574 nm) towards various *E. coli* concentrations after detection time of (a) 2, (b) 3, (c) 4, (d) 5, (e) 6, and (f) 7 hour. (Error bars represent the standard deviation of three independent experiments)..... 99

6.6 Two-step detection of *E. coli* cells at low concentrations using $T7_{lacZ}$ engineered bacteriophage. Contour plots of absorbance intensities (574 nm) as 2D function of detection time and preenrichment time towards *E. coli* cells at the concentration of (a) 10^3, (b) 10^2, (c) 10^1, and (d) 0 $CFU \cdot mL^{-1}$. (The absorbance intensity data shown here represents the average of three independent experiments) 101

6.7 Two-step detection of *E. coli* cells at low concentrations using $T7_{lacZ}$ engineered bacteriophage. Plots of absorbance intensities (574 nm) towards total detection time at the *E. coli* BL21 concentrations of (a) 10^3, (b) 10^2, (c) 10^1, and (d) 0 $CFU \cdot mL^{-1}$. Solid lines indicate the average and ± 3 standard deviation of absorbance intensity of control experiments. (Error bars represent the standard deviation of three independent experiments)..... 102

6.8 High-throughput determination of antibiotic drugs using $T7_{lacZ}$ engineered bacteriophage. (a) Schematic illustration of high-throughputs antibiotic screening by $T7_{lacZ}$ engineered phage infection of *E. coli* BLT5403. Plot of absorbance intensities (574 nm) towards various antibiotics concentrations by $T7_{lacZ}$ engineered phage infection of (b) *E. coli* BLT5403 and *E. coli* BL21. (Error bars represent one standard deviation of three independent experiments) 104

CHAPTER 1

INTRODUCTION

Contamination by pathogenic bacteria is a major concern for human health and wellness. Rapid detection of pathogenic bacteria enables the reduction of food- and water-borne outbreaks in industrial settings, clinical and hospital diagnostics, and water and environmental quality controls as well as in resource-limited settings.[1-2] Most of importance, the bacterial contamination of foods accounts for approximately one-third of global deaths and results in approximately 47.8 million illnesses in United State each year, in addition to costly recalls.[3] The majority bacterial illnesses are a result of an infection or intoxication from *Staphylococcus aureus* (*S. aureus*), *Salmonella typhimurium* (*S. typhimurium*), *Escherichia coli* (*E. coli*) O157:H7, *Listeria monocytogenes*, *Tuberculosis*, *Streptococcal*, *Clostridium perfringens*, and *Bacillus cereus*. Although the use of antibiotics can treat most bacterial infections, several pathogenic bacteria have become resistant to one or more antibiotics, leading to a serious problem. According to World Health Organization, current antibiotics will lose effectiveness to control pathogens over the next 1-2 decades.[4] The presence of multidrug resistant (MDR) pathogens will require the development of new therapies which are effective at killing "super bugs". In the food and hospital processing environment, the formation of bacterial biofilms on the surface of production equipment can increase fouling, promote corrosion, and contaminate product, leading to increased costs and risk.[5] Thus, there is an urgent need to develop accurate and early-stage screening methods to help reduce the risk of these emerging threats in food, medial, and environmental settings.

Common methods to detect and quantify bacteria include traditional plate counting and polymerase chain reaction (PCR). Plate counting allows an estimation of the number of viable bacteria in sample, while PCR enables the detection specific DNA or RNA originating from target bacterial cells. Although these methods can be sensitive and specific, they require significant sample preparation, potentially increasing total assay time beyond 18 hours. There is an on-going challenge in the food and medical fields to reduce the time required for results in order to improve mitigation responsiveness. Thus, a compelling and urgent need exists to improve the current methods for the rapid detection of bacteria. Fortunately, biosensor-based detection strategies are a promising tool to meet the aforementioned criteria. The key components of a biosensor include a recognition element which binds to target analytes, and a transducer which translates the binding event to a measurable signal.[6] The performance of biosensors is determined by response time, dynamic range, limit of detection (LOD), single-to-noise ratio, and specificity.[6] Currently, widespread implementation of biosensors in the real samples is limited by these factors. Nanomaterials have been researched to enhance the performance of biosensors, owing to their unique physicochemical properties. Nanomaterials functionalized with recognition elements have the ability to create advanced recognition and transduction process, which can improve biosensor performance. Specifically, the large surface area of nanomaterials can allow a more efficient capture of analytes during biosensing events. Thus, recognition element-conjugated nanoscale probes can provide an advanced platform for the detection and sensing of pathogenic bacterial cells.

CHAPTER 2

LITERATURE REVIEW

2.1 Introduction

The Centers for Disease Control and Prevention (CDC) estimates bacterial pathogens cause 48 million cases of infection, 128000 cases of hospitalization, and 3000 cases of deaths every year. The conventional method to detect bacteria relies on the colony counting method and polymerase chain reaction (PCR). The colony counting is to estimate the number of viable bacteria in sample, and PCR is based on detecting DNA or RNA originating from target bacterial cells. The conventional methods used to detect and identify pathogenic bacteria are time-consuming and take at least 18 hours from sample to results. Although their high sensitivity and specificity of conventional methods, there is still compelling and urgent need to develop rapid detection methods.

This review will cover the interaction between recognition elements and nanomaterials in biosensors for bacterial detection. The detection and sensing strategies for bacterial cells using nanomaterial-based nanoprobes will be illustrated and discussed. During the sensing events, the appropriate choice of recognition element is a key issue in development of more effective sensors for bacteria. We will highlight the main biosensing recognition elements, including antibodies, aptamers, bacteriophages (phages), and selective ligands. Additionally, this review will suggest future directions to build recognition element-conjugated nanoprobes in order to improve detection and sensing of bacterial cells.

2.2 Fabrication of Nanoscale Probes

Advances in nanotechnology have allowed new nanomaterial-enabled detection strategies for the rapid and sensitive detection of pathogenic bacteria. In order to take advantage of the unique properties of nanomaterials and fabricate bacteria-selective components, recognition elements are modified on the surface of nanomaterials, including gold nanoparticles (AuNPs), gold nanorods (AuNRs), magnetic nanoparticles (MNPs), graphene oxide (GO), quantum dots (QDs), and upconversion nanoparticles (UCNPs). These nanomaterials are functionalized with recognition elements, such as antibodies, aptamers, phages, and selective ligands, to specifically recognize and bind to epitopes on the surface of bacterial cells (Figure 2.1).

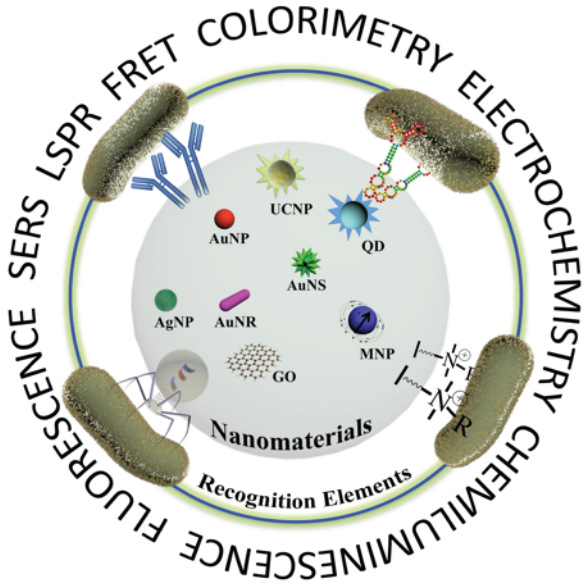

Figure 2.1 Schematic representation showing the fabrication of recognition elements on nanomterials as bacteria-selective nanoprobes to detect and sense bacteria cells.

The immobilization of recognition elements on nanomaterials is an important step in the design of nanoscale probes to enhance biosensor performance. Several methods have been reported to conjugate biological recognition elements on the surface

of nanomaterials, including physical adsorption, covalent bonds, and biotin-streptavidin binding.[7] Physical adsorption is a non-specific interaction between the recognition elements and nanomaterial via hydrogen bonds, hydrophobic interactions, and van der Waals forces. Although this method is facile, the random orientation of the biomolecules can result in low target capture efficiency, and possible instability can trigger the release of target bacterial cells when the local environment is altered (e.g. variance in pH, salt concentration, and/or temperature). To circumvent these issues, a covalent bond is considered an ideal method to immobilize recognition elements on nanomaterials. The amide bond is most commonly used as an intermediate linker to create covalent bonding between the amine groups on the recognition elements and the carboxylic acid groups on the nanomaterials. Since biotin-conjugated antibodies, aptamers, and engineered phages are available, the biotin-streptavidin system has become more popular due to their high binding capacity.

2.3 Antibody-Based Detection of Bacteria Cell

Antibodies (IgG) are large Y-shape proteins and are produced in immune system to identify and detect analytes such as bacterial cells. Antibodies are some of the most commonly used biorecognition elements to capture bacterial cells due to their versatility and ease of integration into biosensing events. The three categories of IgG antibodies are employed in immunology-based assays, including polyclonal, monoclonal, and engineered antibody fragments.

2.3.1 Plasmonic Noble Metal Nanoprobes

Synthesis of gold nanomaterials with varying sizes and shapes (e.g. gold nanospheres, gold nanorods, gold nanowires, and gold nanostars) has been well defined in the previous literature.[6] Differing structures and morphologies result in tunable optical properties in the visible to near-infrared region, providing optical signals for bacterial cell detection. The signals can be observed by monitoring the change of localized surface plasmon resonance (LSPR) within the gold nanomaterials. Although silver nanomaterials also have surface plasmon resonance, the instability in the air and potential toxicity to bacteria can limit their utilization for the detection of bacterial cells.

2.3.1.1 LSPR for Bacteria Cell Detection

Due to the unique properties of LSPR, noble nanoparticles modified with antibodies have been widely used to develop bacteria biosensors. The refractive index change of antibody-conjugated gold nanomaterials causes a shift in the absorbance spectral peaks, thus indicating the presence of target bacterial cells. Also, a plasmon peak shift caused by LSPR can be used to determine the presence of *Salmonella* cells as a result of the binding between the epitopes of target bacterial cells and antibody-conjugated AuNPs.[8] However, the poor detection limits of antibody-conjugated AuNPs limit their practice for bacteria detection. AuNRs have been suggested as a replacement for similar sized AuNPs due to their inherently higher sensitivity to a local dielectric environment.[9]

Wang *et al.* developed a sensor using antibody-conjugated AuNRs to detect *E. coli* cells. As shown in Figure 2.2a, AuNR nanoprobes were fabricated by functionalizing AuNRs with anti-*E. coli* antibodies, which served as the recognition elements to capture

target bacterial cells. The transmission electron microscopy (TEM) micrographs in Figure 2.2b also allowed visualization of the binding between the nanoprobes and target bacterial cells. The specific binding between the AuNR nanoprobes and bacterial cells resulted in a redshift. With an increase of target *E. coli* cell concentration, a larger redshift and lower intensity of longitudinal peak bands were observed (Figure 2.2c). The results indicated that a limit of detection as low as 10^2 CFU·mL^{-1} was achieved in less than 30 minutes. Furthermore, multiple pathogenic bacterial strains can be detected using different types of antibody-functionalized AuNR nanoprobes. For example, anti-*E. coli* and anti-*S. typhimurium* antibodies-functionalized onto AuNRs with different aspect ratios can simultaneously detect *E. coli* and *S. typhimurium* cells at the concentration of 10^4 CFU·mL^{-1}.[9] AuNRs bifunctionalized with magnetic nanoparticles and antibodies were also developed to detect target bacterial cells based on plasmonic resonance. Here, the magnetic properties of the binanoprobes were used to separate, purify, and concentrate the target bacterial cells.[10]

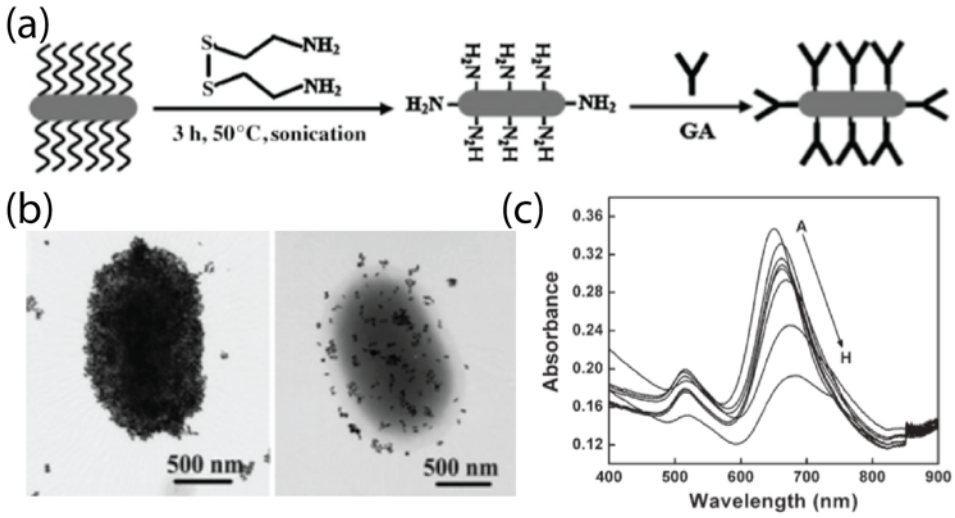

Figure 2.2 (a) Schematic representation of the synthesis of anti-*E. coli* antibodies-conjugated AuNRs nanoprobes. (b) TEM images of the specific interaction of anti-*E. coli* antibodies-conjugated AuNRs with *E. coli* bacteria cells with different coverage. (c) UV-vis absorbance spectra of anti-*E. coli* antibodies-conjugated AuNRs with various concentrations of *E. coli* bacteria cells (from 10 to 10^6 CFU·mL^{-1}).

2.2.1.2 Size Depended Colorimetric Detection

Although the LSPR technique is relatively simple, the requirements of skilled operators and sophisticated instruments result in challenges to scale-up for commercial applications in low-resource settings. Fortunately, colorimetric assays can help overcome these issues by developing portable, easy-to-use, and user-friendly devices for *in-situ* analysis. The aggregation and disaggregation of plasmonic nanomaterials with appropriate sizes has been reported for the analysis of metal ions, anions, small organic molecules, proteins, and oligonucleotides.[6] As a result of being triggered by inter-particle crosslinking or being destabilized aggregation of plasmonic gold nanomaterials in the presence of target analytes, the color of the detection solution changes from red to blue or the reserves at the nanomolar concentration of target analytes, respectively. This color change can be visually observed by the naked eye. The principle behind this system is that gold nanomaterials modified with antibodies reduce the distance between the

individual gold nanomaterials, resulting in inter-particle plasmon coupling and color change. The antibodies on the gold nanomaterials can specifically recognize and bind to the target whole bacterial cells through antibody-antigen interactions.

Singh *et al.* reported anti-*E. coli* antibody-conjugated AuNRs to selectively detect *E. coli* O157:H7 in an aqueous solution at a concentration as low as 50 $CFU \cdot mL^{-1}$.[11] Their results indicated the intensity of two-photon Rayleigh scattering of antibody-conjugated AuNRs increased 40 times in the presence of various competing *E. coli* cell concentrations. The schematic in Figure 2.3a shows the mechanism for the detection of *E. coli* cells using anti-*E. coli* antibody-conjugated AuNR nanoprobes. Although the size of bacterial cells (1-3 μm) is much larger than that of AuNRs, numerous of antibody-conjugated AuNRs can attach to one bacterial cell, resulting in the aggregation of AuNRs. Depending on the concentration of bacterial cells, the degree of aggregation can result in different color shifts, ranging from dark green to blue (Figure 2.3b). The aggregation of antibody-conjugated AuNRs on the surface of bacterial cells was imaged using TEM (Figure 3c). The two-photon scattering intensity change of the detection solutions against various concentrations of target bacterial cells are shown in Figure 3d. The intensity of the new band appearing around 950 nm was used to indicate the aggregation of AuNRs after the addition of target bacterial cells (Figure 3d). In their report, the specificity of antibody-conjugated plasmonic nanoprobes was demonstrated against competing bacterial cells, including *E. coli* O157:non-H7 and *E. coli* O157:NM. Similarly, antibody-conjugated oval-shaped gold nanoparticles have been utilized for colorimetric detection of *S. typhimurium* based on the aggregation of plasmonic

nanoprobes. As target bacterial cell concentrations increase, the color of the detection solutions changes from pink to blue.[12]

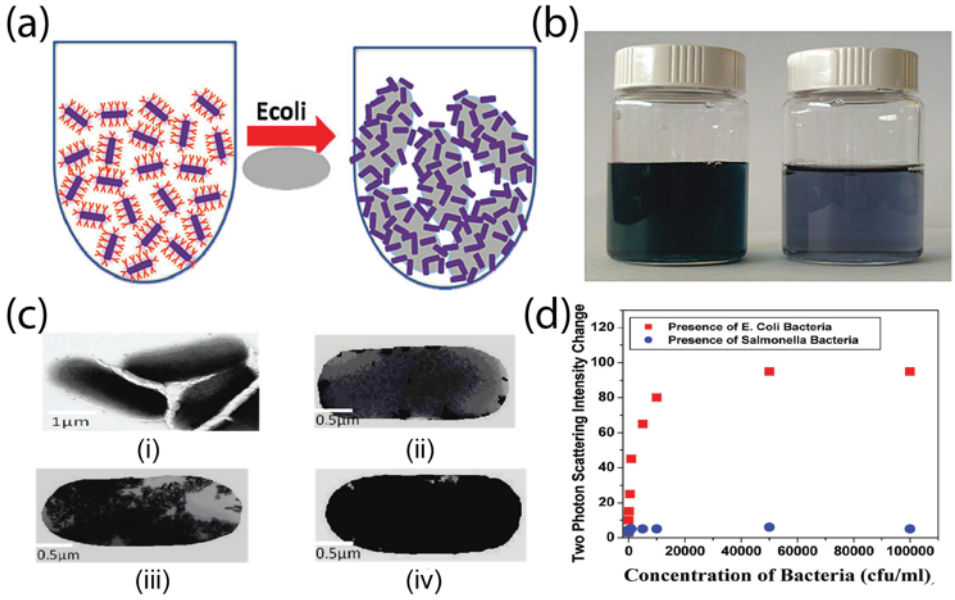

Figure 2.3 (a) Schematic representation of colorimetric detection of *E. coli* bacteria cells using anti-*E. coli* antibody-conjugated gold nanorods. (b) Photograph of colorimetric change after adding *E. coli* bacteria cells. (c) TEM images of aggregation of anti-*E. coli* antibody-conjugated AuNRs on the surface of *E. coli* bacteria cells with various concentrations (i. control; ii. 10^2; iii. 8 x 10^4; and iv. 10^7 CFU·mL^{-1}) (d) Plot of two photon scattering intensity change against bacteria concentrations.

2.3.2 Magnetic Nanoprobes

Immunomagnetic separation (IMS) consists of antibody-conjugated magnetic beads (1-3 micron in diameter) as a powerful tool to separate, concentrate, and purify target bacterial cells from complex matrices. The flexibility of this method allows it to be combined with numerous detection methods, including fluorescence, colorimetric, electrochemical, chemiluminescent, surface-enhanced Raman scattering (SERS), surface plasmon resonance (SPR), and quartz crystal microbalance (QCM). Although IMS is widely used, low capture efficiencies limit its application in complex matrices. To increase capture efficiency, superparamagnetic magnetic nanoparticles (e.g. Fe_3O_4 and

Fe_2O_3,) have been reported to increase capture efficiency for pathogenic bacteria separation from food samples because of their increased surface to volume ratio. [13]

When detecting in complex samples, magnetic separation without centrifugation can increase detection sensitivity by purifying target bacterial cells to reduce the interference from other compounds. It is well known that MNPs modified with antibodies can recognize and attach to the antigens on the surface of bacterial cells. As shown in Figure 2.4, the bound bacterial cells can be separated from sample solutions using an external magnetic field. The capture efficiency, calculated using the equation shown in Figure 2.4, was introduced to measure the performance of antibody-conjugated magnetic nanoprobes.[14]

The most commonly used magnetic nanoparticle for bacteria separation is iron oxide (Fe_3O_4) MNPs. These nanoparticles have been reported to provide a capture efficiency of greater than 90% in real food samples.[15] Unfortunately, the MNPs, having a diameter of 90 nm, required one hour for separation due to low magnetic prosperities. Overnight separation is recommended for commercial dispersed MNPs under 30 nm in diameter. In order to decrease separation time, metal alloy MNPs, such as $CoFe_2O_4$, $PtFe_2O_4$, and $MnFe_2O_4$, were bio-functionalized for bacterial separation as well as biomedical applictions.[16] Multifunctional magnetic nanoprobes have also demonstrated to simultaneously separate and detect bacterial cells. For example, antibody-modified Fe_3O_4/TiO_2 core/shell magnetic nanoprobes were used to separate and detect *Salmonella* strains.[17] Wang *et al.* reported the use of antibody-conjugated AuNRs decorated with Fe_3O_4 MNPs, including Fe_3O_4-AuNR-Fe_3O_4 nanodumbbells and a Fe_3O_4-AuNR necklace, for multiple pathogenic bacteria detection.[10]

IMS can be a useful tool for separating bacteria from complex matrices, such as food. Capture efficiency, antibody cost, and total assay time are the main challenges for the implementation of IMS in low-resource settings.

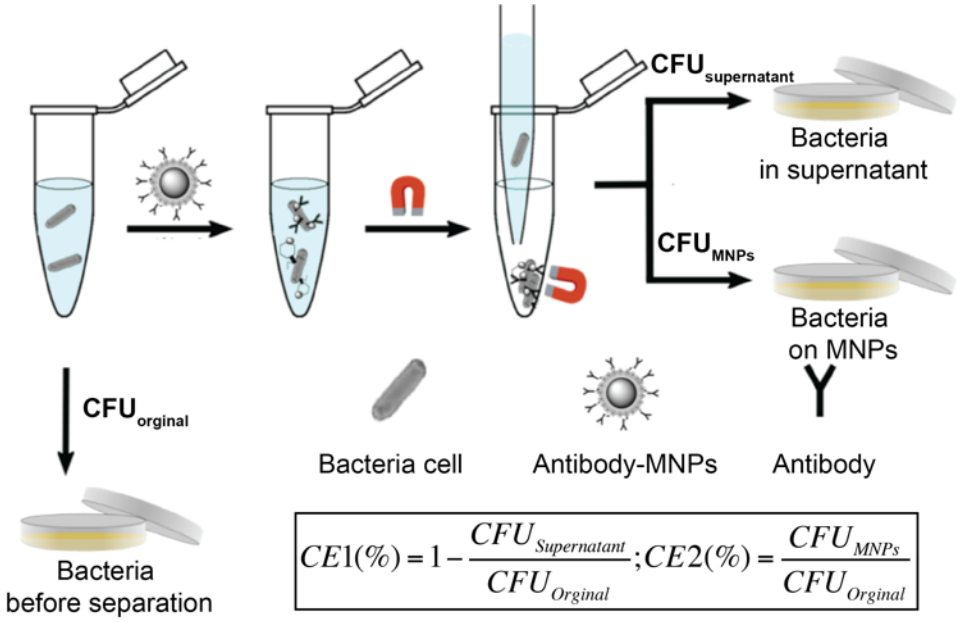

Figure 2.4 Magnetic separation of bound bacteria on the magnetic nanoprobes from unbound bacteria in the supernatant. (Where, $CFU_{original}$ is the total number of bacteria cells present in the initial sample, $CFU_{supernatant}$ is the number of bacteria cells which remained unbound to the magnetic nanoprobes, and CFU_{MNPs} is the number of bacteria cells bound to magnetic nanoprobes.)

2.4 Aptamer-Based Detection of Bacteria Cell

Aptamers, consisting of single stranded nucleic acids (ssDNA or RNA), offer several advantages over the antibody-based recognition elements for the capture of bacterial cells. Aptamers are low-cost, chemically stable, and can be synthesized at a large scale. Due to their small size (typically 3-5 nm), aptamers can exhibit high binding affinity for target bacterial cells, resulting in a decrease in the overall detection limit. Aptamers can be designed for a variety of target bacteria using Systematic Evolution of Ligands by Exponential enrichment (SELEX), and have a three-dimensional configuration to bind epitopes on the surface of bacterial cells.[18] During the process, a

large DNA library is added into a solution containing bacterial cells and incubated. The unbound DNA is then separated from bacterial cells, and bound DNA is eluted and amplified via PCR. The SELEX process is then repeated until the DNA has a high affinity for the target bacterial cells. During the synthesis process, aptamers can be functionalized with –SH, -NH_2, and -COOH groups, providing an easy way to immobilize aptamers to nanomaterials. Aptamer use in both fluorescence and SERS-based detection methods will be described in this section.

2.4.1 Fluorescent Nanoprobes

Fluorescent nanomaterials are advantageous over common fluoropheres due to their large extinction coefficients and high photostability. Thus, the utilization of fluorescent nanoprobes has opened a new area for advanced fluorescence analysis and imaging. In addition to their high photostability, fluorescent nanomaterials with narrow and size tunable emission spectra allow researchers to precisely label target bacterial cells. Most importantly, fluorescent nanoparticles with differing colors, modified with varying recognition elements can be used to detect various types of bacterial cells simultaneously.

Based on fluorescence resonance energy transfer (FRET), nanomaterials, such as AuNPs and GO, can serve as fluorescence quenchers to detect bacterial cells. Aptamers conjugated with fluoropheres can interact with quencher nanomaterials, turning off the visible fluorescence via FRET. In the presence of the target bacterial cells, the aptamers recognize the bacterial cells and release from the surface of the nanomaterial quencher. The resulting increase in fluorescence is used to quantify the concentration of bacterial cells (Figure 2.5a). By employing this principle, Duan *et al.* used a FAM-aptamer/GO

complex as a nanoprobe to detect *S. typhimurium* with a dynamic range from 10^3 to 10^8 CFU·mL^{-1} and a detection limit of 100 CFU·mL^{-1}.[19] Furthermore, Zuo *et al.* applied aptamer-functionalized graphene oxide nanoprobes in a microfluidic biochip to detect *Lactobacillus acidophilus* (Figure 2.5b,c).[20] The limit of detection was determined to be 11 CFU·mL^{-1}, within the assay time of 10 minutes.

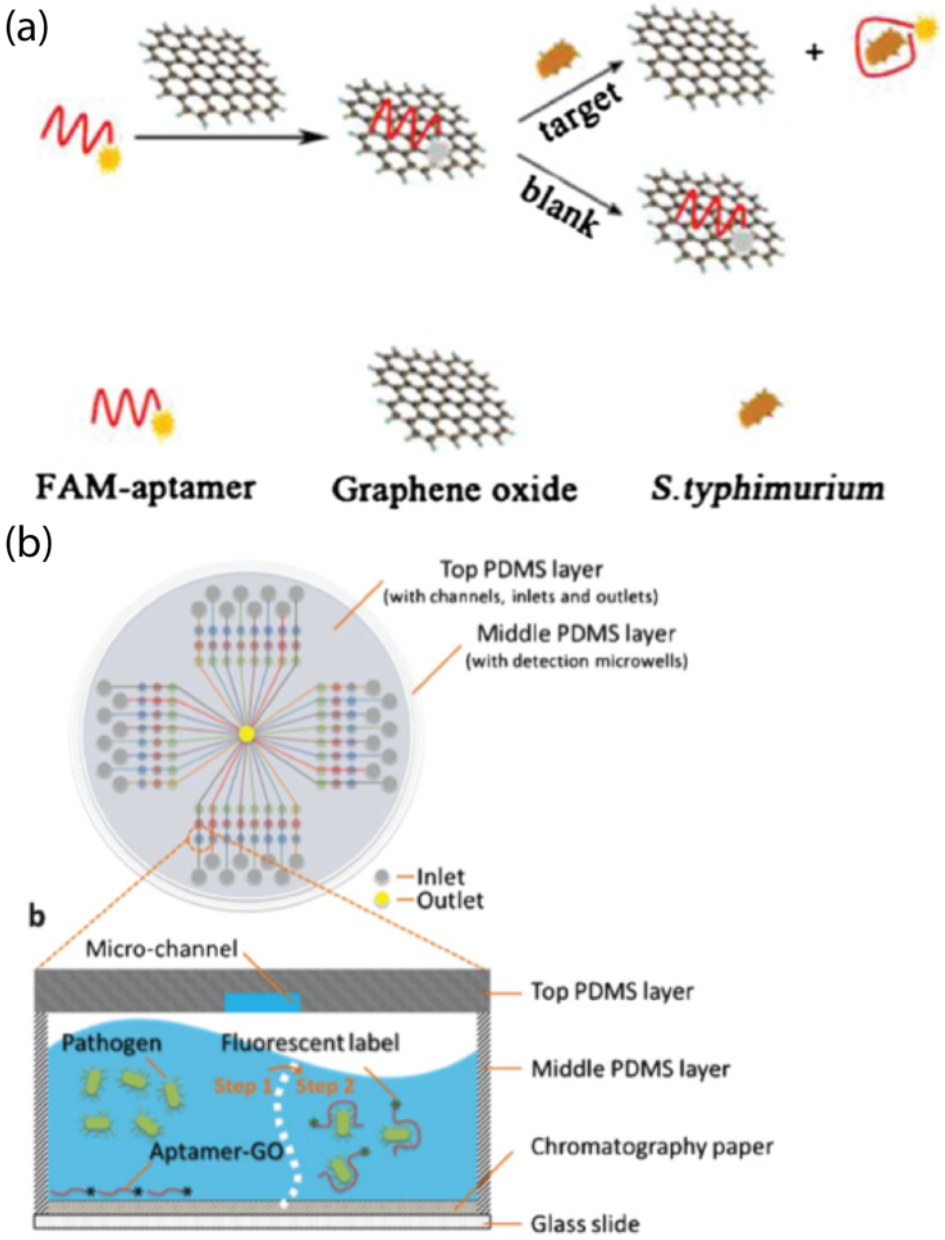

Figure 2.5 (a) Schematic illustration of graphene oxide sensing platform for the detection *S. typhimurium* (Bacteria cell concentration can be detected by turning on the fluorescence signal after the aptamer is bind to target bacteria cells). (b) Schematic representation of the PDMS/paper hybrid microfluidic chips for one step pathogenic bacteria detection. (c) Illustration of the pathogenic bacteria detection principle inside the microfluidic channels.

2.4.1.2 Fluorescence Nanomaterials for Labeling

The combination of aptamers and fluorescent nanomaterials as a fluorescence label has been used in several studies. Because the bacterial surface contains numerous possible binding moieties such as polysaccharides, proteins, and flagella, Kim *et al.* used a cocktail of aptamers with various targets to detect *E. coli* cells (Figure 2.6a).[21] As shown in Figure 2.6b, a mixture of aptamers resulted in a higher fluorescence signal than did any single aptamer used, suggesting that a cocktail of aptamers could enhance the sensitivity for the detection of bacterial cells. Their report indicated that an 18-fold lower limit of detection was achieved using a cocktail of aptamers to detect *E. coli* bacterial cells when compared with a single aptamer.

The ability to detect multiple bacteria types simultaneously is advantageous in many fields including medical diagnostics, food safety, and environmental monitoring. Researchers have demonstrated the ability to perform multiplex detection using several aptamer-nanoprobe combinations during a single assay. Duan *et al.* reported dual-color aptamer-conjugated fluorescent nanoprobes to simultaneously label and detect *S. typhimurium* and *S. aureus*.[22] In the presence of target bacterial cells, the fluorescent nanoprobes attached to target bacterial cells, providing fluorescence readout using a 980 nm laser. This proposed method had a good dynamic range of 10^1-10^5 CFU·mL^{-1} and excellent detection limit of 5 CFU·mL^{-1} for *S. typhimurium* cells and 8 CFU·mL^{-1} for *S. aureus* cells. The same researchers used aptamer-conjugated, dual-color quantum dots to simultaneously detect *Vibrio parahaemolyticus* and *Salmonella typhimurium*.[23] Fluorescence-based nanoprobes containing aptamers show good promise for multiplex

and sensitive detection of bacteria. However, their use in complex matrices may result in quenching of the fluorophores.

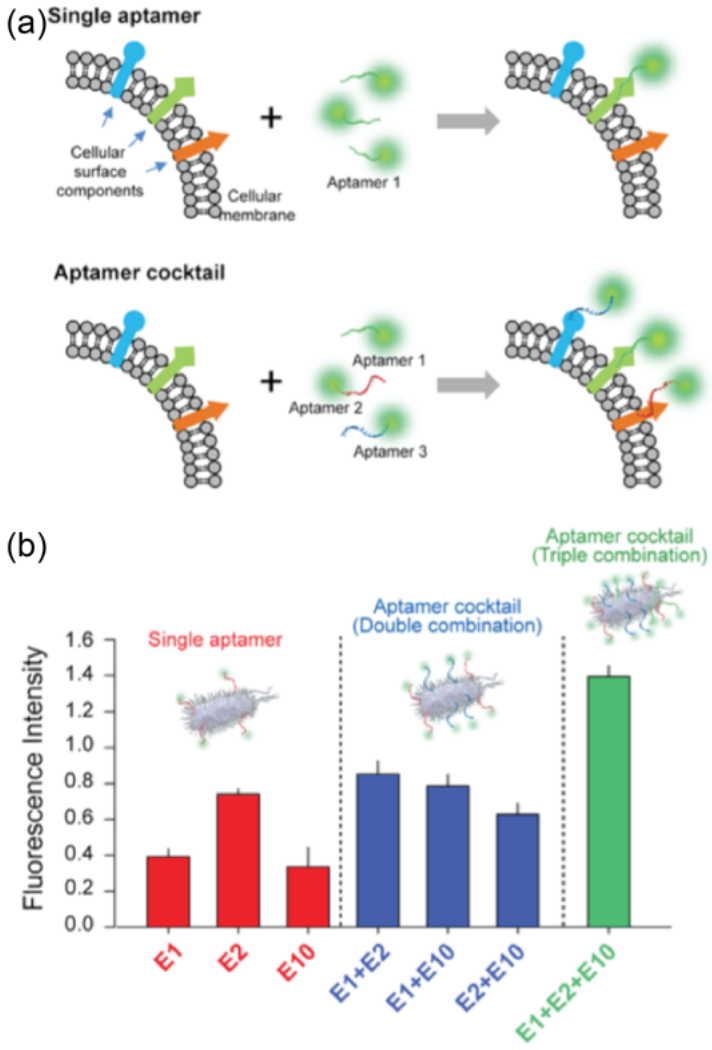

Figure 2.6 (a) Schematic illustration of single enhancement by cocktail aptamers for bacteria cells detection. (b) Fluorescence intensity of bacteria cell suspensions obtained after the fluorescence nanoprobes labeled with single, double, and triple aptamers.

2.4.2 SERS-Based Nanoprobes

Since initial reports of surface-enhanced Raman scattering (SERS) in 1964, metallic nanoparticles have attracted increasing attention for SERS-based detection of chemical and biological agents.[24] The vibrational or rotational transitions on the Raman spectrum corresponding to specific molecular structures on the surface of bacterial cells,

providing a set of chemical fingerprints. The fingerprint spectra are helpful in distinguishing different types of bacterial cells. The Raman signals of bacterial cells, which are normally very weak, can be selectively and sensitively enhanced using plasmonic metal nanomaterials modified with recognition elements. This modification allows for the detection of low bacteria concentrations. The enhancement factors for SERS are generally attributed to a combination of electromagnetic and chemical mechanisms. The chemical mechanism is responsible for SERS enhancement by nanoprobes, explained by the interaction between the electrons from the target bacterial cells and the metal nanomaterials.[25]

The basic principle behind aptamer-SERS for the detection of bacterial cells involves the utilization of aptamer-conjugated nanomaterials with numerous "hotspots", providing a strong SERS signal. Both the aptamer and the nanoprobes are labeled with Raman reporter molecules. On the aptamer-based Raman nanoprobes, the aptamer can specifically bind to target bacterial cells. The Raman reporter molecules are then used to quantify the concentration of bacterial cells. Ravindranath *et al.* demonstrated a cross-platform approach to simultaneously detect three pathogens using three aptamer-conjugated nanoprobes modified with different Raman reporter molecules.[26] The total detection time was less than 45 minutes, and a detection limit of 10^3 CFU·mL^{-1} was obtained. Similarly, a AuNRs-enhanced SERS aptasensor has also been developed for the simultaneous detection of *S. typhimurium* and *S. aureus*.[27] As shown in Figure 2.7a, AuNPs were labeled with Raman reporter molecules and two types of aptamers as nanoprobes for the detection of bacterial cells. Here, MNPs were also modified with two types of aptamers to capture and concentrate *S. aureus* and *S. typhimurium* cells. As

shown in Figure 2.7b, the peaks at 1333 cm^{-1} and 1582 cm^{-1} indicate the presence of *S. aureus* and *S. typhimurium*, respectively. The intensity at the specific peaks from the Raman reporter molecules contributed to the low detection limit of 35 $CFU \cdot mL^{-1}$ for *S. aureus* and 15 $CFU \cdot mL^{-1}$ for *S. typhimurium*.

SERS-based detection of bacteria through aptamer nanoprobes has shown selective and sensitive results. The need for SERS equipment may hinder widespread usage of this method in low-resource settings. Compared to antibodies, both fluorescent and SERS aptamer-based nanoprobes present a low-cost solution to more expensive antibodies.

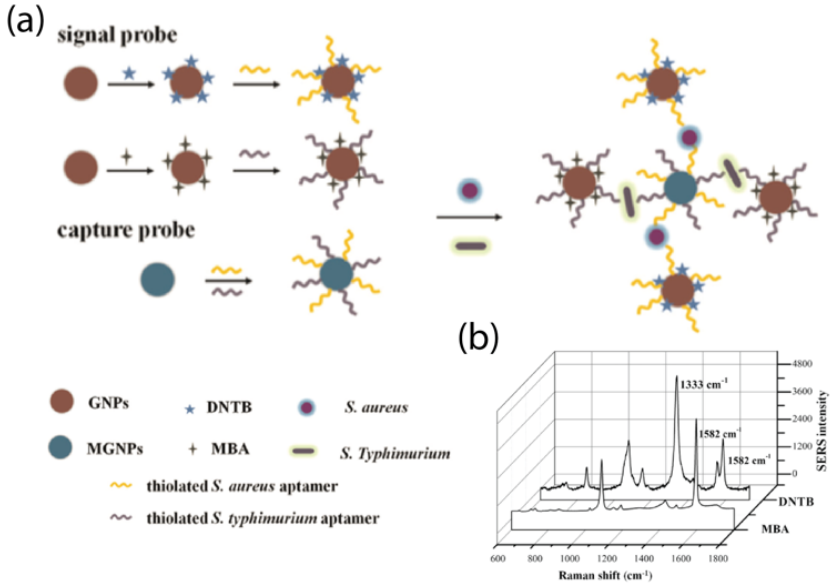

Figure 2.7 (a) Schematic illustration of the aptamer-conjugated nanoprobes for simultaneous detection of *S. aureus* and *S. typhimurium* based on SERS reporter molecules on AuNPs. (b) The Raman spectra of reporter molecules indicating the present of *S. aureus* and *S. typhimurium* in detection solution.

2.5 Bacteriophage-Based Detection of Bacteria Cell

The disadvantages of antibodies and aptamers, which include batch-to-batch variations, robustness in complex matrices, and relatively high cost, have led to research towards alternative biorecognition elements. Bacteriophages, also known as phages, are

bacteria-infecting viruses consisting of nucleic acid, protein capsid, and tail fibers. The tail fibers serve as recognition elements which can specifically recognize and bind to receptors on the surface of target bacterial cells. Depending on the particular phage, the bacteria host range can be either narrow or broad. The sizes of most phages are approximately 100 nm, which makes them ideal to be used as bio-nanomaterial probes for bacteria detection. In addition to their target specificity, another key feature of phages is their ability to distinguish viable versus inactive host bacterial cells. This is because phages can only replicate and express enzymes within viable bacterial cells.[28] The specificity of a phage-based detection system requires careful host-range screening of phage libraries. This has allowed the development of detection systems specific for *Escherichia coli*, *Vibrio cholera*, *Bacillus anthracis*, and *Listeria monocytogens*. These phage-based detection assays are advantageous because they are rapid, sensitive, specific to host bacterial cells, low-cost to produce, and they detect only viable cells. Also, it is relatively easy and inexpensive to synthesize and purify phage, providing a new platform to detect bacteria. Thus, bacteriophages offer significant advantages when considering solutions for bacterial cell detection.

2.5.1 Phage Lysis Assays-Based Detection

Phages are obligate intracellular parasites, which can only replicate within target bacterial hosts.[28] The phage amplification assays are illustrated in Figure 2.8. Following attachment to a suitable host cell, the phage will take over the cell's machinery to replicate DNA, synthesize proteins, and finally lyse the host cells to release the replicated virus. The released phage can then find another suitable host cell and initiate a new infection cycle. At the end of incubation, the number of phages can be quantified using

conventional plating methods. The increased number of phages in solution can be used to calculate the concentration of target bacterial cells. Based on phage amplification assays, some commercial diagnostic kits have been available for the detection of *S. aureus*, *Yersinia pestis*, and *Mycobacterium tuberculosis*. Although low detection limits have been demonstrated, these methods are time and labor consuming. Phage amplification assays have been combined with other technologies, such as mass spectrometry, enzyme-linked immunosorbent assay (ELISA), and PCR to decrease the total detection time.[29-30] For example, Martelet *et al.* developed a highly sensitive strategy for rapid and unambiguous detection of viable *E. coli*.[29] The amplified phages were quantified using mass spectrometry combined with liquid chromatography. Their results indicated a limit of detection as low as 1 CFU·mL^{-1} for viable *E. coli* in food matrices following an 8 hour infection. Furthermore, the advantageous properties of phage amplification-based assays can be utilized to detect bacteria without producing resistant bacteria, and also be used to determine antibiotic resistance.

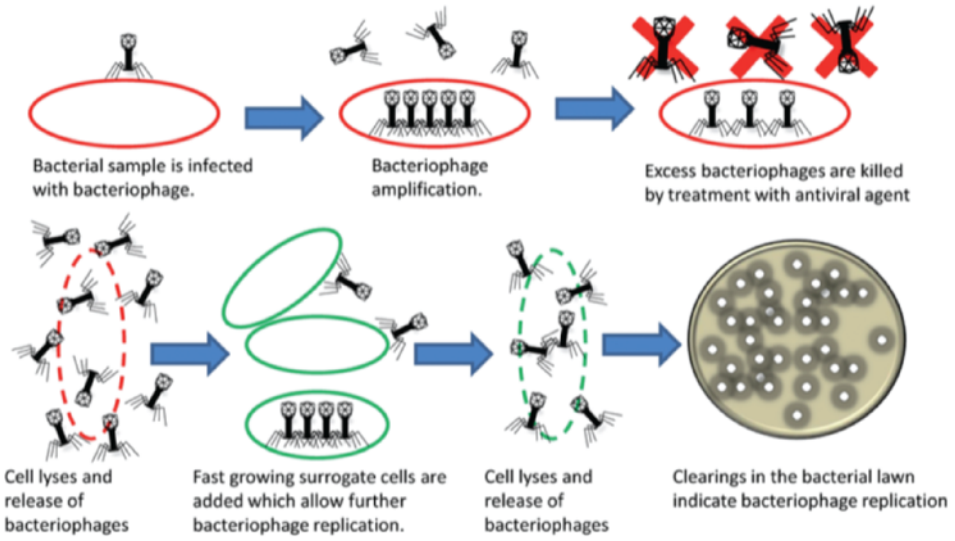

Figure 2.8 Schematic illustrations of bacteriophage replication assays.

After the phage infection cycles, the intracellular components are released from the host cell and can be used as an indicator for the target bacterial cells. Some examples of intracellular components include β-galactosidase, adenosine triphosphate (ATP), and adenylate kinase. The enzymatic activity of phage-mediated released β-galactosidase was quantified using colorimetric, electrochemical, and chemiluminescent strategies. Derda *et al.* reported a colorimetric method to detect 50 CFUs of *E. coli* cells in 1 Liter of water in less than 4 hours.[31] After adding luciferase and luciferin, the released ATP produced a bioluminescence signal. Their reports indicated the detection of *E. coli* and *S. newport* (selected as Gram positive and gram negative bacteria models) with a detection limit of 10^3 CFU within 1 hours and 2 hours, respectively.[32] Amperometric detection of *Enterobacteriaceae* cells in river water was performed, and reached a limit of detection at 5×10^4 CFU·mL^{-1} with an incubation of 2 hours, and 10 CFU·mL^{-1} after a pre-enrichment of 7 hours.[33] Although phage lysis assays can produce a low limit of detection within a short time, a background signal is difficult to avoid. Thus, advanced technology combined with phage lysis assays need to be developed for future studies.

2.5.2 Engineered Phage replication assays

Engineered phages based on genetic engineering technologies are able to transfer genes of interest into specific target bacteria, which then express and amplify the gene product. This amplification allows for rapid and robust detection of bacteria. Therefore, engineered phages provide a potential low-cost tool for specific, rapid, and sensitive detection of bacteria. In order to reduce the background signal and decrease the variations between different bacteria strains, phage components (e.g. capsid proteins, nucleic acid) have been labeled with fluorescence using genetic engineering to act as a bio-nanoprobe

for bacterial cell detection. Due to the relatively large surface area of capsid proteins, phage heads labeled with a fluorescent tag can increase the sensitivity. A common fluorescent tag is green fluorescence protein (GFP), which is added on the small outer capsid protein on the phage head.[34] Recently, engineered phages carrying an enzymatic reporter gene have attracted increasing attention for bacterial cell detection. Firefly luciferase, the most commonly used enzyme, has been reported to detect various bacterial cells.[35] In addition, T7 phages were engineered to carry alkaline phosphatase or tobacco etch virus protease gene, generating phage-based platform for bacteria detection. [36-37]

Edgar *et al.* reported a rapid and simple method to detect *E. coli* (Figure 2.9).[38] The T7 phage was engineered to express biotinylation peptide on the phage capsid proteins. During the phage infection cycle for bacteria cell detection, the biotinylation peptide is biotinylated inside the host bacterial cells. Streptavidin-coated quantum dots were used to label biotinylated phages for fluorescent quantification. The detection limit of *E. coli* cells was shown to reach as low as 10 bacterial cells per milliliter, which had a 100-fold amplification of readout signal over the background within 1 hour. This method helps solve the issue of background signal interference commonly seen with phage lysis assays.

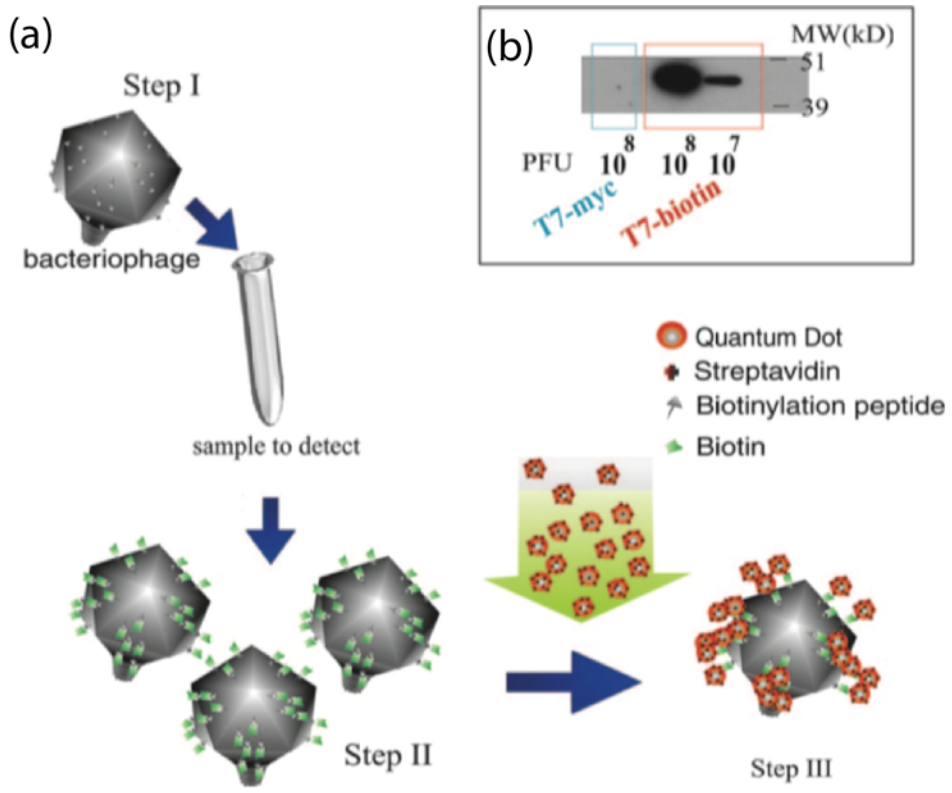

Figure 2.9 (a) Schematic representation of bacteria detection using engineered T7 phages labeled with quantum dots via streptavidin-biotin interaction. (b) Western blot analysis of T7biotin and T7control phage particles.

2.5.3 Phage-Nanomaterial Hybrids

Other methods include replacing antibodies with phages on magnetic beads, and phage-coating magnetic beads in combination with other technologies. These methods have successfully detected several pathogenic bacteria.[39] Taking advantage of the high surface-to-volume ratio of MNPs, Chen *et al.* fabricated T7 phage-based magnetic FeCo nanoprobes for bacteria separation.[14] The FeCo MNPs were functionalized with streptavidin, which were bound by biotinylated T7 phages via streptavidin-biotin interaction. The TEM micrographs of streptavidin coated FeCo MNPs, biotinylated T7 phages, and T7 phage-MNPs complex were shown in Figure 2.10a-c. Their reports indicated similar bacteria capture efficiency between antibody- and phage-conjugated

nanoprobes (Figure 2.10g). However, phages served as nanoprobes provided some advantages, including relative ease of production, ability to distinguish between viable and inactivated bacterial cells, and controllable host range. Moreover, phage-conjugated nanoprobes take the advantage of reliable specific binding, low-cost production at a large scale, as well as high tolerance to temperature and pH.

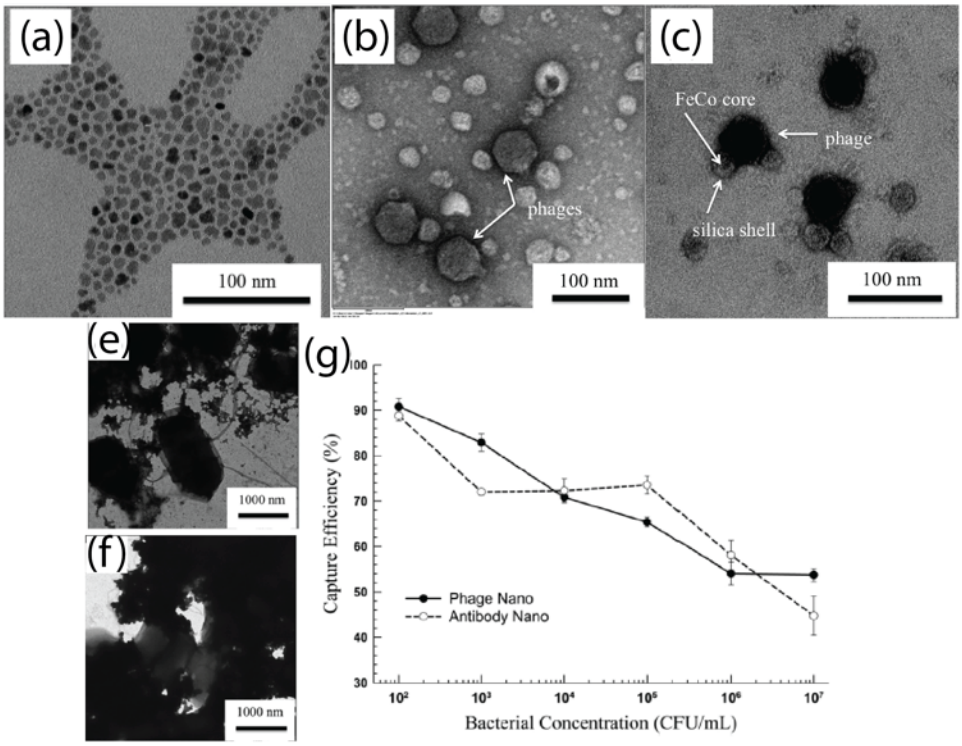

Figure 2.10 TEM images of (a) FeCo MNPs, (b) negatively stained T7 phage particles, (c) positively stained biotinylated phage bound to streptavidin-coated FeCo MNPs, (e) antibody-conjugated MNPs attached on the surface of bacteria cells, (f) phage-modified magnetic nanoprobes attached on the surface of bacteria cells. (g) Comparison the capture efficiency between antibody- and phage-conjugated magnetic nanoprobes.

2.6 Electrostatic Interaction-Based Sensing of Bacteria Cell

Unlike antibodies, aptamers, and bacteriophages, the selective recognition-based sensing is to non-specifically detect bacterial cells by the reversible binding between nanoprobes and target bacterial cells. Compared with specific recognition elements, the selective recognition can be used to detect and recognize multiple target bacterial cells.[40]

Such selectivity-based approach can provide a sensing platform to either detect a wide range of bacterial strains or recognize an individual bacterial cell strain.

2.6.1 Selective Detection of Bacteria Cell

Positively charged nanomaterials have the ability to bind to negatively charged protein surfaces through electrostatic interactions. Several nanomaterials, such as gold nanoparticles, carbon nanotubes, and graphene oxide, have been reported to interact with enzymes, inhibiting enzymatic activities. Based on the reversible interaction, the recovery of enzymatic activity can be used as an indicator of bacterial cell concentration. Li *et al.* synthesized positively charged graphene oxide to inhibit β-galactosidase (β-gal) activity for the colorimetric detection of bacterial cells and sensing of antibiotics.[41] Also, enzymatic activity has been reversibly inhibited by positively charged polyethyleneimine-coated AuNPs to detect Gram-positive or Gram-negative bacterial cells in drinking water as low as 10 $CFU \cdot mL^{-1}$ via simple visual readout.[42]

Rotello and coworkers has reported the synthesis of cationic AuNPs for the selective detection of bacterial cells in differing detection formats.[43-45] Because of electrostatic interactions, the enzymatic activity of β-gal was inhibited by cationic AuNPs which featured quaternary amine head groups. In the presence of bacterial cells, AuNPs were released from the AuNPs/β-gal complex and bound to the surface of the bacterial cells, resulting in the recovery of enzymatic activity (Figure 2.11a). The colorimetric results and absorbance intensities versus bacterial concentrations are shown in Figure 2.11b,c, indicating an obtained detection limit of 100 $CFU \cdot mL^{-1}$.[43] Furthermore, the detection system was inkjet-printed on paper for low-cost diagnostics in contaminated drinking water. As seen in Figure 2.11d, the AuNPs/β-gal complex and colorimetric

substrates were co-patterned on the paper strip. After dipping the test strip into a bacterial solution for 5 minutes, *E. coli* XL1 (10^2 CFU·mL^{-1}) and *B. subtilis* (10^3 CFU·mL^{-1}) can be detected (Figure 2.11e).[44] After the β-gal is released from the AuNPs/β-gal complex, the enzyme activity can also be monitored and quantified using electrochemical strategies. Electrochemically, *E. coli* and *S. aureus* can be detected with high sensitivity (10^2 CFU·mL^{-1}) within 1 hour.[45] While selective detection can provide rapid and sensitive detection of bacteria, these methods need to be validated in complex matrices, such as food.

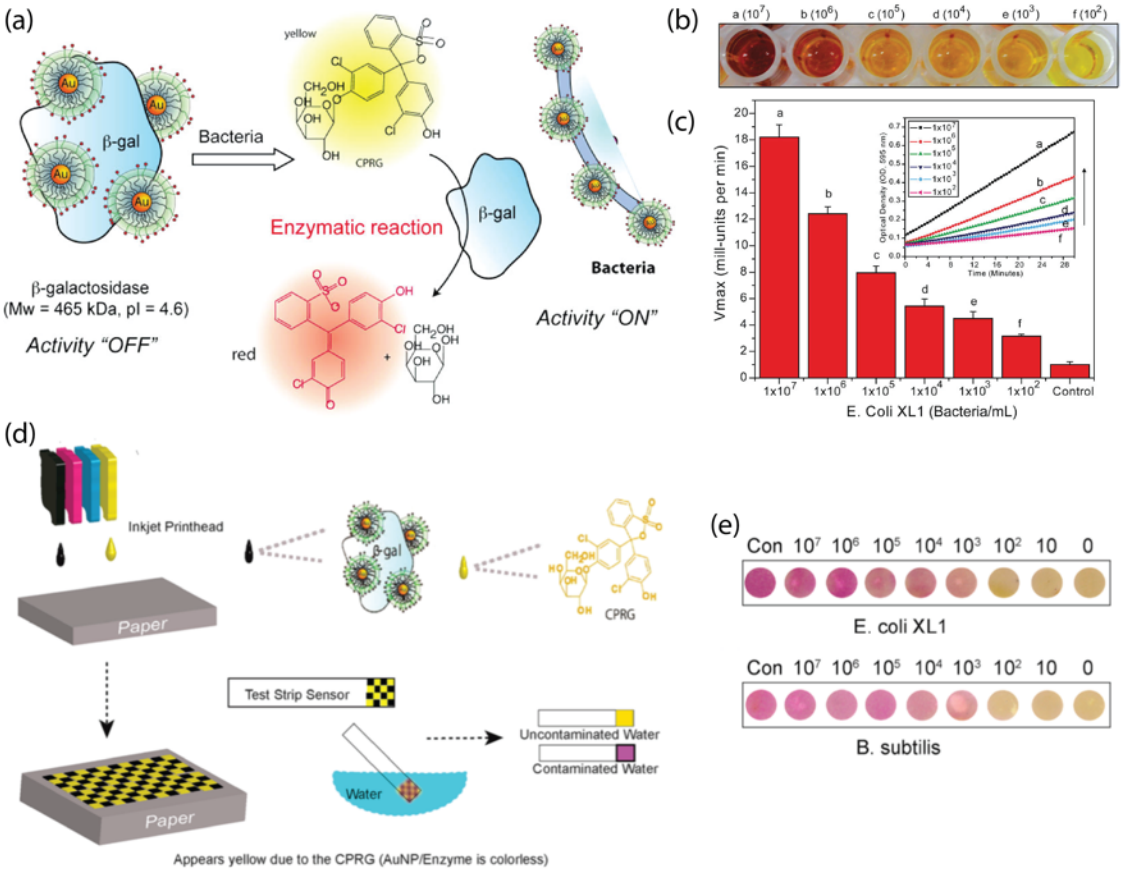

Figure 2.11 (a) Schematic illustration of selective detection of bacteria cells based on the switchable interaction of positively charged AuNPs and negatively charged enzyme. (b) Photograph and (c) absorbance intensity at the wavelength of 595 nm of the detection of bacteria cells with different concentrations. (d) Inkjet printing scheme for the fabrication of test strips. (e) Photograph of inkjet printed test strip for the Gram positive and Gram negative bacteria detection.

2.6.2 Array-Based Sensing of Bacteria

Array-based sensing attracts considerable attention as a detection platform, because of its independent selectivity for complex target bacterial cells. Typically, a set of selective nanoprobes recognizes a set of target bacterial strains, generating patterns. Much like mammalian olfaction, the generated patterns, formed by differential interactions between nanoprobes and bacterial cells, can serve as fingerprints to identify and analyze the bacterial cells.[40] As shown in Figure 2.12a, nanoprobe A-G were interacted with bacteria 1-4, resulting in multiple responses to form array-based patterns. The bacterial strains can be identified by analyzing the multiple response data using principle component analysis (PCA) or linear discriminant analysis (LDA).[40]

Philips *et al.* have demonstrated an array-based sensing of bacteria within minutes, using AuNPs and poly (para-phenyleneethynylenen) (PPE), a fluorescent polymer.[46] The AuNPs were modified with three different quaternary amine functional head groups, which can quench the fluorescence polymers based on FERT. In the presence of bacterial cells, the fluorescent polymers are released from the AuNPs/PPE complex (Figure 2.11b). Due to the differential binding affinities between different AuNPs and bacterial cells, multiple fluorescence readouts were recorded and analyzed using LDA. As shown in Figure 2.12c, each cluster represents one kind of bacteria. Twelve kinds of bacterial strains, including Gram-negative and Gram-positive bacteria, can be detected and discriminated. Interestingly, the same strains with different substrains (e.g. *E. coli* BL21, *E. coli XL1*, and *E. coli* DH5) can also be differentiated. Due to the complex compound in biofilms, it is channeling to discriminate biofilm bacteria strains. Based array-based sensing, Li *et al.* have developed a rapid and effective multichannel sensor to

discriminate bacteria strains in biofilms.[47] The results indicated that the multichannel sensor could also identify nonpathogenic and pathogenic bacteria. While the array-based sensing provided a powerful platform to analyze multiple targets at the same time, more research is needed to assess viability in complex matrices.

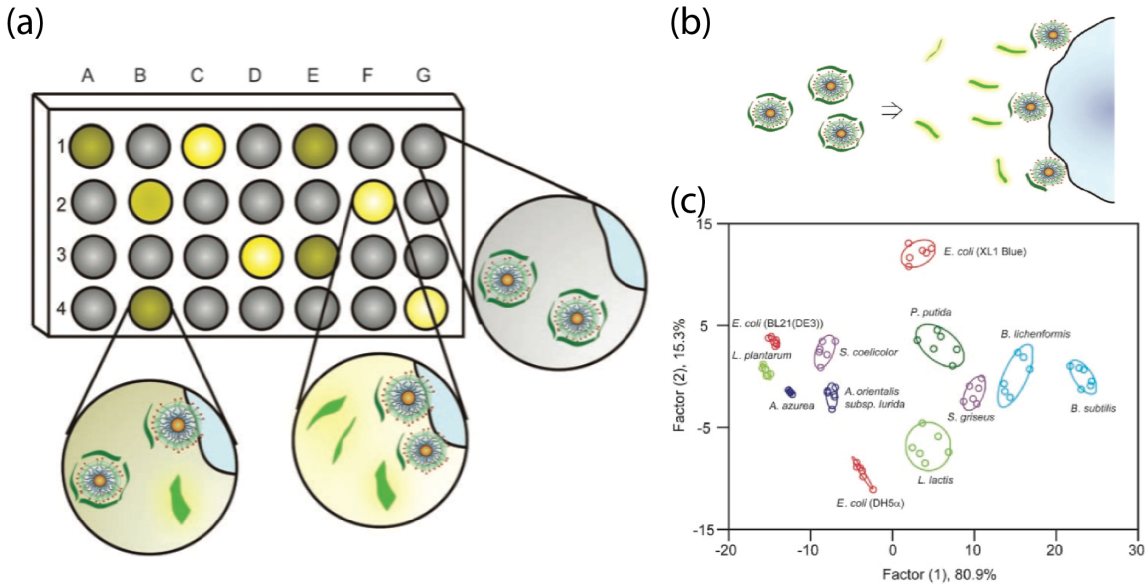

Figure 2.12 (a) Schematic illustration of the signal pattern generation using array-based sensing. (b) Schematic representation of the detection of bacteria strains using turning-on fluorescence array sensors. (c) Canonical score plot for the fluorescence array patterns calculated using LDA.

2.7 Other recognition element-based detection of bacteria

Some small molecules, including carbohydrates, lectin, and vancomycin, have emerged as important recognition elements on nanomaterials for the detection of bacteria. Due to their excellent stability to temperature or pH variations, these small molecules have attracted attention for mediating interactions between nanomaterials and bacterial cells. These small recognition elements have a strong affinity to bind a broad range of bacterial cells, which are suitable for the detection of unanticipated bacteria. Compared with antibodies or aptamers, these small molecules have much higher recognition element

densities on the surface of nanomaterials, providing strong affinity for the capture of bacterial cells.

Carbohydrates (polysaccharides or oligosaccharides) have been modified on nanoparticles as recognition elements to capture bacterial cells. EI-Boubbou *et al.* have used mannose- and galactose-functionalized MNPs to discriminate the *E. coli* strain.[48] After carbohydrates are conjugated with proteins or lipids, the formed glycoproteins or glycolipids can also recognize and bind to specific bacterial cells. Lectin, the most typical glycoprotein, can bind to N-acetyl glucosamine of peptidoglycan on the surface of bacteria. Lectins have previously been bound within columns to capture bacteria in a liquid sample. Additionally, they have been bound to magnetic beads to continuously remove microorganisms from blood.[49] Furthermore, vancomycin, a glycopeptide antibiotic, have been functionalized on MNPs to trap Gram positive or negative bacterial cells.[50] While these methods allow for strong binding events, there is potential for interference from food matrices.

2.8 Conclusions

The development of advanced nanoprobes is important for the detection and sensing of pathogenic bacterial cells. Recognizing the importance of the interaction between recognition element and bacterial cells is helpful to design specific detection strategies to capture bacterial cells. The choice of suitable nanomaterials provides sensitive signal transduction methods to detect bacterial cells. Selection of the proper combination of recognition elements and nanomaterials enable researchers to build diagnostic platforms for a broad purpose. In this review, we have summarized how the recognition elements on nanomaterials as nanoprobe to detect bacteria. Although many

researchers report using these nanoprobes, more sensitive and specific nanoprobe-based detection assays (being able to detection bacteria with 1 $CFU \cdot mL^{-1}$) are compelling of need to advance this rapidly changing area. Additionally, research is needed to examine the feasibility of these nanoprobes in applicable matrices, such as food, medial, and environmental samples. The most important factors to consider when fabricating a nanoprobe include manufacturability, reproducibility, assay time, cost, specificity, sensitivity, and ability for on-site detection of bacterial cells. The advancement of nanoprobes for bacterial cell detection has the ability to impact multiple industries, such as food safety, clinic diagnostics, and environmental monitoring. However, the potential toxicology of nanomaterials on human and environmental health should be taken into consideration when designing for daily use.

CHAPTER 3

DETECTION OF *ESCHERICHIA COLI* IN DRINKING WATER USING T7 BACTERIOPHAGE-CONJUGATED MAGNETIC PROBE

3.1 Introduction

In developing countries, the lack of clean drinking water and sanitation is a critical health issue.[112-114] The World Health Organization (WHO) estimated that 1.5 million children die from diarrheal diseases every year, 88% of which were caused by unsafe drinking water supply and inadequate sanitation.[112] One of major causes is from contamination water with *Escherichia coli* (*E. coli*).[115] The *E. coli* in drinking water mostly comes from domestic wastewater discharge or other sources such as livestock manure.

The Food Safety Modernization Act now required the testing of agricultural water for "generic *E. coli*". Although many of these organisms are non-pathogenic, they serve as indicators for bacterial contamination. A current method for bacteria detection in drinking water is through the detection of an indicator strain such as *E. coli*. A commonly used method for indicator strain detection relies on selective growth media that contains inhibitors to prevent unwanted bacteria from growing. The more widely used method for *E. coli* detection in drinking water is determination of β-galactosidase activity.[81-83, 89, 115-117] This enzyme is released by the bacteria and indicates the ability of the organism to metabolize lactose. For routine monitoring of agricultural water, generic *E. coli* has been used as an indicator of water quality, with a sample limit of 235 CFU·100 mL^{-1} and a rolling 5-sample mean of 126 CFU·100 mL^{-1}.[118] However, the analysis procedure takes at

least 18 hours from sample to results.[18] Therefore, there exists an urgent need to develop an inexpensive, rapid and reliable method to detect *E. coli* in drinking water.

Bacteriophages (phages) are viruses that infect bacteria, and are widely distributed in our environment. Phage can specifically recognize and attach to a host bacterial cell, commandeering the host cell's "machinery" into producing large quantities of new phage virons. At the end of an infection by a lytic phage, the host cell is enzymatically lysed and the newly assembled phage virons are released into the environment to find additional hosts.[72] There is renewed interest in phages as detection probes due to their specificity, speed of infection, and ability to introduce novel genetic material into the cell.[119, 120] Since phages can only replicate within a viable host, phage-based detection schemes are able to distinguish between live and inactivated bacteria.[69] This strategy is an improvement over DNA or antibody based detection assays,[121] as their targets may still be present (nucleic acids or epitopes) even if the pathogen of concern has been successfully inactived, thus resulting in a false positive. As a result, many studies have attempted to leverage phage-based schemes to detect pathogenic bacteria, such as *Staphylococcus aureus*, *Yersinia pestis* and *Mycobacterium tuberculosis*.[89, 122-124]

β-Galactosidase (*β*-gal), encoded by the *lacZ* gene, is an important enzyme for the growth of *E. coli*. *β*-Gal catalyzes the hydrolysis of lactose into galactose and glucose, thus providing a carbon source for *E. coli* growth. Isopropyl *β*-D-thiogalactopyranoside (IPTG) is known to induce the expression of *β*-gal during the growth of *E. coli*. Several previous studies have used IPTG induced expression of *β*-gal in electrochemical detection schemes for *E. coli* in drinking water.[82, 116, 125, 126] The detection limit of several similar techniques for *E. coli* strains are summarized and compared in Table 3.1. While

sensitive, these detection methods require advanced instrumentation and professionally trained operators, making their use problematic in resource-limited settings. Colorimetric assays, that can be visually interpreted represent an alternative method, is more amenable to resource-limited settings. Furthermore, recent developments in digital imaging and image processing greatly simplifies the quantitative analysis of colorimetric assays and avoids the use of advanced and expensive instruments.[127, 128]

Table 3.1 Summary and comparison of techniques for detection of *E. coli* stains.

Detection method	Detection time	Sensitivity	Reference
Electrochemistry	Less 1 hour	2×10^{6} CFU·mL^{-1}	116
Electrochemistry	6-7 hours	20 CFU·mL^{-1}	116
Electrochemistry	2 hours	6×10^{5} CFU·mL^{-1}	82
Electrochemistry	7 hours	10 CFU·mL^{-1}	82
Luminescent	8 hours	40 CFU·mL^{-1}	83
Luminescent	12.5 hours	1 CFU·mL^{-1}	89
Colorimetry	Less 4 hours	50 CFU·mL^{-1}	81

In this study, T7 bacteriophage covalently conjugated to carboxylic acid-modified magnetic beads through an amide bond were used to capture and infect target bacteria (*E. coli* BL21). The captured *E. coli* were then separated prior to lysis from the initial sample using a magnetic. Following separation, the *E. coli*-phage-bead complex was placed in buffer and allowed to lyse as part of the natural infection cycle. The lysis released *β*-gal from the capture cells, which then catalyzed the hydrolysis of a colorimetric substrate to provide visual signal (Figure 3.1). The bacterial concentration in drinking water was then quantified by measuring the color change via camera-generated RGB values.

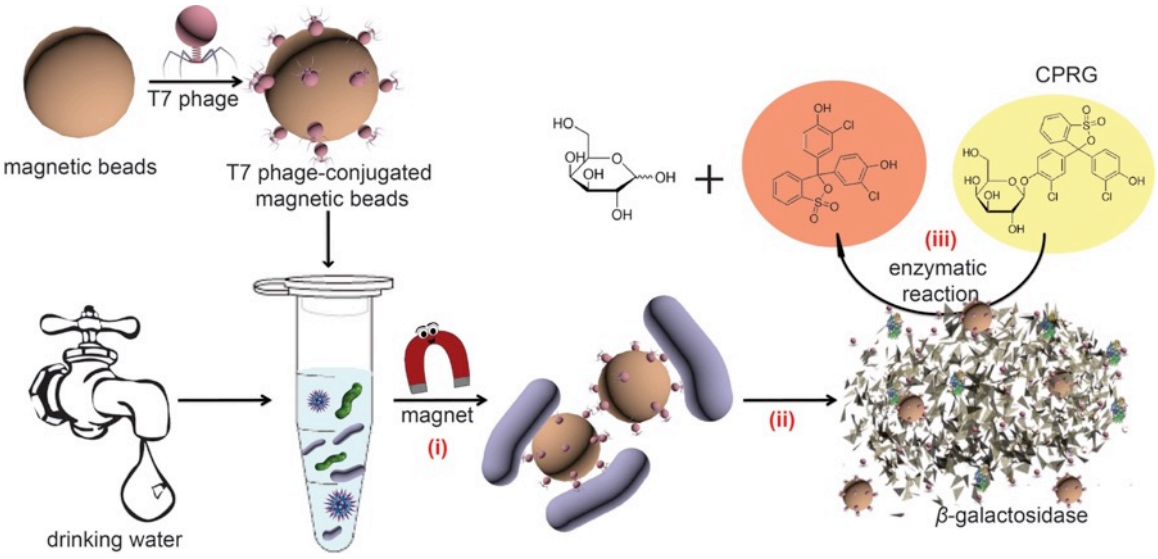

Figure 3.1 Schematic representation of detection of *Escherichia coli* in drinking water using T7 bacteriophage-conjugated magnetic probe. Three steps were involved: (i) Separation of *E. coli* from drinking water using T7 bacteriophage-conjugated magnetic probe to; (ii) T7 bacteriophage infection of *Escherichia coli* and the consequent release of *β*-gal. (iii) *β*-gal catalyzed CPRG hydrolysis to produce colorimetric readout.

3.2 Experimental Section

3.2.1 Chemicals and Materials

2-(N-Morpholino)ethanesulfonic acid (MES) hydrate, 1-ethyl-3-(3-dimethylaminopropyl)-carbodiimide hydrochloride (EDC) and N-hydroxysuccinimide (NHS) were purchased from Acros Organics (Morris Plains, NJ). Bovine serum albumin (BSA), isopropyl *β*-D-1-thiogalactopyranoside (IPTG), glutaraldehyde, sodium chloride, potassium chloride, sodium phosphate dibasic, potassium phosphate monobasic, tryptone, yeast extract and agar were purchased from Fisher Scientific (Fair Lawn, NJ). Chlorophenol red-*β*-D-galactopyranoside (CPRG) was purchased from Roche Diagnostics (Indianapolis, IN). Magnetic beads were Dynabeads® MyOne™ carboxylic acid from Invitrogen (Oslo, Norway). The filter with 0.45 μm pore size (Millex) and syringe with 20-mL volume (BD) were also purchased from Fisher Scientific (Fair Lawn, NJ). All chemicals were reagent grade and used as received. Aqueous solutions were

prepared using Mill-Q water with 18.2 mΩ·cm at 25 °C from Thermo Scientific (Asheville, NC). All media, buffer and plastic/glassware were sterilized by autoclaving at 121 °C for 30 min.

3.2.2 Instrumentation.

Scanning electron microscopy (SEM) images were obtained using an FEI SEM Magellan (Hillsboro, OR) with current of 13 pA and voltage of 1 kV. The absorbance intensities were recorded using a UV-Vis spectrophotometer from Biotek (Synergy™ 2,Winooski, VT). The photographs were taken using a portable iPhone 5 camera from Apple (Cupertino, CA).

3.2.3 Preparation of T7 Bacteriophage-Conjugated Magnetic Beads (Phage-MBs)

The T7 phage-MBs were prepared according to a previously reported method with a slight modification.[129] The amine groups on the surface of T7 phages were covalently bound to carboxylic acid modified magnetic beads by an amide linkage. The magnetic beads (100 μL, 10 mg·mL^{-1}) were washed three times with MES buffer and then suspended in MES buffer (1 mL). EDC (200 μL, 20 mg·mL^{-1}) and NHS (100 μL, 20 mg·mL^{-1}) were added and incubated for 30 min at room temperature with gentle agitation. The magnetic beads were washed three times with ice-cold phosphate buffered saline (PBS) buffer to remove excess EDC and NHS, and finally dispersed in PBS buffer (1 mL). Then T7 phage stock in PBS buffer (100 μL, 10^{11} PFU·mL^{-1}; PFU, plaque forming units) was added to the beads and agitated overnight at 4 °C. The magnetic beads were washed at least three times with PBS buffer to remove excess T7 phage. The beads were then resuspended in PBS buffer containing 0.1% BSA (1 mL, 1 mg·mL^{-1}) and incubated for 2 hours at 4 °C to block residual sites on magnetic beads. Finally, the T7

phage-MBs were stored in PBS buffer (1 mL) at 4 °C for further use. For SEM images, the samples were incubated in 2 % glutaraldehyde solution overnight at 4 °C, then dehydrated using serially diluted ethanol solution.

The phage titer was enumerated following standard plaque assay procedure. Briefly, the stock solution of T7 phage-MBs was 10-fold diluted into serial concentrations. 100 μL of each solution was added into a sterile tubes containing 200 μL of a fresh overnight bacteria culture at room temperature. Then, approximately 3 mL of melted top agar (50 °C) were added into these tubes. The mixtures in the tubes were immediately poured in a standard luria broth (LB) agar plates. The plates were placed in the incubator at 37 °C until clear plaques were seen.

3.2.4 Bacteria Culture

Prior to each experiment, a single colony of *E. coli* BL21 was selected from an previously streaked LB plate and grown in LB broth overnight at 37 °C with 200 rpm agitation. The culture was then centrifuged at 6000 g for 2 min, and resuspended in in PBS buffer. This centrifugation step was repeated for a total of three times. This bacterial working stock solution was then serially diluted into desired concentrations for further usage. Each concentration of bacteria was plated on LB agar plate to confirm the viable counts ($CFU \cdot mL^{-1}$).

3.2.5 Colorimetric Detection of E. coli BL21 Using T7 Phage-Conjugated Magnetic Probes

The working *E. coli* stock was serially diluted into the following concentrations using PBS buffer: 10^4, 10^5, 10^6 and 10^7 $CFU \cdot mL^{-1}$. Aliquots (1 mL) of each concentration were added to sterile centrifuge tubes for detection. PBS buffer was used

for control experiment. Next, T7 phage-MBs (100 μL, 1 mg·mL^{-1}) were added to the above samples. The samples were incubated for 15 min at room temperature, and the bacteria were separated using magnet for 2 min. The supernatant was removed and the bacteria-bead complex was washed three times with PBS buffer. The beads were then resuspended in PBS buffer (220 μL) and CPRG (30 μL, 8 mM). Samples were incubated for 2 hours at 37 °C. 200 μL of each sample were transferred into 96-well plate. The absorbance values were determined using a UV-Vis spectrophotometer at a wavelength of 595 nm. Following color development, a digital image of each sample was taken. The circles with same diameter were selected from each well to represent each sample. The RGB channel and value were obtained using ImageJ 1.48 V (Wayne Rasband, Madison, WI).

3.2.6 Detection of E. coli in Drinking Water

The drinking water sample was collected from water fountains at University of Massachusetts, Amherst. A filter with 0.45 μm pore size was used to prevent large substances/aggregates (including most of the bacteria) in drinking water from interfering the interactions within our system. An aliquot of this pre-filtered water was used as negative control and another three were inoculated with *E. coli* BL21 to a final concentration of 100 and 1,000 CFU·mL^{-1}. 100 μL of each water sample was pipetted into sterile flasks, and combined with 0.9 mL of LB liquid medium containing 0.2 mM IPTG. The mixtures were incubated for 5-8 hours at 37 °C with 200 rpm agitation prior to measurement.

After incubation for a predetermined time, T7 phage-MBs (100 μL, 1 mg mL^{-1}) were added into the negative control and two drinking water samples, respectively.

Following incubation for 15 min, the bacteria were separated with a magnet. The magnetic bead-bacteria complex was washed three times. The samples were re-suspended in PBS buffer (220 μL) and CPRG (30 μL, 8 mM) and incubated at 37 °C for 2 hours. The absorbance values were measured using 96-well plate reader at a wavelength of 595 nm. All experiments were performed with independent triplicates.

3.2.7 Statistical Analysis

All data is presented as mean ± standard deviation (SD) from at least three replicates. The *t*-test was conducted to determine if each set of data was significantly different from the corresponding control set. One star (*) signifies a difference ($0.01 < p < 0.05$) and two stars (**) represented the significant difference ($p < 0.01$) between the two compared sets of data.

3.3 Results and Discussion

3.3.1 Covalent Immobilization of T7 phage on Magnetic Beads and Separation of *E. coli* BL21

Phage-conjugated magnetic beads (phage-MBs) are a better performing alternative to immunomagnetic separation (IMS) for the separation of bacteria.[130, 131] For example, P22 phage has been reported to separate *Salmonella* using tosyl-activated magnetic beads.[97] T4 phage coated Dynabeads have also been used to increase the sensitivity of *E. coli* K12 detection.[129] In this study, the magnetic beads were coated with carboxylic acid. The size of the magnetic beads was approximately 1 μm. During the immobilization reaction, water-soluble EDC and NHS were used to create an amide bond between carboxylic acids of magnetic beads and primary amines on the phage. BSA was used to block remaining active sites in order to avoid non-specific binding between the

magnetic beads and target bacteria. The attachment of T7 phage on magnetic beads was evaluated using scanning electron microscopy (SEM) and plaque assays. The microscopic characterization of non-immobilization and immobilization of T7 phage are shown in Figure 3.2a-d. The carboxylic acid modified magnetic beads had a smooth shell. Following immobilization, the T7 and BSA coated beads appear to have a more uneven surface suggesting a surface coating has been achieved. Given the initial phage concentration of $(2.5 \pm 0.4) \times 10^{11}$ PFU, the number of magnetic particles 7×10^{7} magnetic beads, and the number of phage $(1.2 \pm 0.5) \times 10^{11}$ PFU remaining in the aspirated conjugation solution, we estimated the number of phage immobilized on each particle was approximately 1,871 PFU. Furthermore, T7 phage-MBs were able to initiate phage infection in *E. coli* BL21, as demonstrated by plaque assays, indicating successful conjugation of active T7 phage. The T7 phage-MB solution was tittered to contain $(5.7 \pm 0.2) \times 10^{7}$ PFU·mL^{-1} of phage on appropriately 7×10^{7} beads·mL^{-1}. The difference between the number of phage captured and that tittered was due to the fact that each bead will act as "infective center" and produce a single plaque on a lawn of bacteria, despite having $>10^{3}$ PFU phage bound to it.

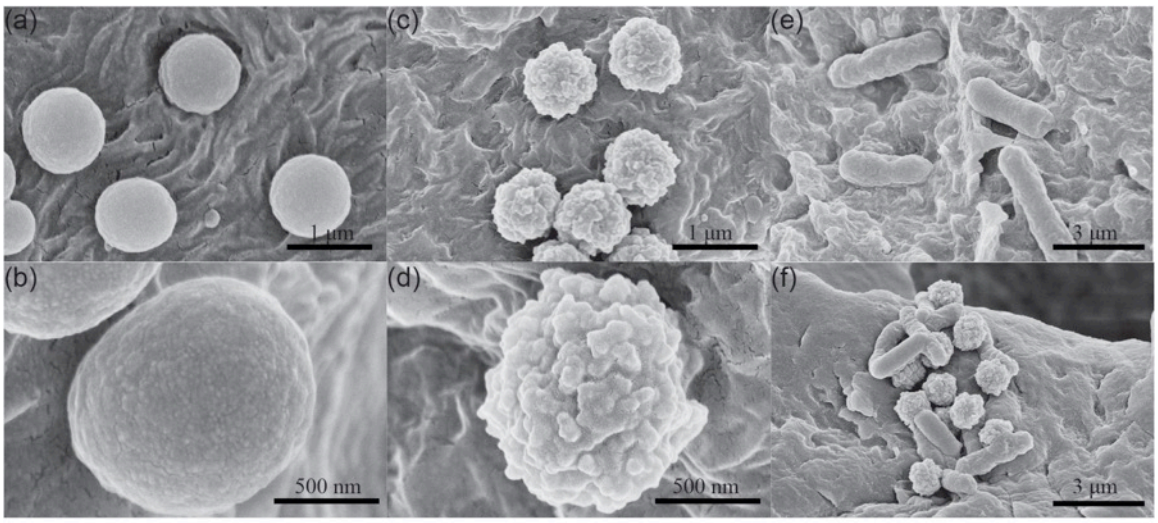

Figure 3.2 SEM images of (a) and (b) carboxylic acid coated magnetic beads, (c) and (d) T7 bacteriophage-conjugated magnetic beads, (e) *E. coli* BL21 cells and (f) *E. coli* BL21 cells attached to T7 bacteriophage-conjugated magnetic beads through tail fiber.

T7 phage specifically attaches to *E. coli* strains through recognition of lipopolysaccharide (LPS) as a receptor by the phage tail fiber protein.[132, 133] The binding between the tail fiber protein and lipopolysaccharide on the bacteria is quite strong and irreversible, allowing for the bacterial separation from complex matrices using phage-MBs. This binding of T7 phage-MBs to *E. coli* cells was also characterized using SEM. Figure 3.2e shows an SEM image of unbound *E. coli* BL21 while *E. coli* BL21 bound by T7 phage-MBs was achieved (Figure 3.2f). As shown in Figure 3.2f, T7-phage MB bound to single and multiple bacterial cells can be observed, as well as bacterial cells bound by multiple T7-phage MBs.

3.3.2 Optimization of Detection Conditions

E. coli BL 21 was harvested following an overnight growth at 37 °C. The culture was centrifuged and the bacterial pellets were washed three times with PBS buffer, and then resuspended in 1 mL of PBS. The suspension was serially diluted to achieve three concentrations: 10^5, 10^6 and 10^7 CFU·mL^{-1} in PBS buffer. PBS buffer was used as

negative control in the detection experiments. The *β*-gal activity of different concentrations of *E. coli* BL21 was determined by absorbance using CPRG as the colorimetric substrate. The absorbance of 200 µL samples in a 96-well plate was measured at a wavelength of 595 nm.

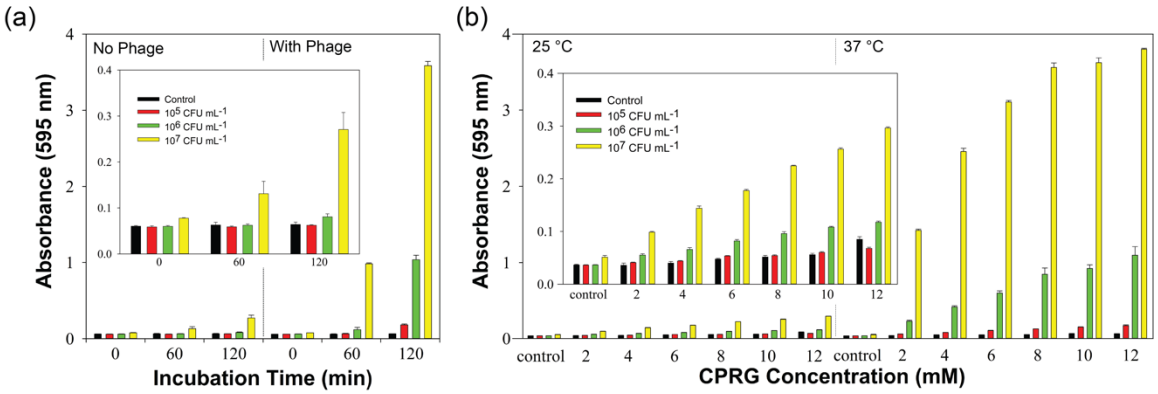

Figure 3.3 Colorimetric response of released *β*-gal from *E. coli* BL21. (a) Detection of *β*-gal activity from *E. coli* BL21 cells (0, 10^5, 10^6 and 10^7 CFU·mL^{-1}) after incubated with phage or phage free buffer for 0, 1 and 2 hours. (b) Detection of *β*-gal activity from *E. coli* BL21 cells (0, 10^5, 10^6 and 10^7 CFU·mL^{-1}) after incubated with CPRG solution (0, 2, 4, 6, 8, 10 and 12 mM) at 25 °C and 37 °C. Error bars represent the standard deviation of a minimum of three replicates.

T7 phage is a lytic phage resulting in bacterial cell lysis occurs at the end of infection cycle. The lysis of the infected cells results in the release of intracellular components, including *β*-gal, into the sample solution. To determine the concentration of *β*-gal released from T7 lysed bacteria cells, varying concentrations of bacteria (0, 10^5, 10^6 and 10^7 CFU·mL^{-1}) were either incubated with 30 µL of a 1.37×10^8 PFU mL^{-1} of T7 phage or a phage-free solution at 37° and the absorbance was measured at 0, 60 and 120 minutes. This colorimetric method was able to detect *β*-gal activity from phage-lysed cells when the initial cell concentration was 10^6 CFU·mL^{-1} after 60 minutes and 10^5 CFU·mL^{-1} after 120 minutes. For comparison, this resulted in one log increase in sensitivity, respectively, when compared to the phage free control (Figure 3.3a). *β*-Gal is

a common intracellular enzyme and therefore solutions without phage infection were able to generate a weak colorimetric signal. This signal could be explained by the release of *β*-gal into solution by natural cell lysis or the diffusion of CPRG across the cell membrane into the bacteria cells.[82, 134, 135] As seen from Figure 3.3a, the absorbance increased with the increase of incubation time due to increased substrate utilization. A reaction time of 2 hours was selected as optimal for the enzymatic reaction.

Additional parameters for the colorimetric readout were optimized. The effect of temperature on the colorimetric detection was first studied using 25 and 37 °C. A greater colorimetric response was observed at 37 °C against 25 °C. This is not surprising as 37 °C is known to be an optimal temperature for *E. coli* growth, T7 phage replication, as well as for the *β*-gal enzymatic reaction.[82, 136] Additionally, phage adsorption has been shown to be relatively temperature independent. This would allow for a more reliable separation (vs. antibodies) in resource-limited settings.[137] The concentration of colorimetric substrate was also an important factor influencing the absorbance. Increasing concentrations of *E. coli* were incubated for 2 hours at 37 °C with various concentration of CPRG solution (0-12 mM). The absorbance increased with increasing the concentration of CPRG and tended to level off after a concentration of 8 mM (Figure 3.3b). Hence, a CPRG concentration of 8 mM was selected for further enzymatic experiments.

Reaction conditions for all additional tests were thus performed using: 1.37×10^8 PFU of T7 phage and 8 mM of CPRG at 37° for 2 hours, which allowed an efficient phage infection and enzymatic reactions to generate enough colorimetric signal.

Simultaneous addition of phage and CPRG was used to allow the enzymatic reaction to produce a faster colorimetric signal.[83, 136]

3.3.3 Analytical Performance of *E. coli* BL21 Using T7 Bacteriophage-conjugated Magnetic Beads

Under optimal conditions, T7 phage-MBs were introduced to detect different concentrations of *E. coli* BL21 cells. T7 phage-MBs were able to capture and infect bacteria cells, subsequently releasing *β*-gal into the sample solution. Different concentrations (10^4, 10^5, 10^6 and 10^7 CFU·mL^{-1}) of bacteria cells were incubated with T7 phage-MBs for 15 minutes. PBS buffer was used as negative control. After separation and three-time washing, CPRG was added and the mixture was incubated for 2 hours. The T7 phage MBs were separated for 2 minutes using a magnet (Figure 3.4a) and the clear supernatant was transferred into a 96-well plate to obtain the absorbance readout. The red color of the enzymatic product increased with the increasing bacterial concentration, and a concentration of 1×10^4 CFU·mL^{-1} produced a signal that can be distinguished visually (Figure 3.4b). The absorbance recorded at the wavelength of 595 nm showed the same trend with increased bacteria concentrations (Figure 3.4c). Based on the absorbance, we could reproducibly detect bacteria concentration at 1×10^4 CFU·mL^{-1} ($p < 0.05$), which corresponds with the visual results. The use of the magnetic beads has several benefits for detection. First, they allow for the concentration of bacterial cells, thus improving detection. Second, they allow for the separation of the bacteria from matrices like: milk, orange juice, turbid water and so on, that would otherwise interfere with colorimetric assays.[81, 83]

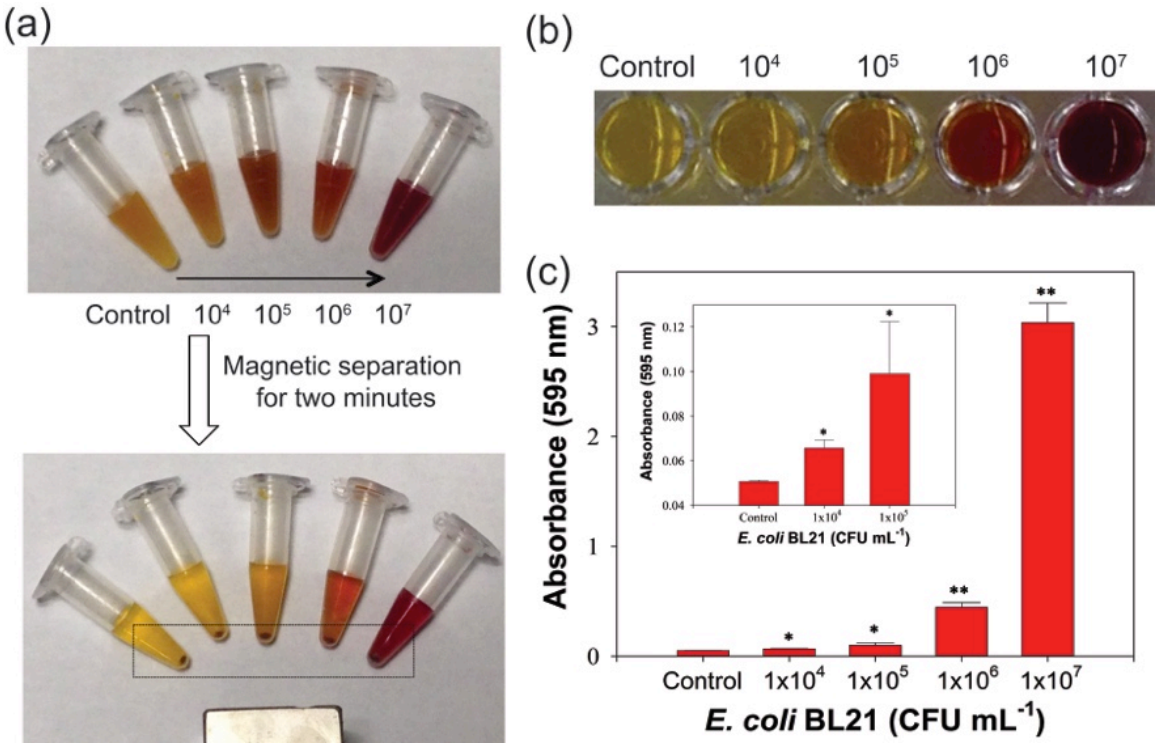

Figure 3.4 (a) Photographs of bacteria detection at different concentrations before and after magnetic separation. (b) Photograph of colorimetric response and (c) absorbance upon different bacteria concentrations. Error bars represent the standard deviation of a minimum of three replicates.

Smartphone-based technology has become increasingly more popularly for use in analytical diagnostics. Erickson and his co-workers developed a smartphone platform to quantify vitamin D levels and detect pH change in saliva and sweat.[138, 139] Multi-analyte tests based on colorimetry have also been successfully performed using smartphone devices.[140] After obtaining an image from the smartphone, a corresponding app can analyze the RGB values and report the analytical results immediately. Such technology allowed the quick test in low-resource settings such as remote parts of Africa, South America and Southeast Asia which might be lacking professional laboratory facilities.[5, 6, 141-143] In this study, images were taken using an iPhone 5 built-in camera immediately following the incubating for 2 hours. By analyzing original image (Figure 3.5a) using

ImageJ software, the images for red, green and blue channels were obtained (Figure 3.5b). The values for each RGB channel were plotted with bacteria concentration (Figure 3.5c), which also confirmed that a bacterial concentration of 1 $\times 10^4$ CFU·mL^{-1} could be detected ($p < 0.05$).[144]

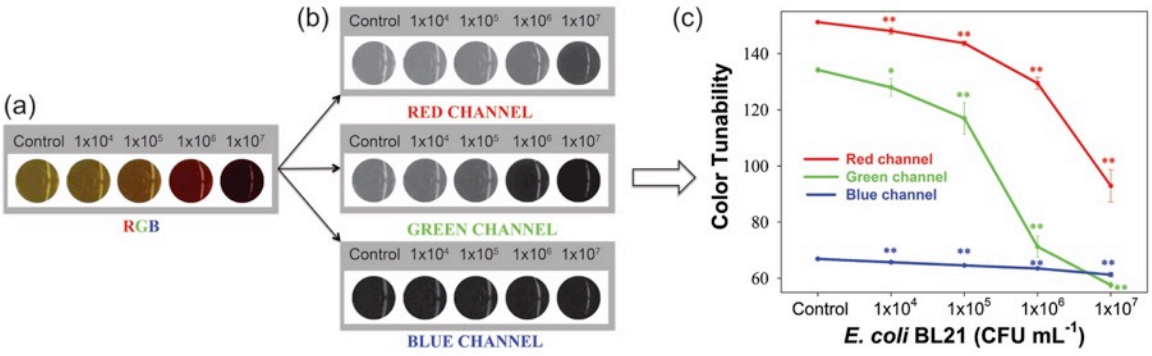

Figure 3.5 Schematic illustration of the RGB values to analyze *β*-gal activity released from different concentrations of *E. coli* BL21 cells. (a) Image of colorimetric response of *β*-gal activity released from different concentration. (b) Red, green and blue channels from original image (a) to different concentration processed using ImageJ. (c) Values of red, green and blue channels obtained from original image (a) to different concentration of *E. coli* BL 21 cells. Error bars represent the standard deviation of a minimum of three replicates.

The specificity of the proposed assay was evaluated using common pathogenic bacteria strains as competitors, including *Salmonella enterica* (*S. enterica*), *Staphylococcus aureus* (*S. aureus*) and *Pseudomonas aeruginosa* (*P. aeruginosa*). The bacteria concentration of each strain in single or mixed competitor solutions was 10^6 CFU·mL^{-1}. A significant change in color and absorbance was observed only with the present of *E. coli* cells (Figure 3.6a-b). These results demonstrated this approach has a good specificity towards *E. coli*.

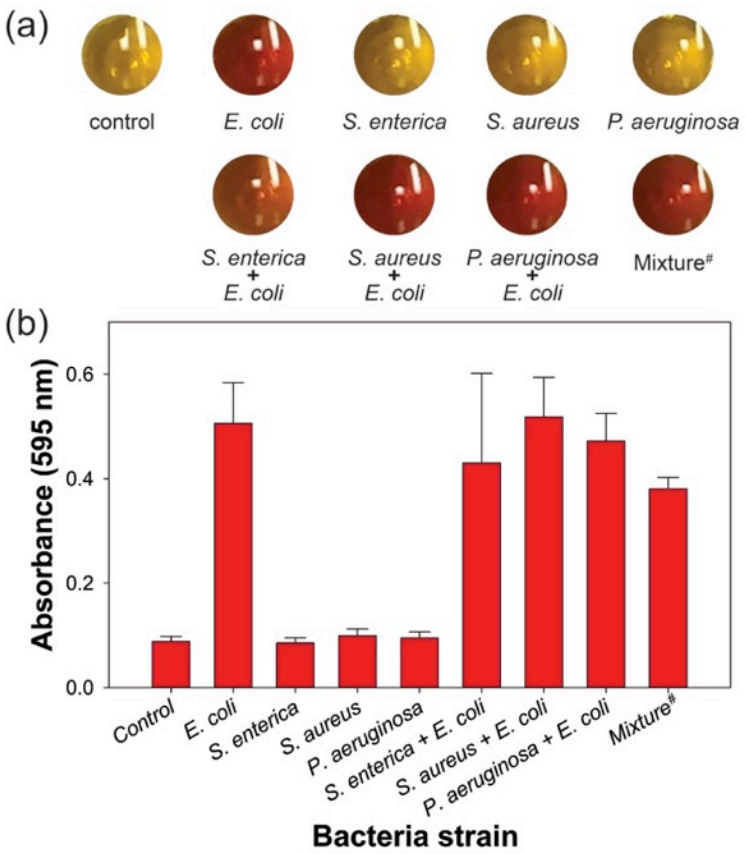

Figure 3.6 (a) Photographs and (b) absorbance of specificity of the T7 phage-conjugated magnetic probes against *E. coli*, *S. enterica*, *S. aureus*, *P. aeruginosa*, *S. enterica* + *E. coli*, *S aureus* + *E. coli*, *P. aeruginosa* + *E. coli* and mixture[#] at concentration of 10^6 CFU·mL^{-1} (mixture[#] represents a mixture of *E. coli*, *S. enterica*, *S. aureus* and *P. aeruginosa*).

3.3.4 Detection of Bacteria in Drinking Water with a Pre-enrich Step

E. coli in drinking water are ideally well below the 1×10^4 CFU·mL^{-1} limit of the colorimetric test. To overcome this hurdle, we investigated using a pre-enrichment step to allow for bacterial growth, subsequently followed by our previously described assay. Water samples were collected from a local water fountain at the University of Massachusetts, Amherst. Different concentrations of bacteria were inoculated into LB liquid medium in the present of IPTG, which was a molecular mimic of CPRG. IPTG can trigger the transcription of *lac* gene in bacteria cells to express more *β*-gal.[82, 116, 145, 146]

IPTG cannot be hydrolyzed by β-gal and its concentration would remain constant in all experiments. Based on the visual images, a 10 CFU·mL^{-1} concentration of bacteria could be detected after a pre-enrichment of 6 hours while a pre-enrichment of 8 hours provided stronger visual signal (Figure 3.7a). As seen in Figure 3.7b, 10 CFU·mL^{-1} bacteria can be detected after pre-enrichment for 5 hours ($p < 0.05$). The reproducibility of the colorimetric assays to detect 10 CFU·mL^{-1} bacteria in drinking water was evaluated. The absorbance of 10 replicates was compared to the control (0 CFU·mL^{-1}). All ten replicated resulted in an absorbance outside at least one standard deviation of the control, indicating that the proposed assays have the ability to detect low bacteria concentration in drinking water (Figure 3.7c).

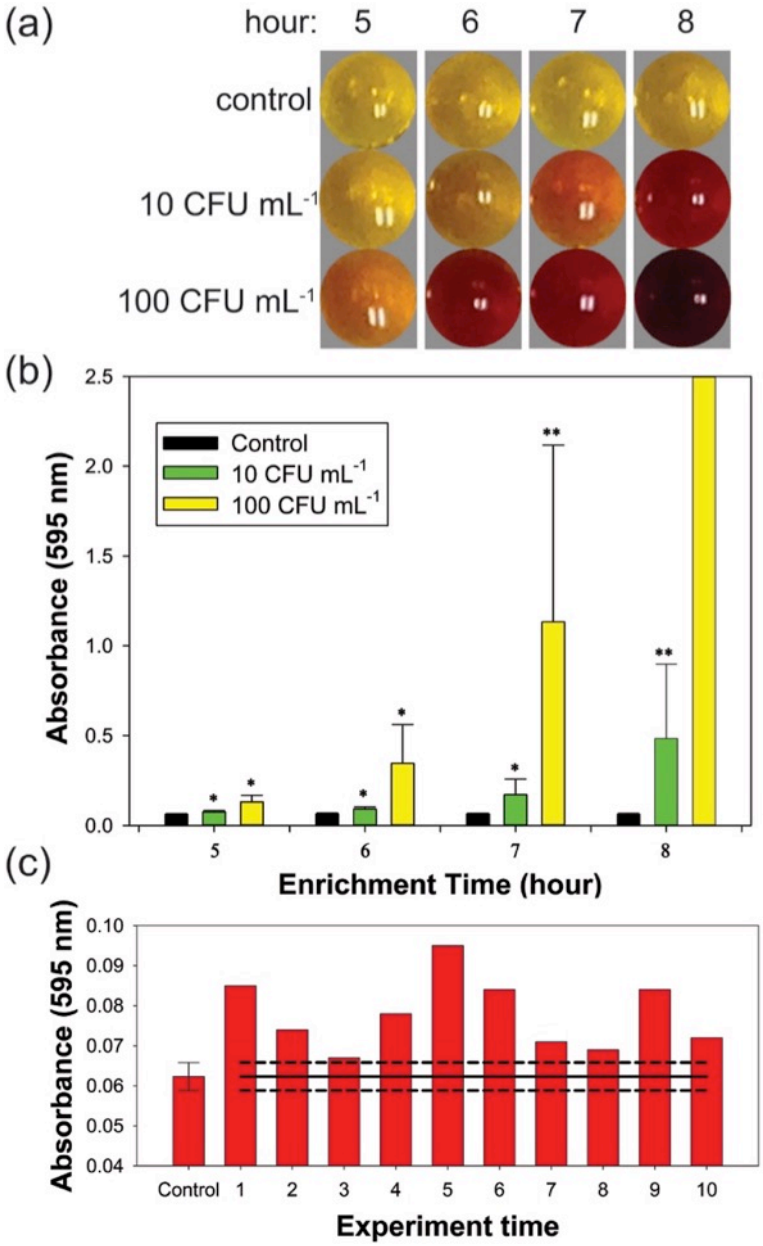

Figure 3.7 Detection of E. coli in drinking water using T7 bacteriophage-conjugated magnetic probe. (a) Photographs and (b) absorbance of detecting bacteria concentrations after 5-8 hours of pre-enrichment. (c) Detection of E. coli at 10 CFU·mL-1 after 5 hours of pre-enrichment for 10 times (the solid line represents the average of absorbance of the control (0 CFU·mL-1) while the dashed lines represent the standard deviation.

3.4 Conclusions

Here, we show the successful use of T7 bacteriophage-conjugated magnetic beads to detect low levels of *E. coli* in drinking water. The T7 phage can specifically recognize

and bind to *Escherichia coli* and the magnetic beads are used to separate and concentrate the bacterial cells from drinking water. After concentration and separation, phages will infect and lyse the host cells, resulting in the release of *β*-gal. The released enzyme can then be readily detected using a colorimetric assay. Compared to antibodies, which are used in standard immunomagnetic separation (IMS), T7 phages are low-cost, animal-free, and can be easily produced.[97, 130] Another benefit to using T7 phage for bacterial separation is their broadly infect *E. coli* with minimal additional specificity,[147, 148] which can allow us to detect an entire genus or species, a range which would be difficult to achieve with antibodies. Although there are strains to known to be resistant, solutions to be resistance has been identified.[148, 149]

Using this proposed strategy, we were able to detect *E. coli* at a concentration of 1×10^4 CFU·mL^{-1} in 2.5 hours. 10 CFU·mL^{-1} of *E. coli* in drinking water can be detected after pre-enrichment for 6 hours. Meanwhile, the high specificity towards *E. coli* and reproducibility of this approach has been demonstrated experimentally. The assay has been designed to allow portability with the use of minimal equipment. This will allow the rapid determination of *E. coli* concentrations in water in settings where proper laboratories are not available. Future work will focus on translating this assay into a portable, rapid and low-cost test strips that are suitable for use in resource-limited setting.

CHAPTER 4

BACTERIOPHAGE-BASED NANOPROBES FOR RAPID BACTERIA SEPARATION

4.1 Introduction

Advances in rapid bacteria detection methods have enabled improvements in speed, sensitivity and specificity in fields such as medical diagnostics, biowarfare detection, food safety, water quality and environmental monitoring. Technologies such as surface plasmon resonance (SPR)[9], surface enhanced Raman scattering (SERS)[150], electrochemical detection,[107, 151] field effect transistor biosensors (FET) and quartz crystal microbalance (QCM)[114, 152] are examples of emerging detection methods, which require a relatively clean sample in a small volume to achieve enhanced sensitivity. Unfortunately, such methods typically require a significant sample purification or preparation step prior to analysis. Analysis of complex samples (containing non-target lipids, proteins, carbohydrates, inhibitors, or other interferents) remains a unique challenge to utilizing such high sensitivity detection methods. Stevens and Jaykus suggested that an ideal separation method should 1) separate the analyte from the sample, 2) remove any possible inhibitors to a downstream detection system, and 3) reduce the sample size while maintaining a high capture efficiency of bacteria.[153]

Immunomagnetic separation (IMS) is a common separation method in which magnetic beads tagged with analyte-specific antibodies are incubated with the analyte. When a magnet is placed near the sample tube, the beads (on which the analyte is bound) are pulled toward the magnet and the remaining liquid sample can be aspirated. IMS beads (typically 1-5 μm in diameter, onto which antibodies for a range of bacterial

analytes are conjugated) are commercially available from several companies. While this method is widely used, improvements to the capture efficiencies and cost would allow the method to become more utilized. Recently, magnetic nanoparticles (MNPs) have attracted attention in various fields such as biomedicine, drug delivery, and diagnostics due to their unique magnetic properties.[41, 154, 155] Magnetic nanoparticles have been reported to efficiently separate *E. coli* O157:H7 in ground beef[35, 36] and *Listeria monocytogenes* from both nutrient broth and milk samples[156]. Unfortunately, traditional iron oxide nanoparticles require extended periods of time to separate due to slow particle velocities.

Bacteriophages, also known simply as phages, are viruses which infect specific bacterial cells. Phages have the ability to very strongly and specifically bind to target bacteria.[68, 133] They are able to recognize a bacterium, infect it, and lyse it releasing hundreds to thousands of replicated phages in the process. Detecting bacteria using engineered phages by fluorescent labeling of phage nucleic acid[157] and phage components[158], phage-integrated colorimetric, fluorescent, and bioluminescent reporter genes[70] and phage-integrated green fluorescent protein[159] has shown promising results.

The use of antibodies for separation can result in inconsistencies due to batch to batch variations. The relatively high cost of antibodies has led to research towards alternative biorecognition elements such as aptamers.[160, 161] Unlike antibodies and aptamers, phages are relatively easy and inexpensive to synthesize and purify. Due to the extremely strong binding affinity,[137] phage have recently been used as low-cost biorecognition elements for bacteria.[133, 162] The host range of bacteriophages can be either extremely wide or narrow allowing for isolation of an entire genus or species.[163] The

phages are also more stable than antibodies with regards to temperature, pH and ionic strength.[164]

The challenge in using infective bacteriophages as recognition elements for separation lies in the infection cycle of the particular phage. The complete infection cycle can last as little as 25 minutes and results in lysed bacteria. Although this could be ideal for downstream genetic analysis such as PCR, if the bacteria have not been separated from the sample solution before cell lysis, the process would fail. Therefore the combination of bacteriophages and magnetic nanoparticles would require separation speeds much faster than those offered by iron oxide nanoparticles which require a significant separation time.

In this paper, we have bound T7 bacteriophage on magnetic nanoparticles for the purpose of separating *E. coli* from a liquid solution. For the nanoparticles, mixed metal oxide (FeCo) magnetic nanoparticles containing 30% cobalt (w/w) were used as core materials. The cobalt allowed improved separation velocities as compared to iron oxide. The magnetic nanoparticles were coated with a silica shell, onto which streptavidin was immobilized for subsequent conjugation of biotinylated T7 bacteriophage and antibodies. The nanoscale phage magnetic probes were used to separate *E. coli* K12 at concentrations ranging from 10^2 to 10^7 CFU mL^{-1}.

4.2 Experimental Section

4.2.1 Synthesis of Oleic Acid Protected FeCo MNPs

The oleic acid protected FeCo MNPs were synthesised according to reported methods with some modifications.[165, 166] $Fe(acac)_3$ (1 mmol, 0.3680 g), $Co(acac)_2$ (2 mmol, 0.5355 g), and 1,2-hexadecanediol (3 mmol, 0.9675 g) were placed into a three-

neck round bottomed reaction flask with dibenzyl ether (50.0 mL). The reaction mixture was stirred for 30 minutes under flowing nitrogen gas to allow the removal of air. The mixture was then slowly heated to 100 °C and kept at this temperature for 10 minutes. The surfactants, oleylamine (4.25 mL) and oleic acid (4.00 mL) were added into reaction flask and the reaction mixture was then heated to 200 °C for 20 minutes. Following the brief incubation, the reaction mixture was heated to reflux (~300 °C) for 60 minutes. During this process, the solution color changed from purple to black, indicating the formation of FeCo MNPs. The black solution was then cooled down to room temperature and the particles were precipitated using ethanol (20 mL) with centrifugation at 7500 x g for 10 minutes. The particles were then washed three times with a mixture of ethanol and hexane (3:1, V/V). Finally, the FeCo MNPs were dispersed in hexane until use.

4.2.2 Preparation of Silica-Coated FeCo Core/Shell MNPs

The silica-coated FeCo core/shell MNPs were prepared using a modification of a previously reported method.[167] Polyoxyethylene(5)nonylphenyl ether (7 mmol, 3.0 g, Igepal CO-520) was dispersed in cyclohexane (50.0 mL). Next, dried FeCo MNPs (10 mg) were transferred into cyclohexane (5.0 mL) and briefly sonicated. The two cyclohexane solutions were mixed until a clear solution formed. Ammonium hydroxide (25%, 0.5 mL) was added to form a clear brown reverse microemulsion. Lastly, tetraethylorthosilicate (30 μL, TEOS) was added, and gently agitated for 48 hours at room temperature. Methanol was added into the solution to remove the excess surfactant and the silica-coated FeCo core/shell MNPs were precipitated and washed three times using sonication and centrifugation with mixture of ethanol and hexane (1:3, V/V). The particles were then redispersed in ethanol until use.

4.2.3 Immobilization of Streptavidin on Silica-Coated FeCo MNPs

The silica-coated FeCo MNPs (10 mg) were placed into a scintillation vial and washed sequentially with 5 mL each of a mixture of DI water and dimethyl sulfoxide (DMSO) (3:7, 5:5, 7:3, V/V). The particles were then washed three times in anhydrous DMSO to minimize the water content. *N, N'*-Carbonyldiimidazole (1.0 mL, 10 mg mL^{-1}, CDI in DMSO) was then added into the scintillation vial. Next, the vial was agitated for 2 hours at room temperature. The MNPs were then washed three times with anhydrous DMSO to remove excess CDI, and washed using ice-cold sodium phosphate buffer solution (0.01 M, pH 7.4, PBS: 10 mM Na_2HPO_4, 1.8 mM KH_2PO_4, 137 mM NaCl, 2.7 mM KCl). The MNPs were redispersed in PBS (5 mL, 0.01 M, pH 7.4), and streptavidin (500 μL, 1 mg mL^{-1} in PBS) was then added to the mixture. The conjugation solution was agitated for 12 hours at room temperature. Following conjugation, the MNPs were washed three times with PBS (0.01 mM, pH 7.4) using magnetic separation and stored at 4 °C.

4.2.4 Quantification of Biotin Capacity of Streptavidin Coated Nanoparticles

Several volumes of streptavidin-coated nanoparticles solution (0, 50, 100, 150, 200, 250 μL, 2 mg mL^{-1}) were washed three times with acetate buffer (1 mL, 0.2 M, pH 5.0, 166 mM sodium acetate trihydrate, 34 mM glacial acetic acid, 0.05% Tween 20), and finally dispersed in acetate buffer (1mL, 0.2 M). Following washing, *d*-biotin *p*-nitrophenyl ester (100 μL, 10 mg mL^{-1} in DMSO, BNPE) was added and incubated for 30 minutes with gentle agitation. The nanoparticles were then washed five times with above acetate buffer (1 mL, 0.2 M) to remove excess BNPE and finally dispersed in NaOH

solution (1 mL, 0.1 M). The BNPE bound to nanoparticles hydrolyzed and produced *p*-nitryl phenol (yellow) which was quantified at 400 nm.

4.2.5 Preparation of Biotinlyted T7 Bacteriophage

T7 bacteriophage was previously genetically modified to express the 15 AA (GLNDIFEAQKIEWHE) biotin ligase (BirA) target on the capsid.[95] The endogenous BirA within *E. coli* was able to conjugate biotin molecules to the phage capsid during replication. *E. coli* BL21 was grown overnight in Luria-Bertani (LB) broth (50 mL, pH 7.4, 10 g L^{-1} tryptone, 5 g L^{-1} yeast extract, 10 g L^{-1} NaCl) at 250 rpm (37 °C). Following the overnight growth, the culture was reinoculated into fresh LB broth (35 mL), and agitated at 250 rpm for 3 hours at 37 °C. After the OD_{600} of the culture reached 0.6–0.8, a high titer biotin T7 phage lysate (5 μL, 10^{10} CFU mL^{-1}) was added and the culture was again incubated for 1 hour at 37 °C until the solution cleared. Following the addition of salt (3 mL, 5 M NaCl), the culture was centrifuged at 7000 rpm for 10 minutes at 4 °C. The supernatant was stored at 4 °C until use.

4.2.6 Preparation of Antibody or Phage Magnetic Nanoprobes

Biotin-modified anti-*E. coli* K12 antibodies (10 μL, 4 mg mL^{-1}) or biotinlyated T7 phage (1 mL, 3.5×10^{10} CFU mL^{-1}) were tagged onto streptavidin-coated nanoparticles (1 mL, 1.8 mg $mL^{-1)}$. The solutions were incubated for 30 minutes with gentle agitation at room temperature. All nanoparticles were washed a minimum of three times with above PBS (0.01 M, pH 7.4) to remove unbound antibodies or phages. The nanoparticles were dispersed in PBS (1 mL, 0.01M, pH 7.4) and stored at 4 °C until use.

4.2.7 Estimation of the Capture Efficiency of Phage or Antibody Probes on Bacterial Separation

E. coli K12 was inoculated into above LB broth (50 mL) and rotated at 250 rpm overnight at 37 °C. Antibody magnetic nanoparticles (100 μL, 1.8 mg mL^{-1}) and phage magnetic nanoparticles (100 μL, 1.8 mg mL^{-1}) were added into bacterial samples (1 mL, *E. coli* K12) in PBS (0.01 M, pH 7.4) with a range of concentrations (102-107 CFU mL^{-1}). The mixtures were incubated 30 minutes for antibody magnetic probes and 15 minutes for phage magnetic probes at 10 rpm at room temperature. The magnetic probes for *E. coli* K12 were separated and washed three times with PBS (0.01M, pH 7.4) by magnetic separation. The concentrations of *E. coli* in the original solution, *E. coli* (phage) in supernatant solution and *E. coli* (phage) on magnetic probes were counted using serial dilutions on LB plates (pH 7.4, 10 g L^{-1} tryptone, 5 g L^{-1} yeast extract, 10 g L^{-1} NaCl, 15 g L^{-1} agar).

4.3 Results and Discussion

4.3.1 Preparation and Characterization of FeCo MNPs

The challenge for using single domain MNPs in magnetic applications is the inherent aggregation which occurs even without an external magnetic field. However, superparamagnetic nanoparticles[168] such as Fe_3O_4, γ-Fe_2O_3, cobalt oxides and mixed metal oxides (without inter-particle magnetic attractive forces) have been utilized in biomedicine, drug delivery and cancer research.[42, 169] Karimi *et al.* reported that 7 nm FeCo MNPs have the highest saturation magnetization compared to the other MNPs with the same size.[42] Mixed metal oxide FeCo MNPs were therefore utilized as core materials for our study.

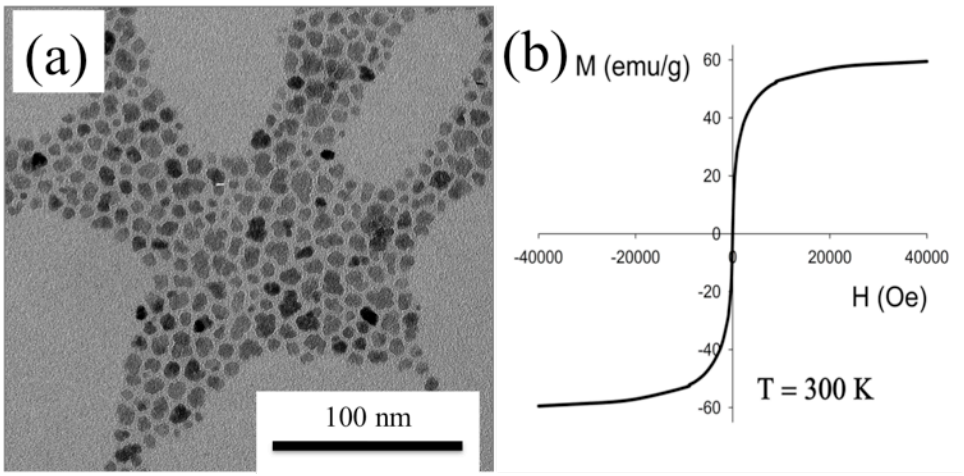

Figure 4.1 (a) Transmission Electron Microscopy (TEM) image of oleic acid protected FeCo MNPs, and b) magnetization curve of FeCo MNPs at room temperature.

Monodisperse FeCo MNPs capped with oleic acid were synthesized using previously reported procedures.[165, 166] Briefly, surfactants were used to surround the iron and cobalt salts resulted in the formation of the initial monomers. When the supersaturated monomers were heated, they became a nucleation site for particle growth. Once cooled, the nanoparticles were able to be dispersed in a non-polar solvent such as hexane due to the hydrocarbon tail of the oleic acid cap. The size of FeCo magnetic nanoparticles was found to be 9.1 ± 2.3 nm in diameter (Figure 4.1a). In order to determine the magnetic behavior of FeCo MNPs, the magnetic hysteresis loops were performed at room temperature (T = 300 K) using a superconduction quantum interference device (SQUID). The FeCo MNPs were found to be superparamagnetic with zero coercivity. The saturated magnetization value of FeCo MNPs at room temperature was appropriately 59 emu g^{-1} (Figure 4.1b), which was similar to previously reported value.[165] As seen in Figure 4.2, the X-ray photoelectron spectroscopy (XPS) analysis of MNPs was shown in -1, indicating the present of Fe (727 eV) and cobalt (787 eV). The FeCo MNPs were able to be separated from hexane with an external magnetic field.

Following removal of the magnetic field, the particles were able to be redisbursed with mild agitation.

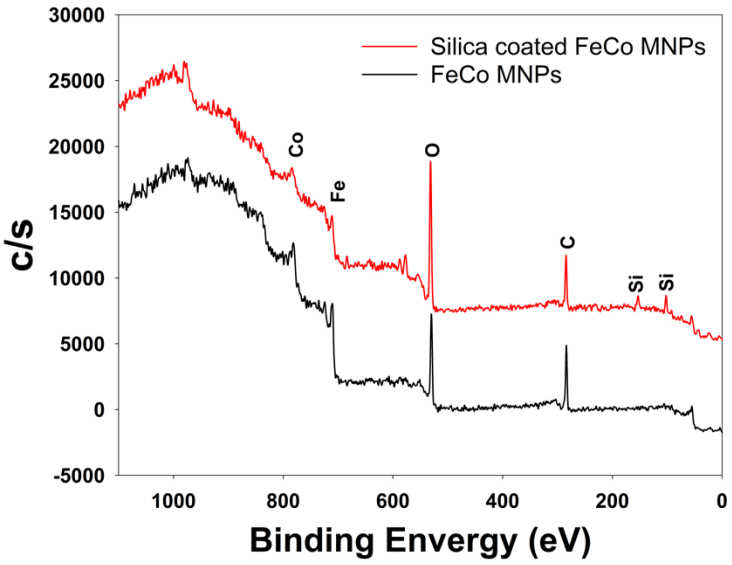

Figure 4.2 The XPS spectra of FeCo MNPs (black line) and silica coated FeCo MNPs (red line).

4.3.2 Immobilization of Streptavidin on FeCo MNPs

The steps to immobilize streptavidin on FeCo MNPs are shown in Figure 4.3a. In order to protect the mental core from the sample matrix, the FeCo MNPs were first coated with a silica shell[170] which also served as a more suitable and convenient functionalizable surface. In this study, we prepared the silica-coated FeCo MNPs using a reverse microemulsion in cyclohexane. A non-ionic surfactant (Igepal® CO-520) was used to suspend the oleic acid-covered FeCo MNPs in aqueous $NH_3 \cdot H_2O$. The surfactant allowed the formation of a water layer on the nanoparticles for hydrolysis of TEOS. The optimal ratio of Igepal® CO-520 to $NH_3 \cdot H_2O$ minimized the number of micelles which contained multiple FeCo nanoparticles in the core. The thickness of silica shell has previously been reported to be tunable from 2 nm to 100 nm.[171] The thickness of silica

layers on FeCo MNPs which were used for this study was 9.0 ± 1.8 nm (Figure 4.3b). The present of silica shell was also confirmed using XPS analysis (Figure 4.2). The TEM image of streptavidin coated on FeCo MNPs is shown in Figure 4.3c. A thin layer of streptavidin can be identified on the surface of the MNPs.

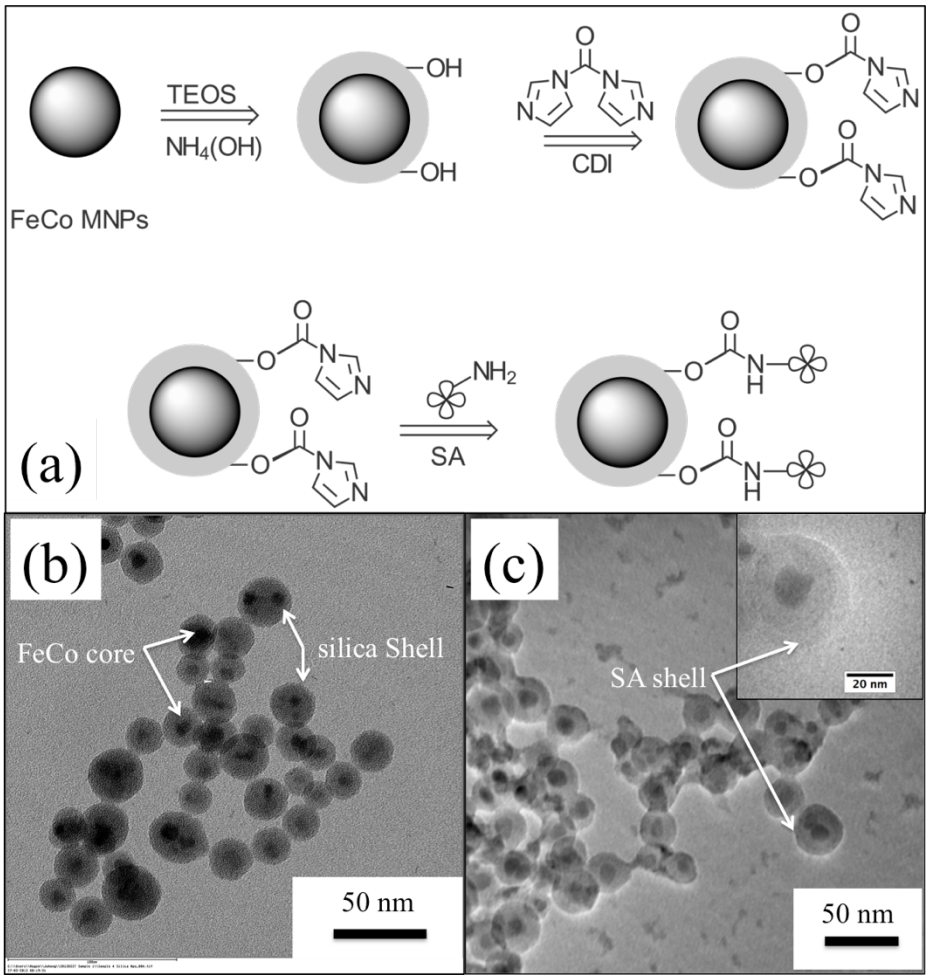

Figure 4.3 Functionalization magnetic nanoparticles. (A) A silica shell was synthesized from tetraethylorthosilicate (TEOS) which was then functionalized with streptavidin (SA) using carbonyldiimidazole (CDI). (b) Transmission electron micrographs of silica-coated FeCo MNPs. c) TEM images of streptavidin coated on MNPs (insets: streptavidin coated on MNPs at high magnification).

This silica layer has the following advantages: 1) it allows convenient conjugation chemistries; 2) it provides a separation of the magnetic cores and reduces aggregation and 3) it decreases non-specific absorption of biological species.[172]

A common method used to immobilize proteins on the surface of nanoparticles is by covalent attachment using 3-aminopropyltriethoxysilane (APTES) and glutaraldehyde.[173] However, Gopinath et al. compared several methods of surface modification and concluded that *N, N'*-Carbonyldiimidazole (CDI) provided an improved direct immobilization of molecules without an intermediate chemical linker.[174] The method used to immobilize streptavidin on silica-coated FeCo MNPs in this study was shown in Figure 4.3a. The CDI was used to activate the silanol group on the surface of silica shell promoting conjugation to a primary amine on the streptavidin protein.

4.3.3 Determination of Biotin Binding Capacity of Nanoparticles

In this study, these nanoparticles were functionalized with streptavidin for the attachment of a biorecognition element (phages or antibodies). In order to fully cover nanoparticles with phages and antibodies, the biotin binding capacities on these nanoparticles were determined. Therefore, the total concentration of biorecognition elements was comparable across all treatments. A colorimetric measurement was performed to determine the biotin binding capacity of streptavidin on the nanoparticle. A solution of *d*-biotin *p*-nitrophenyl ester (BNPE) was reacted with nanoparticle solutions of varying immobilized streptavidin in the biotin binding sites. Following incubation, the magnetic nanoparticles were washed three times to remove unbound NBPE. In the present of NaOH, the bound BNPE was hydrolyzed to produce *p*-nitryl phenol (yellow), which was quantified at 400 nm (Figure 4.4a).[175] The absorbance values of nanoparticles were compared to a standard curve ($R^2 = 0.998$) of *p*-nitryl phenol (Figure 4.4b). Finally, the biotin binding capacity of streptavidin on magnetic nanoparticles was calculated using equation 1:

$$c = \frac{cV}{MW \times m} \times 10^9 \qquad (1)$$

In the above equation, C (nmol mg^{-1}) refers to the biotin binding capacity of streptavidin-coated magnetic nanoparticles, c was the concentration of *p*-nitryl phenol (mg mL^{-1}), V is the volume of hydrolyzed supernatant solution, MW is the molecule weight of *p*-nitryl phenol (g mol^{-1}) and m is the weight of streptavidin-coated magnetic nanoparticles.[175] The biotin binding capacity of streptavidin-coated nanoparticles is 166.95 ± 12.87 nmol mg^{-1}. This represented approximately 8×10^3 biotin binding sites per nanoparticle.

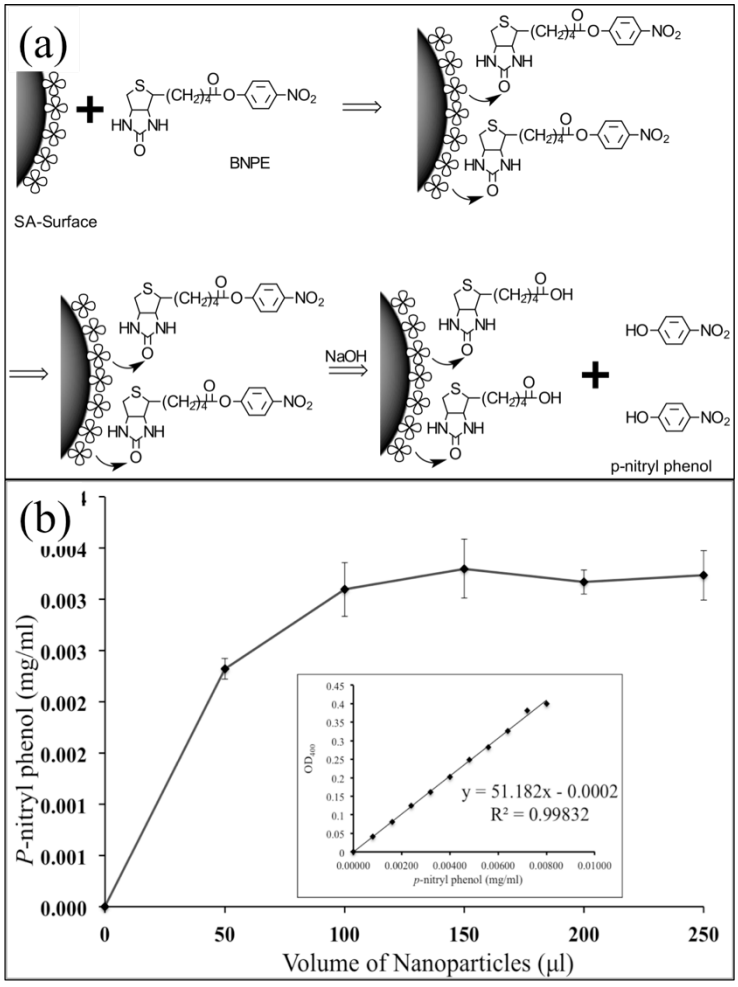

Figure 4.4 (a) Schematic showing the mechanism to measure the biotin binding capacity and (b) biotin binding capacity of streptavidin-coated nanoparticles.

4.3.5 Biofunctionalization of Nanoparticles with Phages or Antibodies

In this study, antibodies modified with biotin were conjugated to streptavidin-coated magnetic nanoparticles. The TEM image of negative uranyl acetate stained biotin-modified T7 phage without nanoparticles was shown in Figure 4.5a. Similarly, T7 bacteriophages, which were genetically engineered to express biotin on the capsid[176] was able to directly bind with streptavidin magnetic nanoparticles (Figure 4.5b). Following standardization of the biotin binding capacity of nanoparticles, the number of phages conjugated on nanoparticles was enumerated following standard plaque assay procedure, resulting in $(1.50 \pm 0.53) \times 10^{10}$ PFU mg^{-1}. Based on eleven TEM images, the phage-MNPs complex was counted and one phage per magnetic nanoparticle accounted for 74% of all phage-MNPs complexes. Phages bounded with two or three nanoparticles were also found (Figure 4.5b).

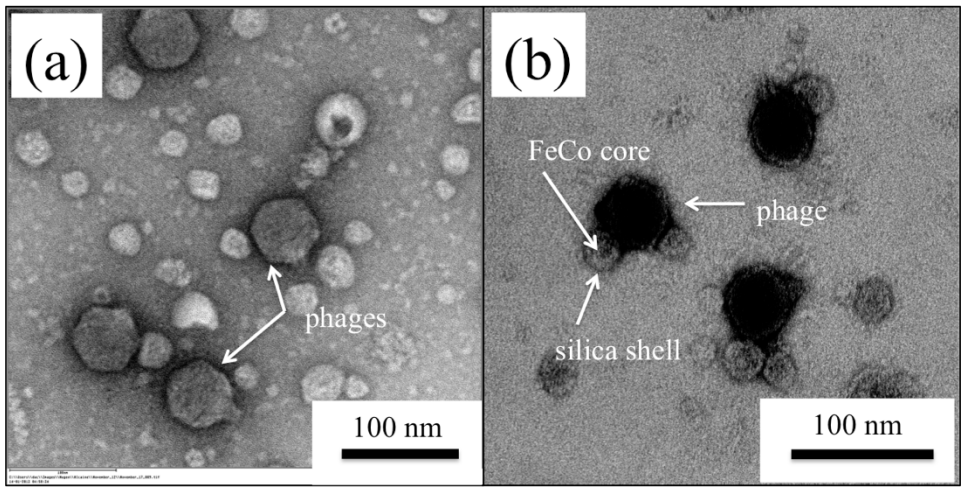

Figure 4.5 TEM images of (a) negative uranyl acetate staining of biotin T7 phage and (b) positive uranyl acetate staining of biotin T7 phage attached to streptavidin-coated FeCo MNPs.

4.3.6 Comparison of the Capture Efficiency between Antibody and Phage-Conjugated magnetic Nanoprobes

Typical IMS beads conjugated to antibodies for specific bacteria are commercially available from several companies.[130, 131] By using nano-scale particles, the capture efficiency is increased. When used to capture E. coli O157:H7 in ground beef, a capture efficiency of over 90% was achieved.[35] Similar results were found by Pappert *et al.* who calculated a 96 ± 6% capture efficiency of *E. coli* from a 10^6 CFU ml^{-1} culture.[36] In this study, the two magnetic nanoprobes (T7 phages and antibodies on magnetic nanoparticles) were used to separate *E. coli* K12 (range: 10^2 to 10^7 CFU mL^{-1}) from 1 mL sample solution. Nanoparticles utilizing an antibody capture were incubated with the bacteria using standard protocols of 30 minutes with mild agitation. A shortened binding time was required for the T7 phages containing particles as 30 minutes could have resulted in lysis of bacteria. Therefore, the phage nanoparticles were incubated for only 15 minutes prior to magnetic separation. Following hybridization, all nanoparticle variants were rapidly separated using an external magnet (Figure 4.6). The capture efficiency was calculated using the equations 2 and 3:

$$CE1(\%) = (1 - \frac{N_a}{N_o}) \times 100\% \quad (2)$$

$$CE2(\%) = \frac{N_b}{N_o} \times 100\% \quad (3)$$

Where, N_o is the total number of *E. coli* K12 cells present in the initial sample (CFU), N_a is the number of *E. coli* K12 cells which remained unbound to the particles (CFU), N_b is the number of *E. coli* K12 cells bound to the particles (CFU).[35] Due to aggregation of the separated nanoparticle/bacteria complex, quantification using standard

plating methods made CE_2 (Equation 3) unreliable. This phenomenon has previously been reported with the magnetic separation of *E. coli*.[35, 156] Therefore, the capture efficiency was reported using CE_1 (Equation 2).

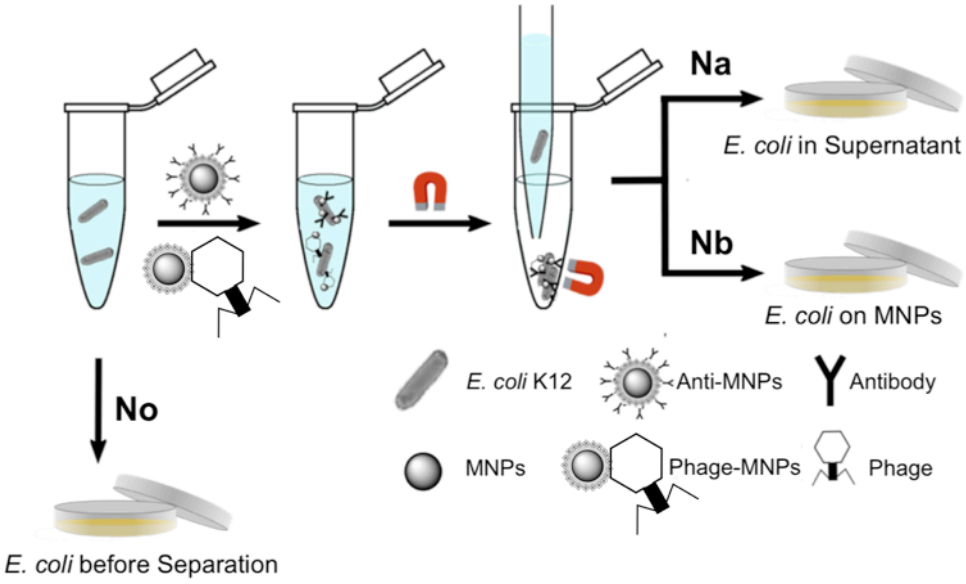

Figure 4.6 Magnetic separation of bound bacteria on the magnetic nanoprobes from unbound bacteria in the supernatant (not drawn to scale).

The separated nanoparticles and bacteria were imaged using transmission electron microscopy (TEM) (Figure 4.7a,b). The capture efficiency (CE_1) of the two magnetic nanoprobes can be seen in Figure 4.7c. In order to determine the specific bind between the nanoprobes and *E. coli* cell, the negative control result of streptavidin coated MNPs was shown (Figure 4.7c). A similar capture efficiency between phage and antibody magnetic nanoprobes was obtained, indicating that phages produced easily and at low cost can replaced the commonly used antibodies for bacteria separation at nanoscale size.

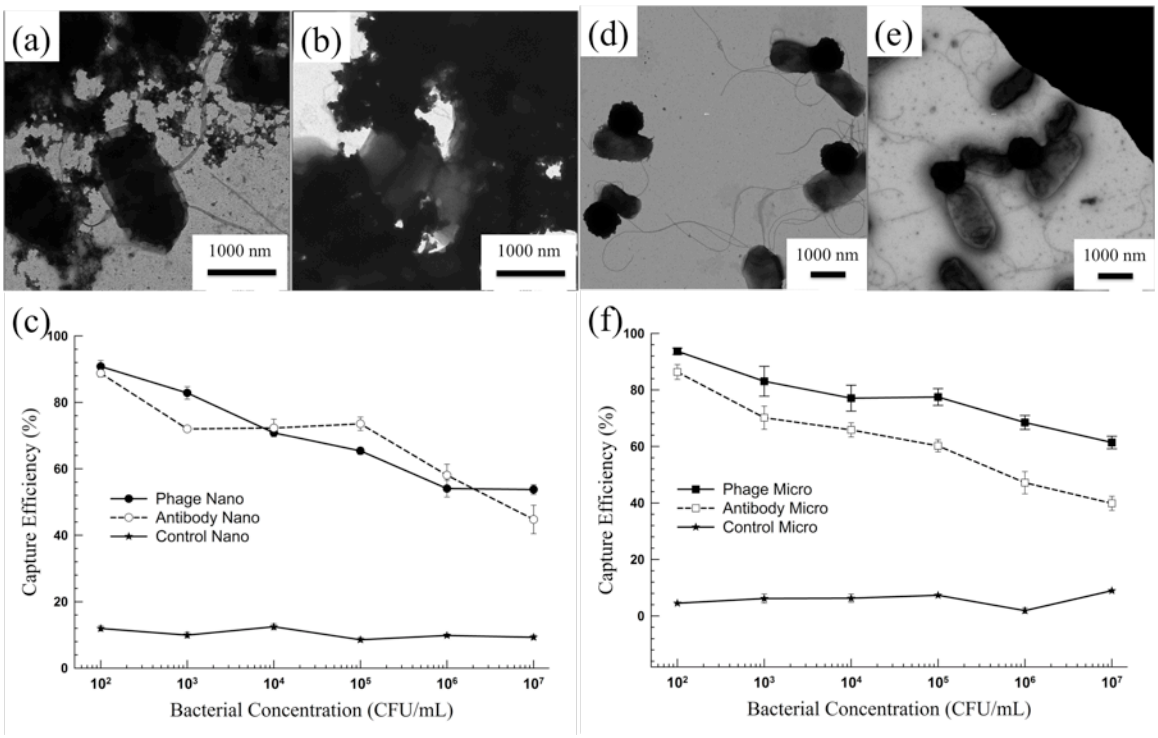

Figure 4.7 TEM images of nanoprobes bound to *E. coli* K12: a) antibody-conjugated nanoparticles, b) phage-conjugated nanoparticles, e) antibody-conjugated microbeads and f) phage-conjugated microbeads, (c) and (f) comparison the capture efficiency between the two magnetic nanoprobes: phage magnetic nanoprobes (solid round line) and antibody magnetic nanoprobes (hollow round line), and phage magnetic microprobes (solid square line) and antibody magnetic microprobes (hollow square line).

In order to further confirm that phages can be used as biorecognition elements for bacteria separation instead of antibodies, magnetic beads at microscale size was measured. The commercial streptavidin-coated magnetic microbeads modified with phages and antibodies were used to separate *E. coli* K12. Firstly, the biotin binding capacity of streptavidin-coated magnetic microbeads was measured using above-mentioned method and 306.54 ± 26.04 nmol mg^{-1}. In order to equal the biotin binding capacity at micro and nanoscale size, the amount of streptavidin-coated microbeads was normalized. Next, phages and antibodies were immobilized on these microbeads for bacterial separation. The TEM images of microbeads and bacteria were shown in Figure 4.7d,e. Compared with antibody magnetic microprobe, phage magnetic microprobe

resulted in a higher capture efficiency (Figure 4.7f). Among all magnetic probes, the lowest capture efficiency was the current standard for IMS which used antibodies on microbeads. Phage-conjugated magnetic probe showed a promising tool for bacteria separation.

4.4 Conclusions

We have developed nanoscale T7 bacteriophage magnetic nanoprobes for the low-cost and efficient separation of bacteria from liquid sample. The capture efficiency at all bacterial concentrations (10^2-10^7 CFU mL^{-1}) was not significantly different between the bacteriophage magnetic nanoparticles and antibody magnetic nanoparticle while using only half the incubation time for phage magnetic probes. Compared with traditional filtration, the key feature using magnetic nanoparticles modified as biorecognize elements is that they can specifically concentrate and separate target bacteria cell. It should also be noted that the application of phages as a detection nanoprobes provides many advantages over other molecular probes due to their relative ease of production, host specificity, ability to distinguish between viable and non-viable cells, and potential for rapid bacteria detection. Additionally, phages are highly stable to temperature, pH variations, organic solvents and degradation by proteases.[177]

While most detection devices require small and relatively clean samples, many sample matrices such as food, soil and feces are inherently complex and contain inhibitors for downstream analytical tools such as PCR. In these cases, a sample preparation step becomes a necessary tool for reliable testing. Additionally, many organisms such as *Listeria monocytogenes*, *Salmonella* spp. and *E. coli* O157:H7 have a zero tolerance in food thus requiring the ability to detect a single organism in a 25 gram

sample. While typical protocols require an enrichment step to grow the organisms, this process takes hours to days and is therefore not suitable to all sample types such as fresh produce. Bacteriophages on magnetic nanoparticles represents an improved separation/concentration tool as compared to the current molecular biology standard, IMS.

In order to eliminate the infectivity of toxicity of bacteriophage for bacteria separation, further studies will focus on conjugating ghost phage (able to bind, but not infect) on nanoparticles to better quantification of the separation ability for target bacterial detection.[178] This will allow a fast and low-cost method to isolate and detect bacteria. Additionally, the separated bacteria would also undergo a natural lysis as part of the infection. This can allow access to the DNA for applications such as QPCR and therefore allow the determination of only viable organisms as infection would not occur in nonviable bacteria.

CHAPTER 5

COLORIMETRIC DETECTION OF *ESCHERICHIA COLI* BASED ON THE ENZYME-INDUCED METALLIZATION OF GOLD NANORODS

5.1 Introduction

Due to their low infectious dose, bacterial infectious diseases result in approximately one third of all global deaths.[7, 107] Accurate and early detection of bacterial pathogens can lead to immediate and effective treatment, which can prevent or curtail foodborne and waterborne pathogen outbreaks.[16] However, many of the current gold-standard methods to identify pathogenic bacteria require at least 18 hours from sample to results.[18] This creates an urgent need to develop rapid and reliable methods to detect bacteria in environmental, food, and water matrices. These methods are also necessary in resource-limited settings.[6, 130, 141, 179] A colorimetric assay that does not rely upon advanced instruments and skilled operators is the most promising method for rapid detection of bacterial pathogens. Furthermore, colorimetric methods linked to enzymatic reactions have been widely accepted for their practicality and simplicity.[16, 105, 180] Enzyme-induced colorimetric detection of bacteria is based on monitoring and measuring a color change resulting from enzymatic activity via a biochemical reaction of corresponding substrates.[105, 180, 181] Unfortunately, the enzyme-induced colorimetric detection do not have sensitive color change, and therefor can only serve as a rough estimation.[182] Hence, a novel enzyme-induced colorimetric assay with high-sensitive color change is of great significance.

Recently, plasmonic noble metal (gold and silver) nanomaterials-enabled colorimetric detection strategies have attracted a wide attention due to their rapid, sensitive, and

unique optical properties.[31, 183, 184] Interparticle crosslinking or destabilized aggregation of plasmonic metal nanoparticles has been reported to detect DNA, cancer cells, heavy metal ions, and bacterial cells.[31, 184] Compared with the similarly sized gold spherical nanoparticles, the gold nanorods (AuNRs) have been reported to perform better due to an inherently higher sensitivity to local dielectric environment.[28, 29] AuNRs have two localized surface plasmon resonance (LSPR) peaks: the transverse LSPR peak and the longitudinal LSPR peak. The transverse LSPR band locates around 520 nm, and the longitudinal absorption band locates from visible to near-infrared (NIR) absorption band depending on the aspect ratio (AP, length divided by width) of AuNRs.[180, 185-188] The longitudinal LSRP peak shifts to shorter wavelength (blue shift) with the increasing of AP.[189] It has been demonstrated that depositing silver shell on the surface of AuNRs can change the AP of AuNRs, resulting in distinctive multicolor change.[186, 190] The changes in color have been successfully utilized in an investigation into the affects of time and temperature on food freshness.[186] Until now, this technique has not been applied to the detection of bacteria in clinic or food samples.

In this work, we utilized enzyme-induced silver metallization on the surface of AuNRs for both high-resolution colorimetric monitoring and measurement of beta-galactosidase (β-gal) activity. The sensing scheme of our proposed method incorporates β-gal for hydrolyzation of substrates into weak reduction agents, which can reduce silver ions to generate a silver shell on the surface of AuNRs. The decrease of AP resulted in the blue shift of the longitudinal LSPR peak of AuNRs and an obvious color change from light green to orange-red. This proposed method was employed to detect *Escherichia coli* (*E. coli*) in aqueous solutions using β-galactosidase activity as a direct readout for *E.*

coli concentrations. The bacterial cells were infected with T7 bacteriophages (phages) in order to release *β*-gal for enzyme-induced colorimetric detection. A phage-based system was advantageous compared to an antibody-based platform because of their specificity for target bacterial cells, their ability to distinguish between live and dead cells, and their low cost.[64, 69, 71, 96] The released *β*-gal induces a metallic silver deposition on the surface of AuNRs. *β*-Gal activity and the blue shift of the longitudinal LSPR peak was directly relative to the concentration of target *E. coli* cells. This enzyme-induced metallization colorimetric assay has the potential to be built into point-of-care devices for detection of bacterial concentration in low-resource settings.

5.2 Experimental Section

5.2.1 Chemicals and Materials

Cetyltrimethylammonium bromide (CTAB), chlroauric acid trihydrate ($HAuCl_4$), L-ascorbic acid (AA), poly (4-styrenesulfonic acid) (PSS), *β*-galactosidase (*β*-gal), *p*-aminophenyl *β*-D-galactopyranoside (PAPG), α-chymotrypsin (ChT), glucose oxidase (GOx), alkaline phosphatase (PhosB), lipase (Lip), myoglobin (Mayo), and bovine serum albumin (BSA) were purchased Sigma Aldrich (Saint Louis, MO). Silver nitrate (AgNO3) was purchased from Acros Organics (Morris Plains, NJ). Sodium borohydride ($NaBH_4$), hydrochloric acid (HCl), O-nitrophenyl-*β*-galactoside (ONPG) sodium chloride (NaCl), potassium phosphate monobasic, sodium phosphate dibasic, agar, tryptone, and yeast extract were purchased from Fisher Scientific (Fair Lawn, NJ). All chemical were used as received. Mill-Q (MQ) water with 18.2 MΩ·cm at 25 °C was used throughout the all experiments.

5.2.2 Synthesis and Coating of AuNRs.

The AuNRs stabilized with CTAB were synthesized using the seed-mediated growth method.[180, 186, 187] For seed solution, $HAuCl_4$ solution (0.25 ml, 0.01 M) was added into CTAB solution (9.75 mL, 0.1 M) under magnetic stirring. The freshly prepared ice-cold $NaBH_4$ solution (0.6 mL, 0.01 M) was then added quickly. The solution was aged for 2 hours at 30 °C before use. The growth solution was prepared by mixing $HAuCl_4$ solution (2.0 mL, 0.01 M), $AgNO_3$ solution (0.4 mL, 0.01 M), HCl solution (0.8 mL, 0.1 M), and CTAB solution (40 mL, 0.1 M). AA solution (0.32 mL, 0.1M) was then added to reduce the gold salt. The seed solution (200 μL) was added until the growth solution became colorless. To grow the AuNRs, the mixture solution was kept at 30 °C overnight. The AuNRs were collected and washed by centrifugation (1000 ×g, 20 minutes) and redispersion in Mill-Q water twice. PSS (0.5 mL, 10 mg mL^{-1}) in NaCl solution (5 mL, 10 mM) was added and incubated for 30 minutes in room temperature. Excess CTAB and PSS were removed by centrifuging twice at 1000 ×g for 20 minutes. Finally, the AuNRs with transverse and longitudinal plasmon bands at 510 and 885 nm were suspended into Mill-Q water. The AuNRs solution was diluted with an expected absorbance intensity of approriately1.000 at 858 nm.

5.2.3 AuNRs-Based Colorimetric Monitoring of β–gal Concentration

Different concentrations of *β*-gal solution (25 μL) were added into PAPG solution (25 μL, 1.2 mM) in centrifuge tubes, respectively. The mixture solutions were gently agitated and incubated at 37 °C for 30 minutes. The enzymatic hydrolyses (50 μL) were added into detection solutions, which consisted of AuNRs solution (100 μL, $Ab_{885\ nm}$ = 1.0), $AgNO_3$ solution (10 μL, 10 mM), and PB (100 μL, 10 mM, pH 7.4). The absorbance

spectra of the resulting solutions (200 μL) were recorded using UV-vis spectrophotometry with a wavelength range of 300-940 nm. The specificity to detect *β*-gal was investigated using competing proteins (ChT, GOx, PhosB, Lip, Mayo, and BSA).

5.2.4 Bacterial Culture and Bacteriphage

The *E. coli* BL21 and T7 phage were used in this study. A single colony of *E. coli* was selected and added into lysogeny broth (LB) and grown overnight at 37 °C under 200 rpm agitation. The *E. coli* stock was prepared by centrifugation at 6000 ×g for 2 minutes and resuspended in PB (10 mM, pH 7.4). The process was repeated for a total of three times. The concentration of *E. coli* cells was enumerated on a LB agar plate to confirm the visible counts ($CFU \cdot mL^{-1}$). The preparation and tittering of T7 phages were reported by our previous publications.[40, 96]

5.2.5 Detection of *E. coli* Using AuNR-Based Colorimetric Assay

The *E. coli* stock was serially diluted into varying concentrations using PB. Each concentration (25 μL) was added into sterile centrifuge tube containing PAPG solution (25 μL, 12 mM), phage solution (50 μL, appropriately 4.4×10^7 $PFU \cdot mL^{-1}$), and PB (150 μL, 10 mM). In order to allow the phage infection and enzymatic reaction, the mixtures were gently agitated and incubated at 37 °C for 2 hours. The enzymatic hydrolyses (50 μL) were added into detection solutions consisting of AuNRs solution (100 μL, $Ab_{885\ nm}$ = 1.0), $AgNO_3$ solution (10 μL, 10 mM), and PB (100 μL, 10 mM). Finally, each produced color solution (200 μL) was measured using UV-vis spectrophotometry from 300 to 940 nm.

5.3 Results and Discussion

5.3.1 Sensing Mechanism of Enzyme-Induced Colorimetric Assay

The principle of the AuNR-based colorimetric assay using enzyme-induced metallization is shown in Figure 5.1. In the absence of *β*-gal, the unhydrolyzed PAPG cannot reduce silver ions to metal silver. The color of the solution remains the color of AuNRs (light pink color). When *β*-gal is present, it converts PAPG into a reducing agent PAP, which in turn reduces silver ions. In the presence of AuNRs, the reduced metal silver coats the surface of AuNRs, resulting in different colors of the detection solution. The color of detection solution varies from light green to orange-red according to the *β*-gal concentration.

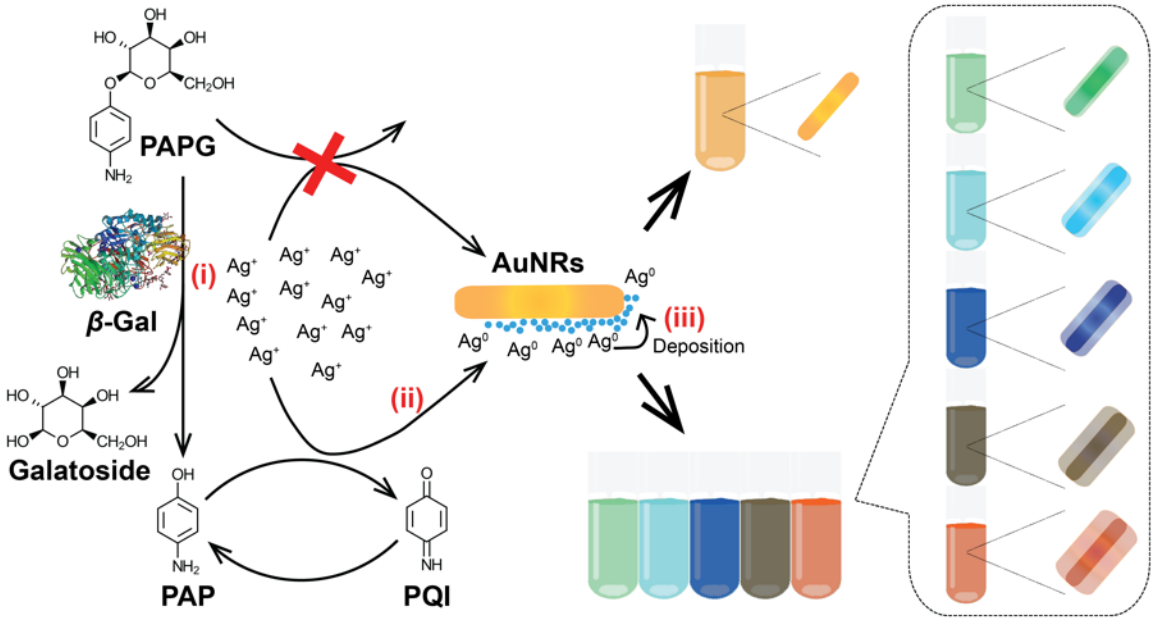

Figure 5.1 Sensing mechanism of enzyme-induced AuNR-based colorimetric assay for the monitoring and measuring of *β*-gal concentration. Three steps were involved: (i) *β*-gal converted PAPG into PAP serving as weak reducing agent, (ii) PAP reduced silver ions to metallic silver, and (iii) the AuNRs were coated with metallic silver, resulting in various colorful detection solutions.

5.3.2 Characteristics and Control Experiments for Enzyme-Induced Colorimetric Assay

AuNR synthesis using different ARs with seed-mediated growth has been reported previously. [185, 191] In this study, AuNRs with an AR of appropriately 5.1 were used for colorimetric detection. The as-synthesized AuNRs had a length of 59.7 ± 8.3 nm and a width of 11.7 ± 1.4 nm. The AuNRs were coated with cetyltrimethylammonium bromide (CTAB), which positively charges them. This resulted in colloidal stability, prevented aggregation, and therefore, the AuNRs were well suspended in the Mill-Q water using CTAB as surfactant.[192] The absorbance spectrum of AuNRs-CTAB shows transverse and longitudinal plasmon bands at 510 and 885 nm, respectively (Figure 5.2). However, AuNRs coated with CTAB were not stable in alkaline solution (pH > 7) due to the weak protection of CTAB.[192] In phosphate butter (PB, pH 7.4), which is preferred in biosensing applications and enzymatic reaction[107, 193, 194], the change in the absorbance spectrum of AuNR-CTAB indicated that the AuNRs were aggregating (Figure 5.2). Although increasing the CTAB concentration was helpful for AuNR stability in PB, excess CTAB also inhibited downstream reactions. In order to stabilize the AuNRs in PB, AuNRs-CTAB were coated with poly (4-styrenesulfonic acid) (PSS).[195] The strong electrostatic attractive interaction between the positively-charged CTAB and negatively-charged PSS allowed the formation of double-layer coating.[196] The absorbance spectra of AuNRs-PSS in Mill-Q water and PB are shown in Figure 5.2. Compared with AuNRs-CTAB in Mill-Q water, the transverse and longitudinal plasmon bands with a slight shift were observed. After adding β-gal into the PAPG, $AgNO_3$, and AuNRs solution, the color change of solution was caused by the deposition of metal silver on the surface of AuNRs.

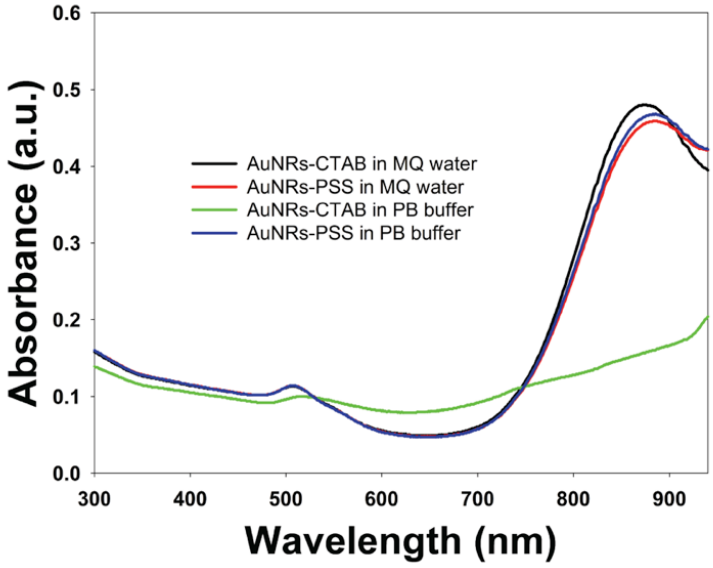

Figure 5.2 The UV-vis absorbance spectra of the AuNRs-CTAB in MQ water (black), AuNRs-PSS in MQ water (red), AuNRs-CTAB in PB (green), and AuNRs-PSS in PB (blue).

In order to confirm the presence of a silver shell on the surface of AuNRs, the morphology of the AuNRs before and after enzyme-induced metallization was characterized using transmission electron microscopy (TEM). The resulting TEM images and energy-dispersive X-ray (EDX) elemental mapping images of AuNRs were shown in Figure 5.3a, b. Previous studies have reported that the metal silver were preferably deposited on the transverse direction (body side) of AuNRs.[186, 197] In our study, the silver shell on the body sides of AuNRs was observed in Figure 5.3b. The deposition of Ag shell on the surface of AuNRs was further investigated using HRTEM-EDX. In Figure 5.3a,b, the corresponding EDX Ag (red color) and Au (green color) mapping images confirmed also the coating of metal silver on the surface of AuNRs.

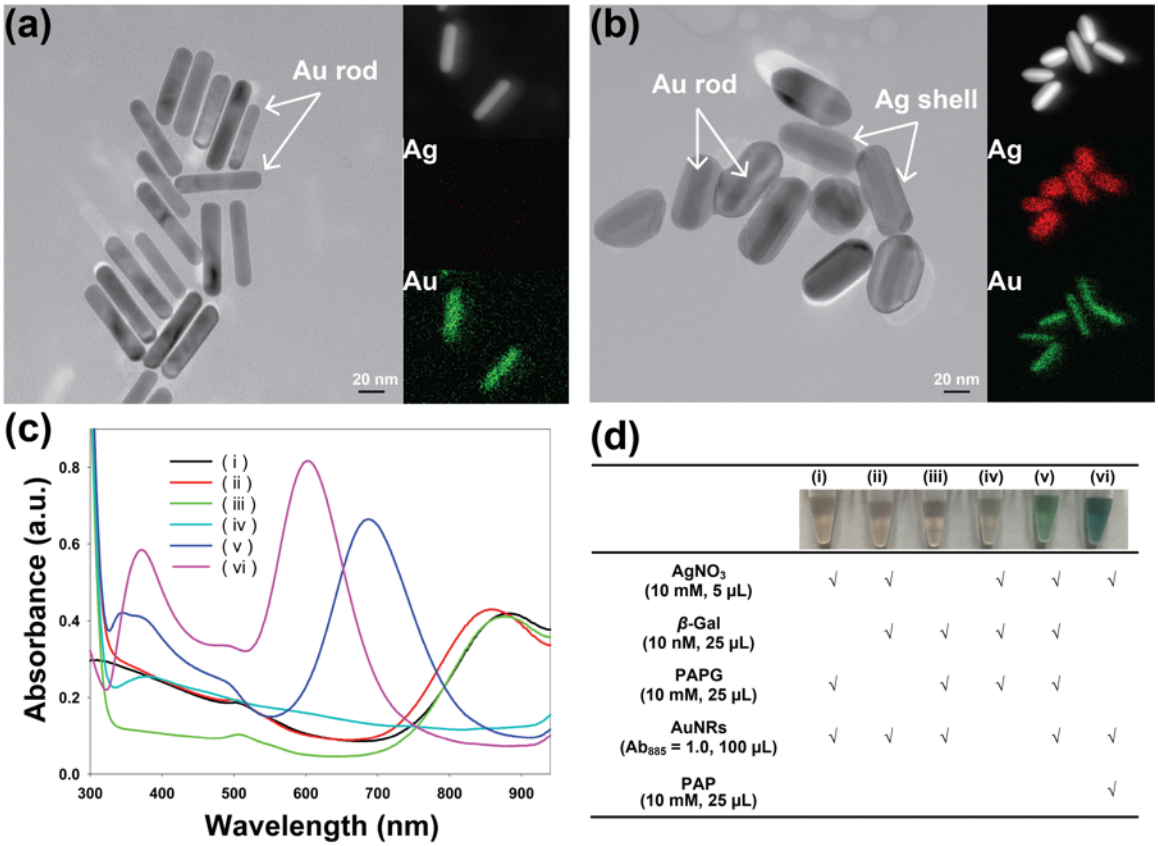

Figure 5.3 TEM images of AuNRs (a) before and (b) after silver deposition (their corresponding EDX elemental mapping images of silver and gold were displayed on the right of their TEM images). Control experiments of the enzyme-inducted metallization colorimetric detection. (c) UV-vis absorption spectra and (d) table of reagents added to each tube of (i) $AgNO_3$ + PAPG + AuNRs, (ii) $AgNO_3$ + β-gal + AuNRs, (iii) β-gal + PAPG + AuNRs, (iv) $AgNO_3$ + β-gal + PAPG, (v) $AgNO_3$ + β-gal + PAPG + AuNRs, and (vi) $AgNO_3$ + AuNRs + PAP.

Because the silver preferably deposited on the transverse direction of the AuNRs rather than the longitudinal direction, it resulted in the decrease of the AR of the nanorod structure. The lower AR the AuNR has, the greater blue shift of the longitudinal LSPR peak is observed in the absorbance spectrum. Moreover, compared with Au nanocrystals of the same shape and size, Ag nanocrystals showed a shorter plasmon resonance.[182, 186] Therefore, the enhanced absorbance intensity and blue shift of the longitudinal LSPR

peak were observed after enzyme-induced Ag metallization on the surface of AuNRs (Figure 5.3c).

This sensing procedure was further tested with the following control experiments: (i) $AgNO_3$ + PAPG +AuNRs, (ii) $AgNO_3$ + β-gal + AuNRs, (iii) β-gal + PAPG +AuNRs, (iv) $AgNO_3$ + β-gal + PAPG, (v) $AgNO_3$ + β-gal + PAPG +AuNRs, and (vi) $AgNO_3$ + AuNRs + PAP. The absorbance spectra of control experiments were shown in Figure 5.3c. The blue shift of the longitudinal LSPR peak occurred in the presence of $AgNO_3$, β-gal, PAPG, and AuNRs. In the absence of β-gal and PAPG, enzymatic hydrolysis (PAP) caused a similar blue shift of the longitudinal LSPR peak, indicating that β-gal and PAPG solutions were key for the reduction of silver ions to form silver shell on the surface of AuNRs. Meanwhile, the color changes of AuNR solutions were observed (Figure 5.3d). These results demonstrated that our design has the ability to specifically detect β-gal concentration.

5.3.3 Optimization of Experimental Conditions for Silver Deposition Reaction

It is clear that β-gal hydrolyzed PAPG to generate PAP, which can reduce silver ions and generate Ag shell on the surface of AuNRs. The change in morphology of AuNRs resulted in the blue shift of the longitudinal LSPR peak and color change of detection solution. Therefore, the concentration of Ag ions and reaction conditions for enzymatic hydrolysis needed to be optimized for improved Ag deposition on the AuNR surface. Based on manufacturer suggestions, the enzymatic reaction was performed at 37 °C. At this temperature, additional reaction parameters including $AgNO_3$ concentration, PAPG concentration, PB concentration, and pH were optimized for further experiments. The blue shift of the longitudinal LSPR peak ($\Delta\lambda_{max}$) was selected as standard for the

performance of silver deposition reaction. First of all, the silver ions concentration was optimized. A high concentration of silver ions can accelerate the reduction reaction, resulting in a thicker Ag shell on the surface of AuNRs (Figure 5.4a). However, high Ag deposits on the AuNRs bodies caused loss of overall nanorod structure, indicating that the AR of AuNRs was close to zero. In the absorbance spectrum, the longitudinal LSPR peak of AuNRs disappeared and a strong plasmon resonance wavelength of silver nanocrystals was observed (Figure 5.4b). Therefore $AgNO_3$ concentration at 10 mM was selected as optimal for silver reduction reaction.

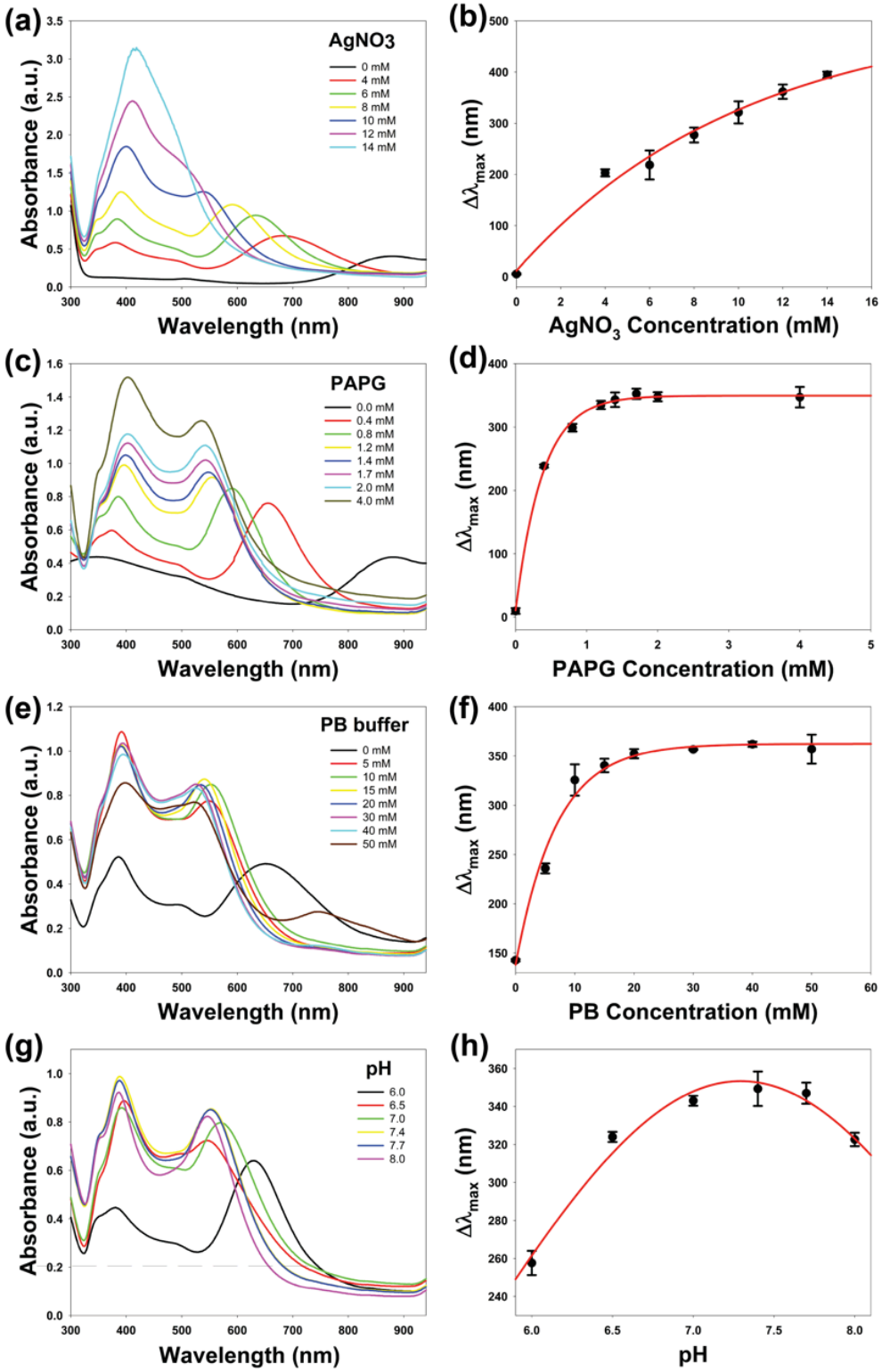

Figure 5.4 The experimental conditions for silver deposition reaction. The effects of silver-depositing AuNRs (a-b) $AgNO_3$ concentration, (c-d) PAPG concentration, (e-f) PB concentration, and (g-h) pH. Error bars represent the standard deviation of three replicates.

Higher PAPG concentration could increase their hydrolysis opportunity by *β*-gal, increasing the blue shift of the longitudinal LSPR peak of AuNRs. The absorbance spectra of varying PAPG concentrations is shown in Figure 5.4d with blue shift of the longitudinal LSPR peak plotted against the PAPG concentration in Figure 5.4c. The blue shift of the longitudinal LSPR peak increased with the increasing of PAPG concentration and stabilized at a concentration of 1.2 mM. Therefore a PAPG concentration of 1.2 mM was adopted for following reactions.

In order to optimize the PB solution for this procedure, varying PB concentrations and pH were studied. A higher base concentration in PB can tolerant the change after adding enzymatic substrate and AuNRs solutions. As shown in Figure 5.4e, the blue shift of the longitudinal LSPR peak tended to level off after a PB concentration of 10 mM, which was selected for the development of the colorimetric detection. The pH of the buffer also influenced the enzyme-induced silver deposition reaction greatly due to optimal pH for enzymatic reaction. As shown in Figure 5.4g, the blue shift in the longitudinal LSPR peak of AuNRs initially increased with the increasing of pH, and then decreased after pH of 7.4. Due to these data, a detection solution consisting of 10 mM $AgNO_3$ and 1.2 mM PAPG in 10 mM PB (pH 7.4) was selected for further colorimetric experiments.

5.3.4 Analytical Performance for Colorimetric Detection of β-gal Concentration

Using the aforementioned optimal conditions, varying concentrations of *β*-gal were used to evaluate the sensitivity and dynamic range of the enzyme-induced metallization colorimetric assay. First, the *β*-gal solutions were incubated with PAPG solution to produce reducing reagent PAP. After incubation for 30 minutes, the

hydrolyzed PAP was added into the detection solution to reduce silver ions. We used the absorbance spectra to monitor the change of AuNRs in varying *β*-gal concentrations (Figure 5.5a). The longitudinal LSPR peak shifted from 885 nm to 520 nm, and the absorbance intensity of longitudinal LSPR peak increased with the increasing of *β*-gal concentrations. The blue shift of the longitudinal LSPR peak ($\Delta\lambda_{max}$) was plotted against the *β*-gal concentration. As shown in Figure 5.5b, the $\Delta\lambda_{max}$ increased with the increasing of *β*-gal concentration, and a dynamic relationship between $\Delta\lambda_{max}$ and *β*-gal concentration in a range from 0.1 nM to 10 nM was observed. The limit of detection (LOD) of 0.128 nM was calculated using $3\sigma_{control}$/slope, where $\sigma_{control}$ was the standard deviation of control samples, and the slope was from the linear range. As shown in Figure 5.5c, the detection solutions exhibited colors from light green to orange-red as compared to the control. The distinct multicolor changes can be easily identified visually or with a reader.[127, 198]

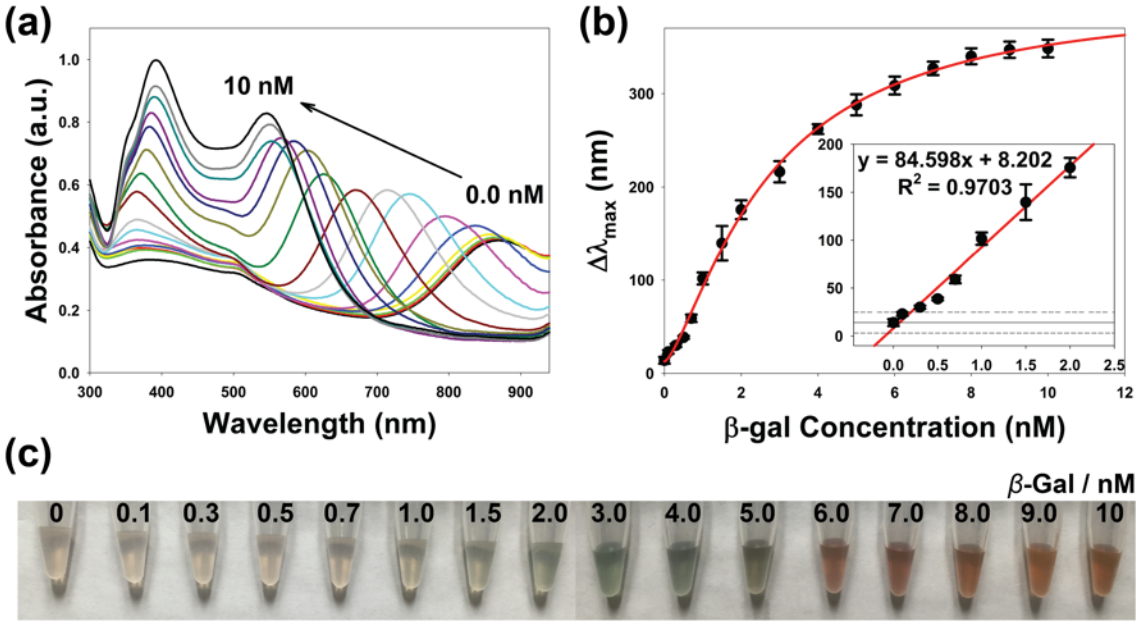

Figure 5.5 The colorimetric detection of *β*-gal concentration using enzyme-induced metallization of gold nanorods. (a) UV-vis absorption spectra, (b) the blue shift in the longitudinal LSPR peak (insert: linear range, the solid and dash lines indicates the average and ± 3 standard deviation of $\Delta\lambda_{max}$ of control samples), and (c) photographs of colorimetric assay toward various concentrations of *β*-gal.

For comparison, conventional colorimetric assay for the detection of *β*-gal concentration using ONPG as enzymatic substrate was performed. As shown in Figure 5.6a, the absorbance spectra of detection solutions indicated the absorbance wavelength at 405 nm had the maximum absorbance intensity ($A_{405\ nm}$). The absorbance at 405 nm versus *β*-gal concentration with ONPG as enzymatic substrate was plotted in Figure 5.6b. It was clearly observed that the absorbance intensity increased with the increasing of *β*-gal concentration and leveled off after the *β*-gal concentration of 2 mM. The dynamic range of conventional colorimetric method was from 0.1 nM to 0.2 nM, which was narrower than that of our present colorimetric assay. Additionally, the limit of detection calculated using $3\sigma_{control}$/slope was 0.163 nM, which was also higher than that of our present colorimetric method. For the conventional method, the color change of the detection solution was from colorless to yellow (Figure 5.6c), which is difficult to

identify without machine assistance. In summary, these results indicated that the ability to monitor and measure *β*-gal activity was improved in limit of detection, dynamic range, and colorimetric output using our present assay.

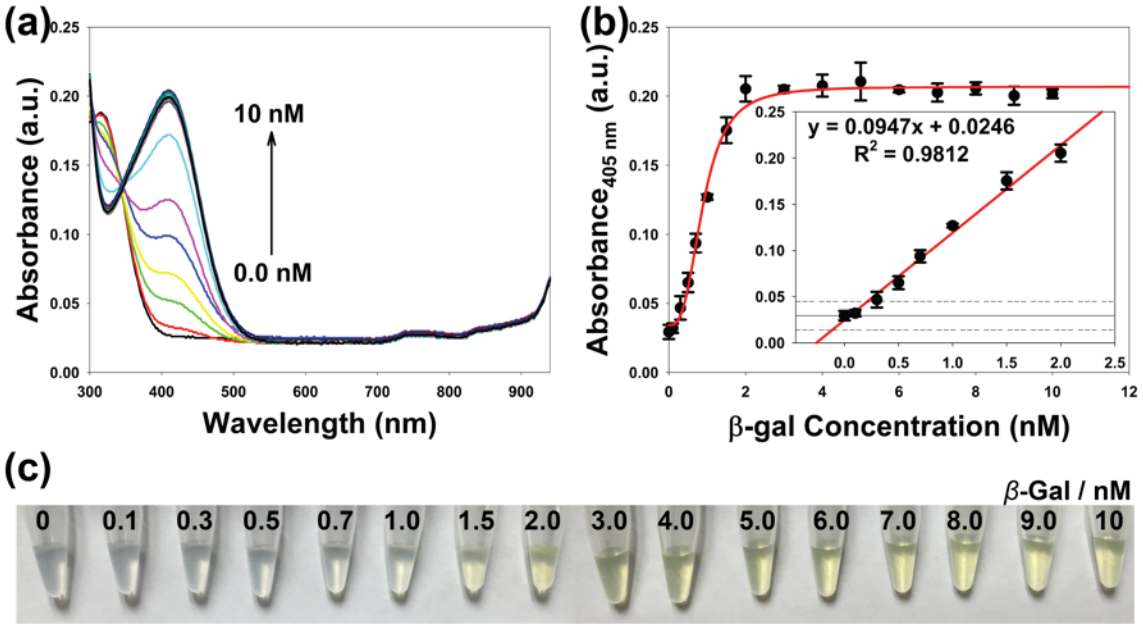

Figure 5.6 The colorimetric detection of *β*-gal concentration using the ONPG-based conventional colorimetric method. (a) UV-vis absorption spectra, (b) the absorbance intensity at the wavelength of 405 nm (insert: linear range, the solid and dash lines indicates the average and ± 3 standard deviation of absorbance intensity of control samples), and (c) photographs of colorimetric assay toward various concentrations of *β*-gal.

In order to evaluate the specificity of our present AuNR-based colorimetric assay for *β*-gal detection, control experiments were conducted using competing proteins [5 nM], including, α-chymotrypsin (ChT), glucose oxidase (GOx), alkaline phosphatase (PhosB), lipase (Lip), myoglobin (Mayo), and bovine serum albumin (BSA). As shown in Figure 5.7a, an obvious blue shift of the longitudinal LSPR peak in the absorbance spectra was observed only in the presence of *β*-gal, and the $\Delta\lambda_{max}$ of competing proteins was also plotted (Figure 5.7b). In contrast to solutions with *β*-gal, we did not observe a change in color in the control experiments, (Figure 5.7b). Thus, these results revealed that

our present enzyme-induced silver metallization on the surface of AuNRs assay had specifically detects β-gal activity.

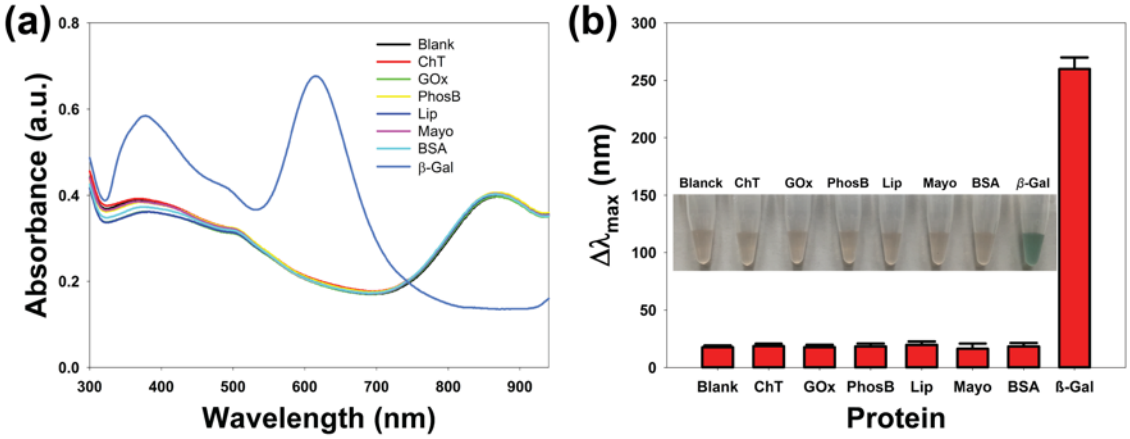

Figure 5.7 The specificity of this proposed method for β-gal against common competing proteins (5 nM): ChT, GOx, PhosB, Lip, Mayo, and BSA. (a) UV-vis absorption spectra of the colorimetric assay toward various protein competitors. (b) The blue shift in the longitudinal LSPR peak of the specificity of β-gal against various protein competitors (insert: the corresponding photographs). Error bars represent the standard deviation of three replicates.

5.3.5 Application for AuNR-Based Colorimetric Detection of E. coli

We tested whether our present enzyme-induced metallization colorimetric assay could be used to detect E. coli cells. β-gal was an essential enzyme in the inducible lactose transport and metabolism system of E. coli, and was used as indicator for their presence.[81-83, 125, 199] Because phages can distinguish between live and inactive bacteria, their use as detection probes avoids false-positive results.[69] As shown in Figure 5.8a, the detection process can be divided into two steps: (i) phage infects the target bacterial cells, resulting in the release of β-gal into the sample solution, and (ii) determination of the released β-gal concentration from bacterial cells was determined using our present colorimetric assays. As a result, the bacterial concentration can be determined using UV-vis absorbance spectra, or conveniently by the naked eyes.

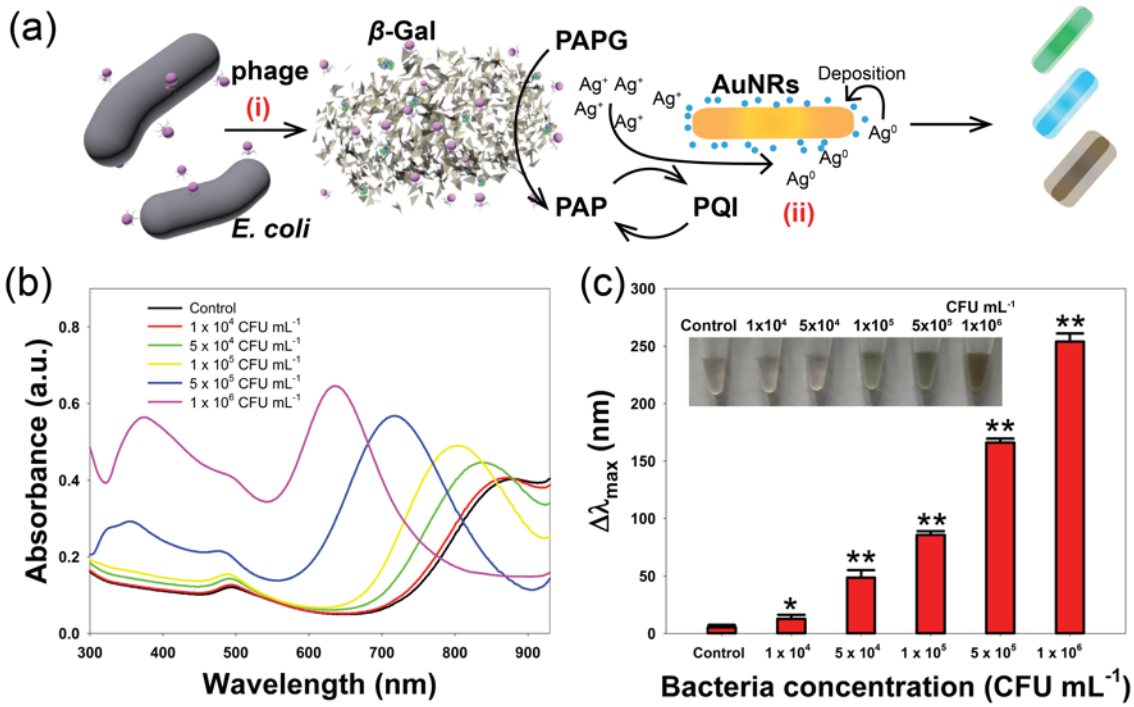

Figure 5.8 (a) Schematic illustration of the enzyme-induced metallization colorimetric assay for the detection of *E. coli* cells: (i) phage infection of *E. coli* cells to release *β*-gal, and (ii) the signal generation based on enzyme-induced silver metallization on the surface of AuNRs. (b) UV-vis absorption spectra of the colorimetric assay toward various *E. coli* BL21 concentrations. (c) The blue shift in the longitudinal LSPR peak towards various *E. coli* BL21 concentrations (insert: the corresponding photographs). Error bars represent the standard deviation of three replicates. Significant values (t-test) were marked by an asterisk (*, $0.01 < p < 0.05$) and two asterisks (**, $p < 0.01$), respectively.

E. coli BL21 was chosen as model analyte and bacteriophage T7 as the infecting phage as published previously.[200] This AuNR-based colorimetric assay combined the advantage of phage-based detection can specifically detection viable *E. coli* cells. As shown in Figure 5.8b, the different blue shifts of the longitudinal LSPR peak were observed. The $\Delta\lambda_{max}$ of different bacterial concentrations were also plotted in Figure 5.8c, revealing that we could reproducibly detect 1×10^4 colony forming units (CFU) mL^{-1} ($p < 0.05$). The photography showed that the color of the detection solution turned from light red to green to pale (Figure 5.8c, insert). In our previous study, the specificity to detect *E. coli* using T7 phage-based method had been reported.[200] Thus, These results

demonstrated that our present colorimetric assay could successfully detect bacterial concentrations.

5.4 Conclusions

In summary, a simple and rapid enzyme-induced metallization colorimetric assay has been successfully employed to monitor and measure *β*-gal activity. Compared with conventional ONPG-based colorimetric assay, our proposed method had lower detection limit (0.128 nM) and board dynamic range (0.1-10 nM) for the detection of *β*-gal concentration. This system also provided a rapid and distinctive colorimetric readout to detect the *β*-gal concentration using bare-eyes. Furthermore, we combined this assay with phage lysis to improve the detection of *E. coli* cells. The proposed technology has the ability to be fabricated into inexpensive, portable, friendly-to-user, and disposable devices, providing a tremendous benefit to their respective industries, especially if used in resource-limited settings.

CHAPTER 6

$T7_{LACZ}$ ENGINEERED BACTERIOPHAGE FOR SIMPLE COLORIMETRIC DETECTION OF VIABLE *ESCHERICHIA COLI*

6.1 Introduction

Bacterial infections remain a critical burden on human health in both developing and developed countries, and are globally responsible for the tens of 10 million deaths[201, 202]. With the increasing prevalence of antibiotic resistance bacteria, these infections further exacerbate the economic and public health costs of treatment[203, 204]. Traditional bacterial detection methods, such as plate counting, can take at least 18 hours after the samples are received to provide results. To ascertain whether an isolate is resistant to a given antibiotic, can take even longer. To meet the growing demand for sensitive and rapid bacteria detection, numerous advanced technologies have been developed to detect bacteria, including polymerase chain reaction (PCR), surface-enhanced Raman scattering (SERS), and surface plasmon resonance (SPR)[16, 205-207]. Although sensitive and accurate, the above-mentioned methods are expensive, require skilled operators, and are unsuitable for use in low-resource settings. Thus, there remains an urgent need to develop innovative, inexpensive, sensitive, and rapid methods for *in-situ* detection of bacteria.

Bacteriophage (phage) is a virus, which can infect specific host bacterial cells. Phage-based amplification assays for bacteria detection have been widely used for food safety, environmental monitor, and clinical diagnosis[70, 71]. Unfortunately, these traditional assays are complicated and the long detection time makes their utilization problematic for rapid detection of pathogenic bacteria. Advances in molecular genetic technologies have provided researchers with new tools to improve upon current phage-based schemes,

allowing for sensitive and rapid bacteria detection using engineered phage. A number of reporter genes, such as green fluorescent protein, tobacco etch virus protease, alkaline phosphatase, and firefly luciferase, have been inserted into phage genomes and subsequently used as reporters to improve bacteria detection[72, 93, 208].

Beta-galactosidase (*β*-gal), encoded by *lacZ* operon, is commonly used as an indicator for the detection of *E. coli* cells in drinking water[81, 83, 115]. Phages have been incorporated into some of these schemes as lytic agents to break the host cell's membrane and release *β*-gal for colorimetric, electrochemical, and bioluminescent detection of *E. coli* cells[81, 83, 125]. The sensitivity of these schemes leaves room for improvement. In our study, in order to improve detection limit of *E. coli* cells via *β*-gal activity, we have engineered T7 phage to carry *lacZ* gene linked to the T7 promoter to induce *β*-gal overexpression during the phage infection cycle. Our strategy for *E. coli* detection is shown in Figure 6.1. After our engineered $T7_{lacZ}$ phages attach to host *E. coli* cell and inject its genome containing our T7 promoter-linked *lacZ* gene into host *E. coli* cell, then *lacZ* transcription will be driven by T7 polymerase and translated into *β*-gal by the bacterial ribosome. At the time of phage-induced lysis, both native and overexpressed *β*-gal will be released into environmental media. Now free from the cell, the released enzyme can catalyze a colorimetric substrate, like chlorophenol red-*β*-D-galactopyranoside (CPRG), to provide a visual signal from yellow to red.

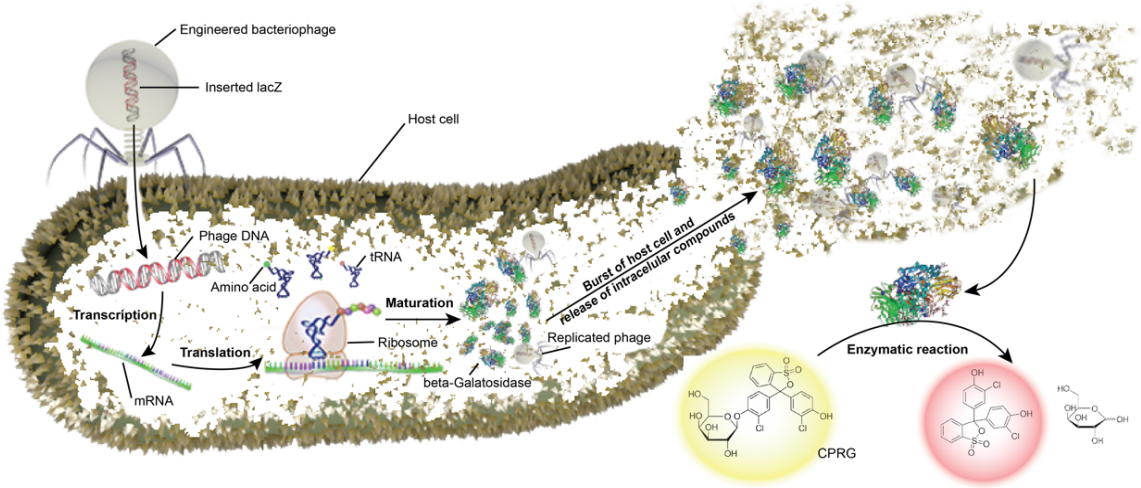

Figure 6.1 1Schematic illustration of E. coli detection using enzymatically active β-galactosidase-overexpressed via engineered bacteriophage. Initial infection of E. coli cells results in rapid propagation of phages and overexpression of β-gal. Upon phage-induced cell lysis, both phages and β-gal are released, leading to subsequent infections and catalysis of chlorophenol red-β-D-galactopyranoside to produce a colorimetric signal.

6.2 Experimental Section

6.2.1 Bacterial strains, bacteriophage, and chemicals

E. coli BL21, *E. coli* BLT5403, and bacteriophage T7Select415-1 were purchased from EMD Millipore (Billerica, MA). The pUC57 plasmid containing *lacZ* operon was synthesized by GenScript (Piscataway, NJ). Phusion PCR kit and restriction enzyme (EcoRI and HindIII) were purchased from New England Biolabs (Ipswich, MA). T4 DNA ligase was purchased from Promega (Madison, WI). The kits for purification of PCR product and restriction digests were purchased from Qiagen (Valencia, CA). Chlorophenol red-*β*-D-galactopyranoside (CPRG) was purchased from Roche Diagnostics (Indianapolis, IN). All other chemicals were purchased from Fisher Scientific (Fair Lawn, NJ).

6.2.2 Construction and purification of engineered bacteriophage

Phage T7Select415-1 kit was used to create $T7_{lacZ}$ phage carrying *lacZ* gene with standard molecular techniques. During phage infection, the engineered $T7_{lacZ}$ phage can overexpress intracellular *β*-gal. The *lacZ* gene, 3075 base pairs in size, was synthesized within pUC57 plasmid. Phusion PCR kit was used to amplify our designed construct. The PCR product was then purified and digested by EcoRI and HindIII. T4 ligase was used to insert our digested construct to T7Select 415 genome vector arms. $T7_{lacZ}$ phage was obtained by packing of the modified *lacZ*-carrying $T7_{lacZ}$ genome using T7Select packing kit. In order to confirm *β*-gal overexpression by $T7_{lacZ}$ phage performance, the *S·Tag* was used to replace our *lacZ* inserted construct to create a control phage ($T7_{control}$), which could not express intracellular *β*-gal during phage infection. The resulting engineered $T7_{lacZ}$ and $T7_{control}$ phages were propagated on *E. coli* BL21 and plated. The isolated plaques were checked for the appropriate size insert using Phusion PCR kit with T7Select Up and Down primers.

Prior to be used for phage-based bacterial detection, $T7_{lacZ}$ and $T7_{control}$ phages were amplified within *E. coli* BL21 and purified. Overnight cultures of *E. coli* BL21 (150 μL) were added into sterile flasks containing LB broth (35 mL) and incubated at 37 C until an OD_{600} of 0.6 was reached. Then a plug of $T7_{lacZ}$ and $T7_{control}$ phage from the confirmed plaques were used to inoculate these cultures, respectively. The flasks were incubated with shaking at 37 °C until lysis (the cultures became clear). Lysed cultures were centrifuged at 7000x g for 10 minutes, and the supernatants were then filtered using 0.2 μm filters. The purified solutions were centrifuged at 35,000x g for 2 hours. Finally, the pellets were resuspended into PBS buffer (4 mL) and stored at 4 °C for subsequent

experiments. The phage titer (PFU mL^{-1}) was enumerated following standard plaque assays.

6.2.3 Bacteria culture

The *E. coli* BL21 was streaked on a LB agar plate. After overnight growth at 37 °C, a single colony was used to inoculate a sterile flask containing 35 mL LB broth, which was then incubated overnight at 37 °C with 200 rpm agitation. The bacteria cells were then centrifuged at 6000x g for 2 minutes and resuspended in PBS buffer. The washing steps were repeated three times. Finally, the optical intensity of cell pellet in PBS buffer was measured and adjusted to 1.0 (~10^8 CFU mL^{-1}) to create a stock solution. Desired bacterial concentrations were obtained by serially dilution of this bacterial stock solution and stored for further use at 4 °C. Bacteria concentration were also confirmed by plating on LB agar plates at time of use.

6.2.4 Comparison of one-step *E. coli* detection using $T7_{lacZ}$ and $T7_{control}$ phage

The activity of β-gal expressed by $T7_{lacZ}$ and $T7_{control}$ phage was investigated using CPRG as colorimetric substrate. The serial dilutions of bacterial stock (25 µL) were added into a sterile centrifuge tubes containing LB broth (190 µL), CPRG solution (10 µL, 24 mM), and engineered phage solution (25 µL, appropriately 10^5 PFU·mL^{-1}). These mixture solutions were incubated for 7 hours at 37 °C with 200 rpm agitation. The absorbance intensity of each solution (200 µL) was measured every one hour using UV-vis spectrophotometer at the wavelength range of 500-650 nm.

6.2.5 Two-step detection of *E. coli* cells using $T7_{lacZ}$ phage

The impact of a preenrichment step on assay sensitivity and detection time was investigated. Bacterial solutions (100 µL) at the concentration of 10^4, 10^3, and 10^2

CFU·mL^{-1} were added to LB broth (760 μL) at 37 °C with 200 rpm agitation. PBS buffer without bacteria cells was used as control. After various hours (1-6 hours) of preenrichment, CPRG solution (40 μL, 24 mM) and engineered phage solution (100 μL, appropriately 10^5 PFU·mL^{-1}) were added into these solutions. The absorbance intensity of each solution (200 μL) was recorded every one hour using UV-vis spectrophotometer at the wavelength range of 500-650 nm for a max total assay time of 7 hours.

6.2.6 Sensing of antibiotic drugs

For high-throughput drug sensing, *E. coli* BLT5403 solutions (25 μL, 10^4 CFU·mL^{-1}) were incubated in LB broth (190 μL) containing different antibiotic drugs with varying concentrations (0, 2, 5, 10, 20, 40, 60, and 100 μg·mL^{-1}) for 3 hours at 37 °C with 200 rpm agitation. CPRG solution (10 μL, 24 mM) and T7$_{lacZ}$ phage solution (25 μL, appropriately 10^5 PFU·mL^{-1}) were then added and incubated for another 2 hours. The solutions were analyzed as above mentioned. The *E. coli* BL21 was used as a control.

6.2.7 Statistical analysis

All data were evaluated for statistically significance using *t*-test and presented as mean ± standard deviation. A star (*) and two (**) indicated that tested set of data had a difference ($0.01 < p < 0.05$) and significant difference ($p < 0.01$) with control set, respectively.

6.3 Results

6.3.1 Construction of enzymatic reporter-produced bacteriophage

We modified T7 bacteriophage, which is an *E. coli*-specific phage and broadly infects *E. coli* strains, to overexpress intracellular *β*-gal during phage infection[209]. This work was achieved by inserting our *lacZ* inserted construct into the T7Select415-1

genome using EcoRI and HindIII restriction enzyme sites (Figure 6.2a-b). In our construction, our *lacZ* gene was preceded by regulator sequences to enable T7 polymerase mediated overexpression, and a ribosome binding site for translation by the bacterial cell (Figure 6.2c). The T7 promoter is a very strong promoter, and is utilized in many gene overexpression schemes. And, a similar overexpression scheme has successfully demonstrated the production of over 200,000 copies of an enzymatic reporter per cell, enabling bacterial detection[93]. Furthermore, as previously described, a stop codon was incorporated upstream of our *β*-gal construct to ensure the enzyme was not fused to capsid in protein when inserted into the T7Select415-1 genome. As a control, T7Select415-1 control DNA, which encodes the *S·Tag*, was inserted into the T7 genome to create $T7_{control}$ phage, which would not express *β*-gal (Figure 6.2d). After propagating our modified phage, lysate were plated and we utilized PCR to select the positive plaques that contained our designed *lacZ* construct and the control DNA.

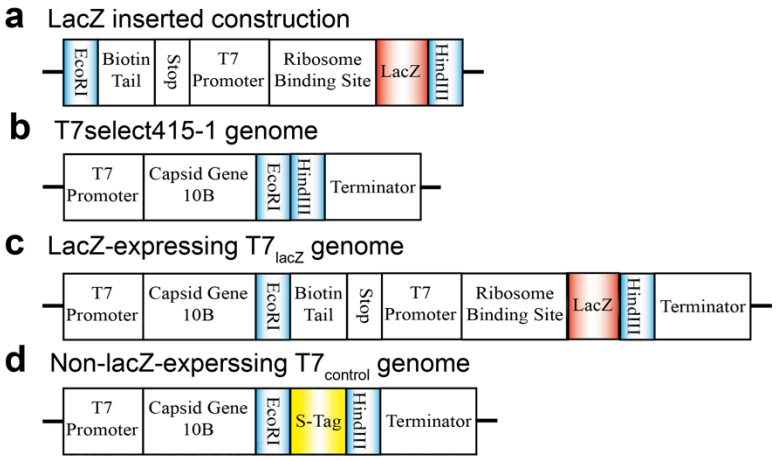

Figure 6.2 Genomes of engineered bacteriophage used for *E. coli* detection. (a) Genome of *lacZ* inserted construction. (b) Genome of T7Select415-1 shows 10B capsid protein and cloning site. (c) Genome of *β*-gal-overexpressing $T7_{lacZ}$ phage created by cloning *lacZ* inserted construction into T7Select415-1 genome. (d) Genome of non-*β*-gal-overexpressing $T7_{control}$ phage created by cloning *S·Tag* into T7Select415-1 genome.

6.3.2 Characterization of enzymatically active engineered bacteriophage

After PCR screening, positive $T7_{lacZ}$ and $T7_{control}$ plaques were re-propagated to investigate the expression of *β*-gal during infection. The enzymatic activity of *β*-gal was monitored using CPRG as colorimetric substrate. We measured the UV-vis absorption spectra of solutions containing *E. coli* BL21, CPRG, and our engineered phage ($T7_{lacZ}$ and $T7_{control}$ phage, respectively) after the incubation of 3 hour (Figure 6.3a). The absorbance intensities at the peak wavelength of 574 nm were plotted towards treatment type (Figure 6.3b). The absorbance intensity of solutions contain cells lysed by our $T7_{lacZ}$ phage was much greater than that of solutions containing cells lysed by our $T7_{control}$ phage, indicating that *β*-gal was overexpressed during $T7_{lacZ}$ phage infection. In order to further confirm that increased absorbance intensity was due to our $T7_{lacZ}$ phage infection, more control tests were studied, including *E. coli* BL21 + $T7_{lacZ}$, CPRG + $T7_{lacZ}$, *E. coli* BL21 + CPRG, $T7_{lacZ}$, CPRG, and *E. coli* BL21. None of these controls results in absorbance intensity equivalent to our *E. coli* BL21 + CPRG + $T7_{lacZ}$, further supporting that the observed increase in absorbance intensity was due to our $T7_{lacZ}$ phage infection. Photographs of detection solution from different treatment types are shown in Figure 6.3b and the red color was observed only in the present of *E. coli* BL21 + CPRG + $T7_{lacZ}$.

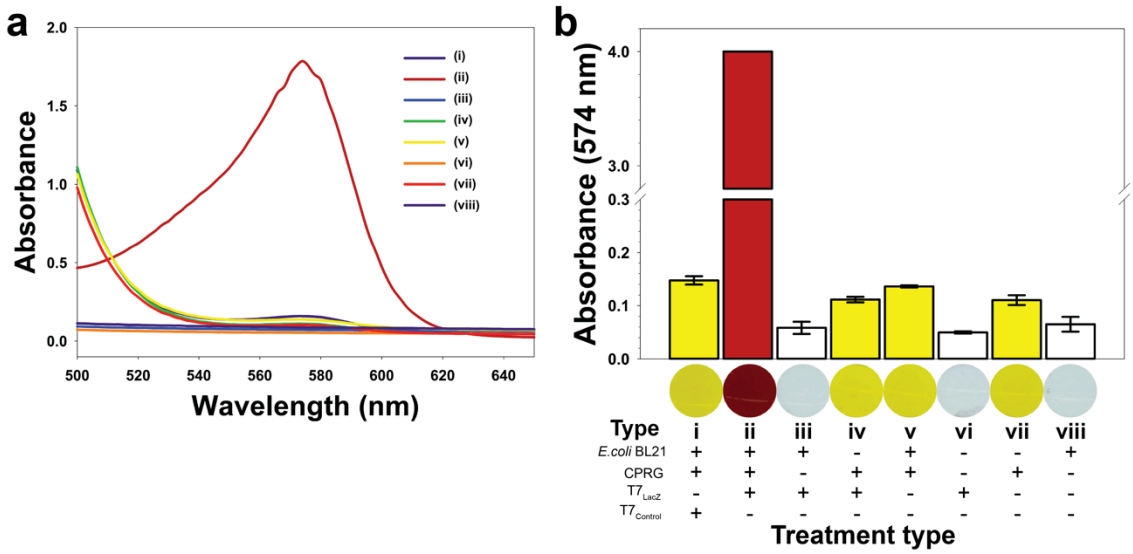

Figure 6.3 Comparison of overexpressed *β*-gal activity with different treatment types. (a) UV-vis absorption spectra of different treatment types and (b) plot of absorbance intensities (574 nm) towards different treatment types of (i) *E. coli* BL21 + CPRG + $T7_{control}$, (ii) *E. coli* BL21 + CPRG + $T7_{lacZ}$, (iii) *E. coli* BL21 + $T7_{lacZ}$, (iv) CPRG + $T7_{lacZ}$, (v) *E. coli* BL21 + CPRG, (vi) $T7_{lacZ}$, (vii) CPRG, and (viii) *E. coli* BL21. (Error bars represent one standard deviation of three independent experiments)

6.3.3 One-step detection of *E. coli* cells using engineered $T7_{lacZ}$ and $T7_{control}$ bacteriophage

We next sought to investigate the ability of our colorimetric scheme to detect *E. coli* cells using $T7_{lacZ}$ and $T7_{control}$ phage. Varying concentrations (10^1 to 10^7 CFU·mL^{-1}) of *E. coli* BL21 in LB broth were incubated with either $T7_{lacZ}$ or $T7_{control}$ phage (10^5 PFU·mL^{-1}) in the presence of CPRG. LB broth without *E. coli* cells was used as a control. Contour plots of absorbance intensities (574 nm) of the colorimetric response as 2D function of *E. coli* BL21 concentration and total detection time using $T7_{lacZ}$ phage and $T7_{control}$ phage are shown in Figure 6.4a-b. The color transition from yellow to red was scaled using absorbance intensity from 0.0 to 4.0 with an interval of 0.5. As shown, the red color indicates the *E. coli* detectable area incorporating both factors (*E. coli* cell concentration and total detection time). With the increasing of detection time, the

detection limit decreased, reaching a limit of 10^2 CFU·mL^{-1} after 7 hours using T7$_{lacZ}$ phage. In contrast, the *E. coli* detection limit using T7$_{control}$ phage never went below 10^5 CFU·mL^{-1} even after incubation of 4 hours. As shown in Figure 6.4a-b, the large difference in the red area clearly demonstrated the improvement in *E. coli* detection by using T7$_{lacZ}$ phage which induced β-gal overexpression and cell lysis against the T7$_{control}$ phage which only resulted in release of endemic β-gal. The corresponding photographs of the colorimetric response are shown in Figure 6.4c-d, which are consistent with absorbance intensity data.

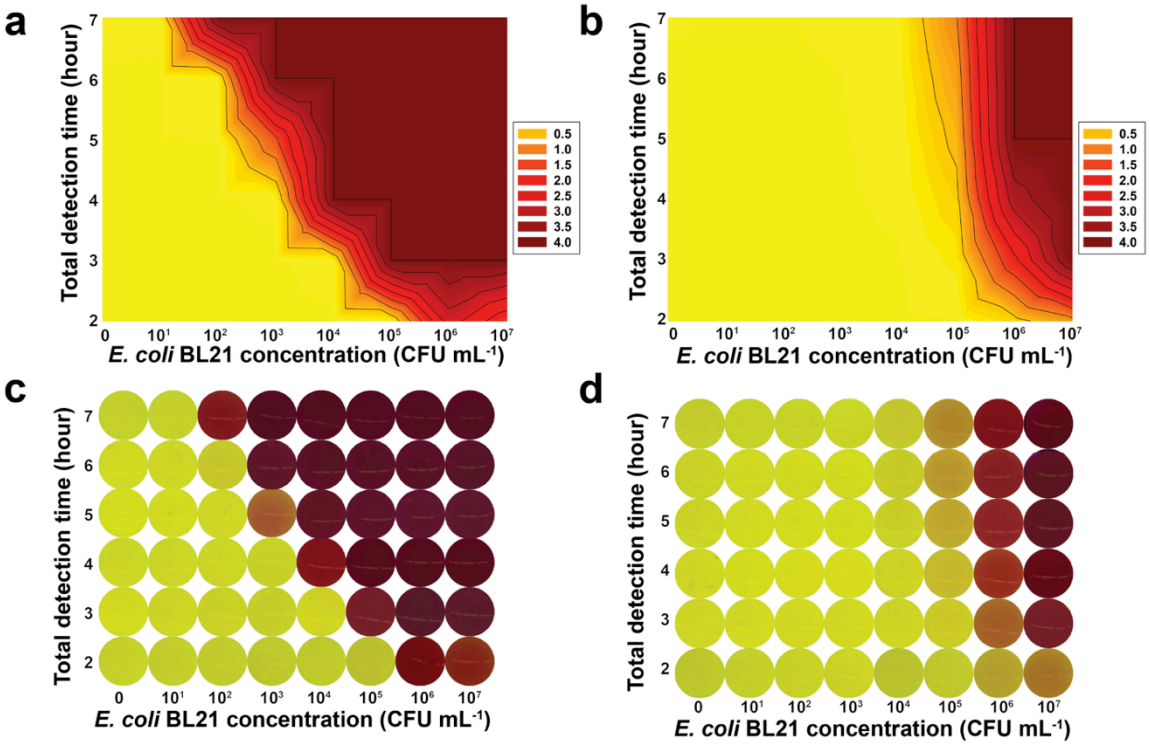

Figure 6.4 Comparison of one-step *E. coli* detection using T7$_{lacZ}$ and T7$_{control}$ engineered bacteriophage. Contour plots of absorbance intensities (574 nm) of colorimetric response as 2D function of *E. coli* BL21 concentration and total detection time using (a) T7$_{lacZ}$ phage and (b) T7$_{control}$ phage. Contour plots of photograph of colorimetric response as 2D function of *E. coli* BL21 concentration and total detection time using (c) T7$_{lacZ}$ phage and (d) T7$_{control}$ phage. (The absorbance intensity data shown here represents the average of three independent experiments)

To further compare the differences in *E. coli* cell detection using $T7_{lacZ}$ and $T7_{control}$ phage, a time course study of bacteria detection can be found in Figure 6.5. Although equivalent *E. coli* cell detection limits were reached using both phages within 3 hours, $T7_{lacZ}$ phage showed a stronger colorimetric response than $T7_{control}$ phage at the same time. After 4 hours, differences became clearer, and a lower limit of detection was obtained using $T7_{lacZ}$ phage. As noted, we were able to detect 10^2 CFU·mL^{-1} after 7 hours using $T7_{lacZ}$ phage, which was driven by phage-overexpressed *β*-gal. Without overexpression of *β*-gal, the endemic enzyme released from *E. coli* cells using $T7_{control}$ phage resulted in a weaker colorimetric response and 100-fold poorer detection limit of 10^4 CFU·mL^{-1} after 7 hours. These results indicated $T7_{lacZ}$ phage, which induces *β*-gal overexpression upon infection, has the potential to improve the sensitivity of *β*-gal-based detection of *E. coli* cells.

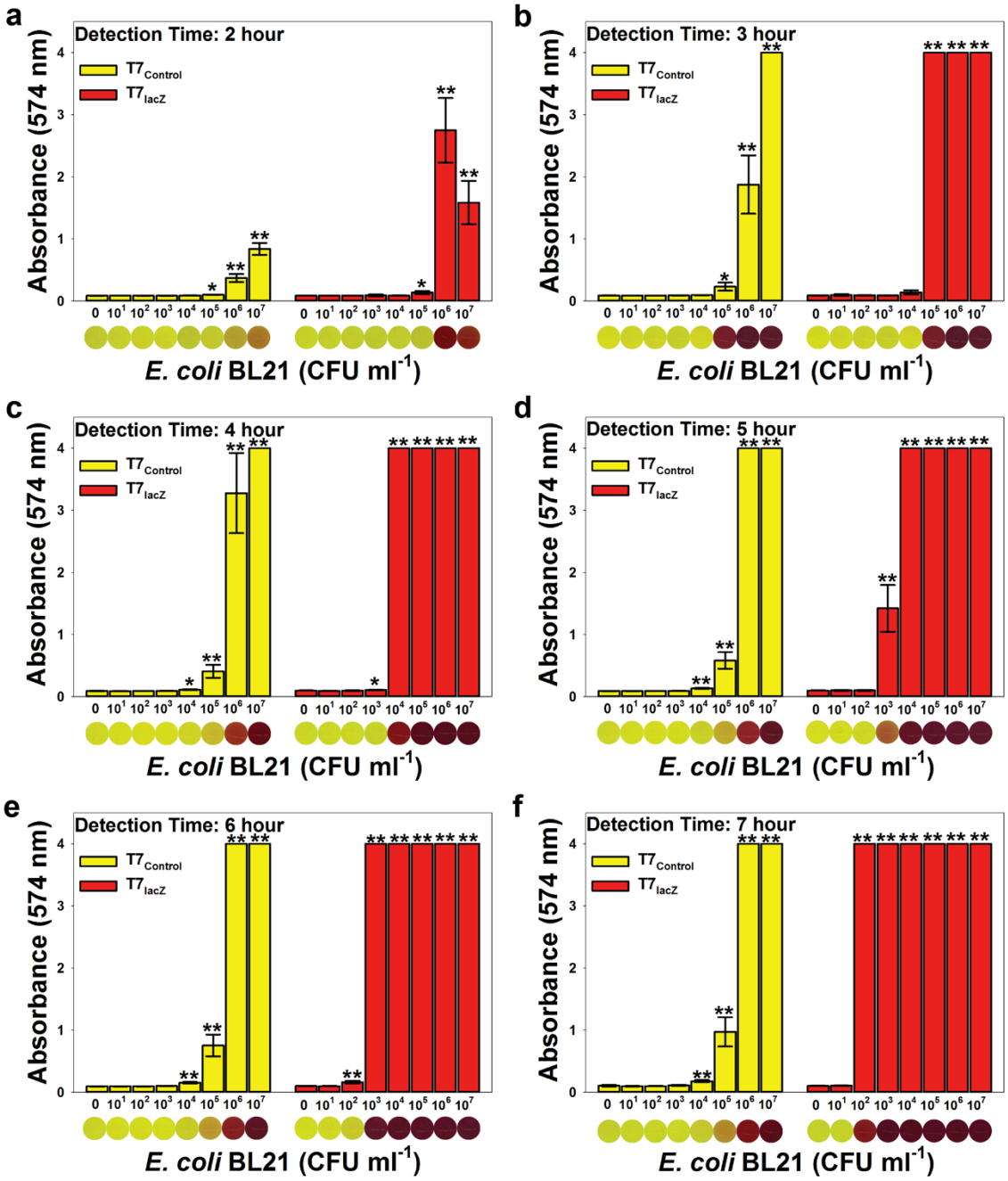

Figure 6.5 Comparison of one-step *E. coli* detection using engineered $T7_{control}$ and $T7_{lacZ}$ bacteriophage. Plots of absorbance intensities (574 nm) towards various *E. coli* concentrations after detection time of (a) 2, (b) 3, (c) 4, (d) 5, (e) 6, and (f) 7 hour. (Error bars represent the standard deviation of three independent experiments)

6.3.5 Two-step detection of *E. coli* cells using $T7_{lacZ}$ engineered bacteriophage

Preenrichments steps are commonly used in bacterial detection methodologies and we were curious as to the extent such a step could improve our detection time or limit. We

diluted an *E. coli* culture to the following concentrations (10^3, 10^2, and 10^1 CFU·mL^{-1}, LB broth was used as control experiment) and allowed them to grow in LB broth for various hours at 37 C°. After a set preenrichment time, T7$_{lacZ}$ phage and CPRG were then added to start the phage infection and reporter enzyme production. The absorbance intensity was measured every hour until a total of 7 hours. Contour plots of absorbance intensities at 574 nm as 2D function of detection time and preenrichment time for each starting *E. coli* concentrations can be found in Figure 6.6. It should be noted that detectable area (red color) decreased with the decreasing of *E. coli* concentration. As expected, no red color was observed in the control experiment.

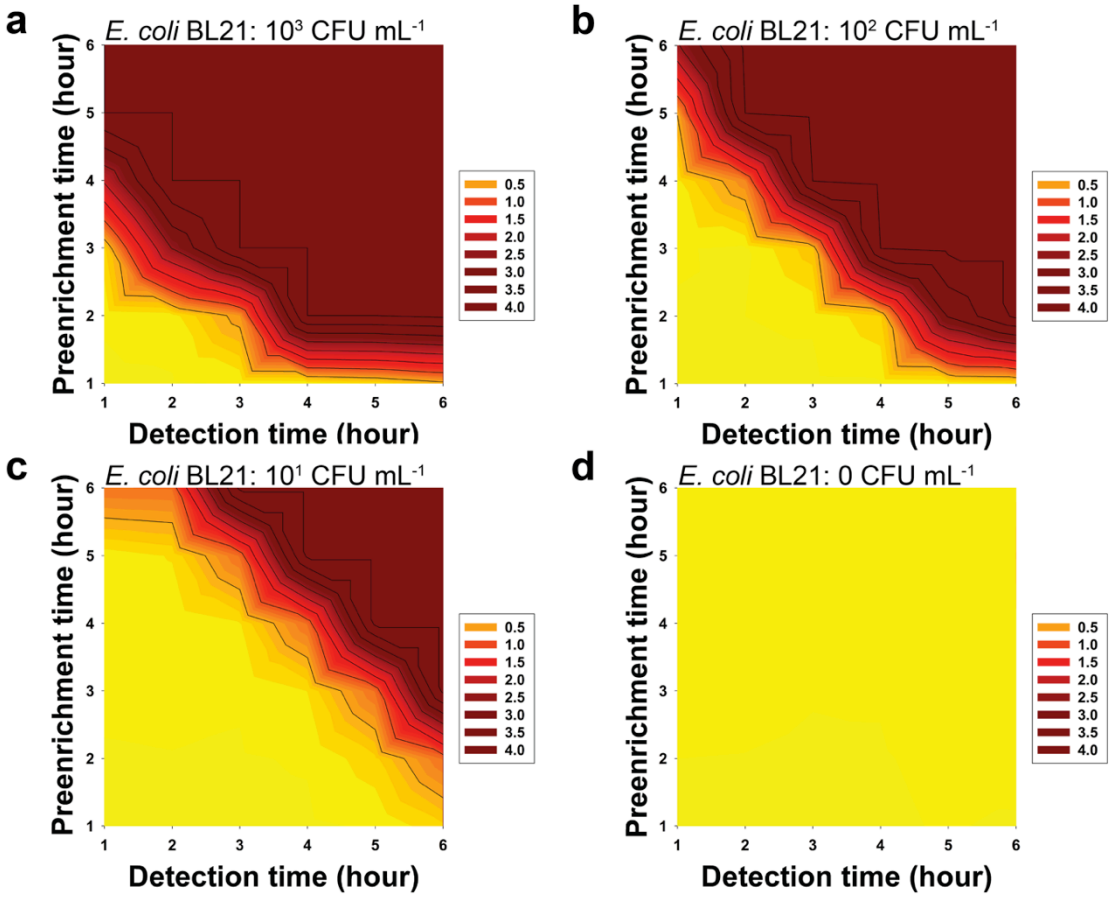

Figure 6.6 Two-step detection of *E. coli* cells at low concentrations using T7$_{lacZ}$ engineered bacteriophage. Contour plots of absorbance intensities (574 nm) as 2D function of detection time and preenrichment time towards *E. coli* cells at the concentration of (a) 10^3, (b) 10^2, (c) 10^1, and (d) 0 CFU·mL^{-1}. (The absorbance intensity data shown here represents the average of three independent experiments)

The number of *E. coli* cells played an extremely important role on colorimetric response. In our study, two-step detection (preenrichment step and detection step) was incorporated to detect *E. coli* cells at low concentrations. Preenrichment allowed *E. coli* to grow to increase *E. coli* cell number, and the detection step was used for phage infection and enzymatic reaction. The absorbance intensity at 574 nm was plotted towards total detection time (less than 7 hours) at different *E. coli* concentrations. As shown in Figure 6.7, we were able to detect *E. coli* cells at the concentration of 10^3, 10^2, and 10^1 CFU·mL^{-1} after total detection time of 5, 6, and 7 hours, respectively. Different

preenrichment times resulted in slightly differences of colorimetric response, indicting that whole detection was mostly contributed by phage infection and enzymatic reaction. This phenomenon can be explained that *E. coli* cells at low concentrations can grow as normal because spare cells in the detection solution decreased the opportunity to be infected by T7$_{lacZ}$ phage.

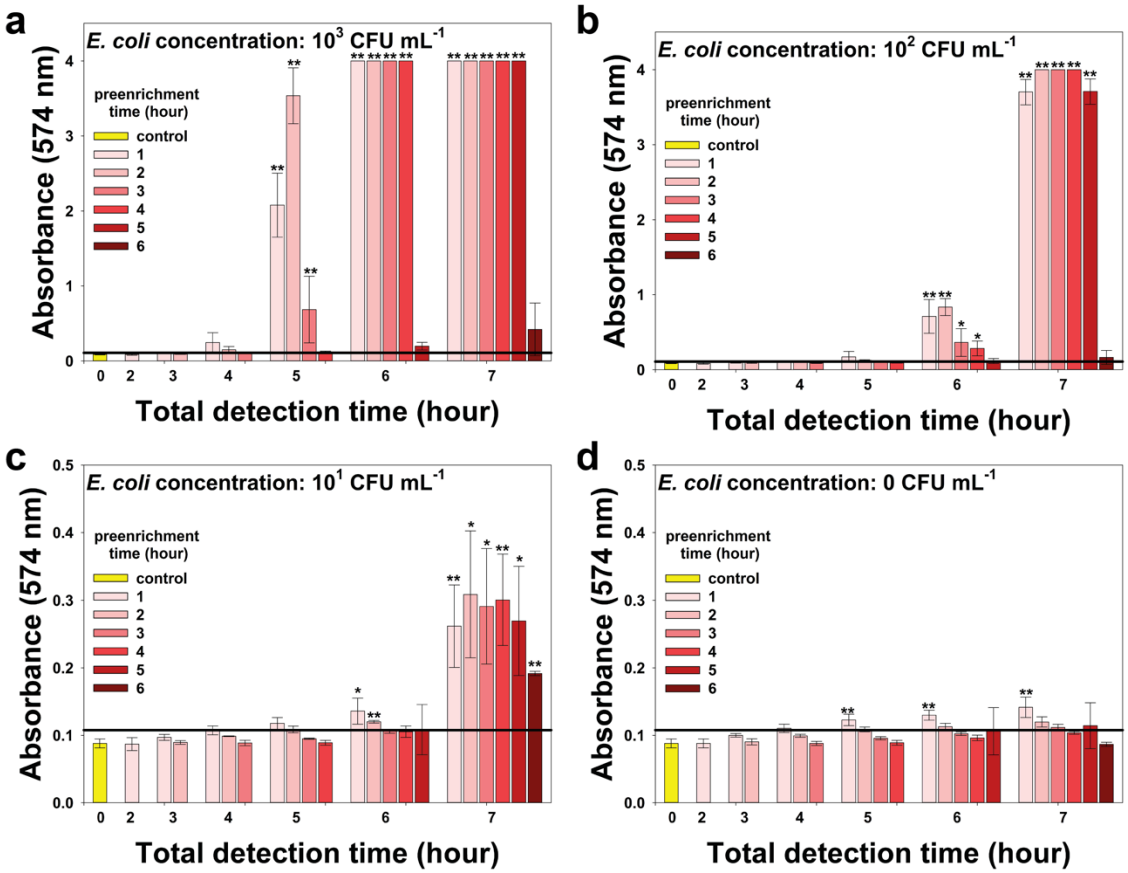

Figure 6.7 Two-step detection of *E. coli* cells at low concentrations using T7$_{lacZ}$ engineered bacteriophage. Plots of absorbance intensities (574 nm) towards total detection time at the *E. coli* BL21 concentrations of (a) 10^3, (b) 10^2, (c) 10^1, and (d) 0 CFU·mL^{-1}. Solid lines indicate the average and ± 3 standard deviation of absorbance intensity of control experiments. (Error bars represent the standard deviation of three independent experiments)

6.3.6 High-throughput sensing of antibiotics

As a proof-of-principle application for phage-based detection, we explored the ability of our modified phage to improve time to result of antibiotic drugs sensing in a high throughput, i.e. 96-well plate, format. The *E. coli* BLT5403, an ampicillin resistant *E. coli* stain, was used as our bacterial model, and we examined phage mediated *β*-gal overexpression in the presence of ampicillin, kanamycin, and ciprofloxacin. The steps of our proposed simple, high-throughput, and phage-based antibiotic drugs sensing scheme are illustrated in Figure 8a. We inoculated *E. coli* BLT5403 cells into LB broth containing different antibiotics at varying concentrations at 37 °C for 3 hours. $T7_{lacZ}$ phage and CPRG were then added to prompt colorimetric response. In the present of effective antibiotic drugs, the proliferation of *E. coli* cells was inhibited, which decreased the expression of *β*-gal after adding $T7_{lacZ}$ phage. Therefore, the detection solution kept yellow. In the present of ineffective antibiotic drugs (ampicillin), the *E. coli* cells exhibited exponential growth. The degree of growth inhibition by antibiotic drugs caused different amounts of *β*-gal expressed by $T7_{lacZ}$ phage, resulting in different levels of red intensities.

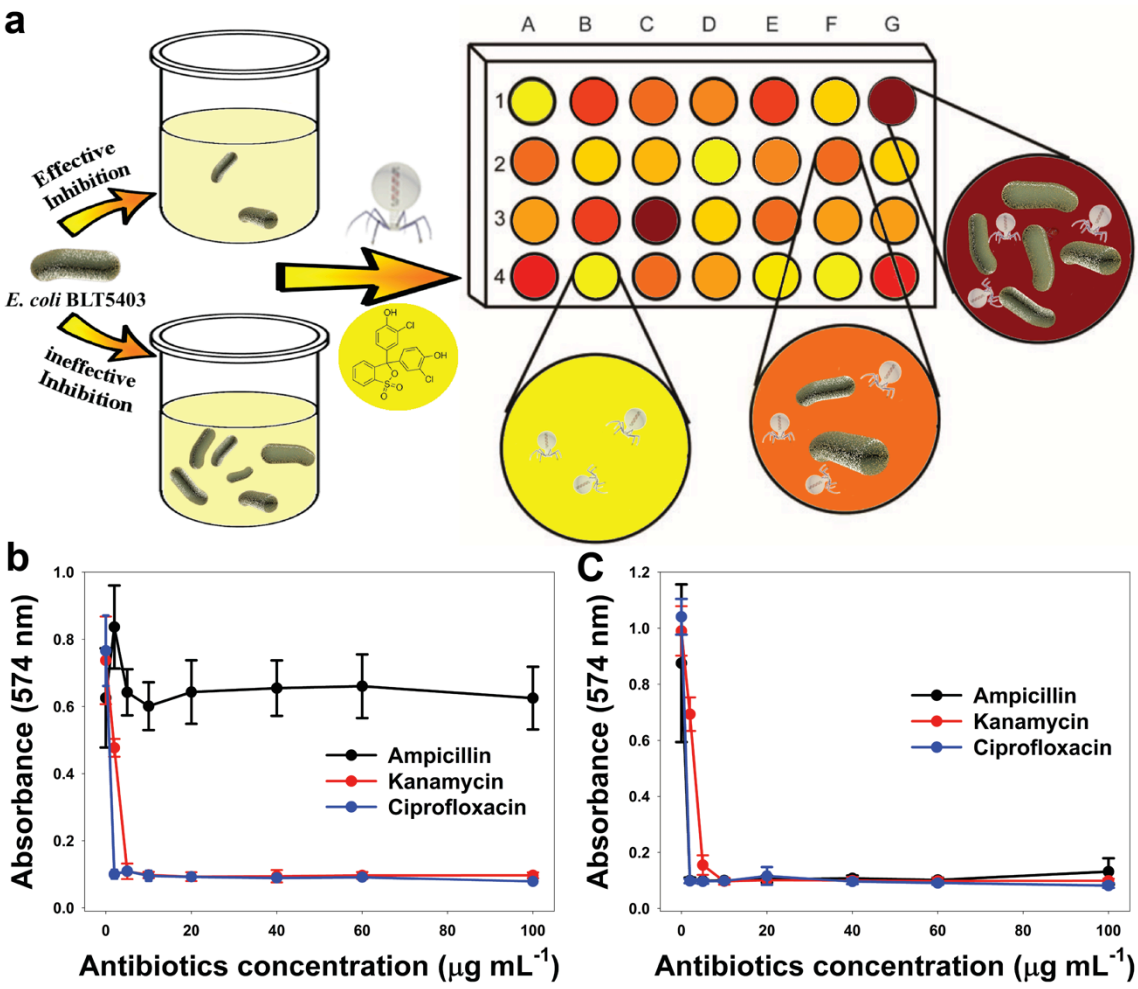

Figure 6.8 High-throughput determination of antibiotic drugs using T7$_{lacZ}$ engineered bacteriophage. (a) Schematic illustration of high-throughputs antibiotic screening by T7$_{lacZ}$ engineered phage infection of *E. coli* BLT5403. Plot of absorbance intensities (574 nm) towards various antibiotics concentrations by T7$_{lacZ}$ engineered phage infection of (b) *E. coli* BLT5403 and *E. coli* BL21. (Error bars represent one standard deviation of three independent experiments)

By analyzing the colorimetric response of the sensing system, we were able to determine the antibiotic drugs. As shown in Figure 6.8b, T7$_{lacZ}$ phage incorporating with *E. coli* BLT5403 was able to sense ampicillin. In the present of kanamycin and ciprofloxacin, absorbance intensity at 574 nm dramatically decreased with the increasing of antibiotics concentration. However, we didn't observe the decrease trend for absorbance intensity at 574 nm in the present of ampicillin at varying concentrations. As

control, T7$_{lacZ}$ phage incorporating with *E. coli* BL21 was used to determinate antibiotic drugs. All the three antibiotic drugs completely inhibited the cell growth, resulting in that all the detection solutions kept yellow (Figure 6.8c). Thus, these results indicated that T7$_{lacZ}$ phage had the potential to determine antibiotic drugs, and even screen new antibiotic drugs.

6.4 Discussion

In this study, we demonstrated that a scheme utilizing engineered T7$_{lacZ}$ phage, that induces β-gal overexpression during infection, resulted in an improved time to and limit of *E. coli* detection in comparison to a scheme utilizing non-reporter enzyme-produced phage. The colorimetric response from phage-mediated β-gal enzymatic activity was driven by two factors. The first factor is the number of *E. coli* cells infected by our phage, which was impacted by initial cell concentration, preenrichment time, and phage concentration. After low concentration of *E. coli* cells was inoculated into fresh LB broth, the cell proliferation started. It is no doubt that higher initial cell concentration and longer preenrichment time could quickly increase the number of *E. coli*. In addition, phage concentration played an important role for the cell number. The *E. coli* cells at low concentrations decreased the probability to be infected by phage, resulting in more time for cell proliferation. The second factor was enzymatic reaction, which triggered the readable signal. Reaction time as well as pH and temperature had a significant effect on the enzymatic product. Like the number of *E. coli* cells affected by phage concentration, phage concentration could determine enzymatic reaction time. In conclusion, phage concentration was a key parameter to balance cell growth time and enzymatic time to reach best detection efficiency.

The efficiency of detection was judged by their specificity, sensitivity, and speed. In previously reported publication, the specificity of T7 phage for *E. coli* detection has been demonstrated in the presence of competitive bacterial species, including *Salmonella enterica*, *Staphylococcus aureus*, and *Pseudomonas aeruginosa*[96]. In this study, we demonstrate the sensitivity of our scheme, though there is trade off between sensitivity and time to result. Several methods could be used to further improve the detection limit or shorten the detection time using engineered T7$_{lacZ}$ phage. For example, promoter optimization could allow for increased β-gal product[176]. A more sensitive transduction method could be used to monitor the activity of β-gal, like an ultrasensitive enzymatic reaction incorporating redox cycling or multi-enzyme labels[210]. There is also the potential to use a concentration step, like membrane filtration, to increase *E. coli* concentrations prior to the addition of T7$_{lacZ}$ phage[81, 83, 97]. In our DNA construct, a biotin tag was fused to the phage capsid protein, which in the future may enable us to bind our engineered phages to streptavidin-conjugated magnetic beads allowing further schemes that combine sample purification, concentration, and detection[40].

While our proof-of-principle is limited to detection of *E. coli* cells, there is clear potential to adapt our phage-mediated reporter design to other phage that target other bacterial pathogens with public health relevance, such as *Salmonella* and *Listeria monocytogenes*. There is also the potential, as we grow our understanding of phage infections, that genetic technologies will allow us to modify phage proteins responsible for cell attachment, and thus allowing us to redefine the host range of our T7$_{lacZ}$ phage[211]. Phage cocktails have also gained a wide interest in the areas of phage therapy, reduction of biofilm, and prevention of pathogenic disease[212-215]. A cocktail of β-gal active

engineered phage may also be a potential route to broaden our range of detectable bacterial strains.

As a proof-of-principle application, T7$_{lacZ}$ phage incorporating with ampicillin resistance *E. coli* had been demonstrated to sense ampicillin against kanamycin and ciprofloxacin. This design could be used to sense other antibiotic drugs using T7$_{lacZ}$ phage combining with other antibiotic resistance *E. coli* strains. In addition, our T7$_{lacZ}$ phage may be used to determine antibiotic susceptibility of *E. coli* strains by monitoring bacteria growth in antibiotic LB broth. As shown in Figure 6.8b and Supplementary Figure 6.8c, both *E. coli* BL21 and BLT5403 showed a higher minimal inhibitory concentration (MIC) for kanamycin than ciprofloxacin. Our proposed methods to sense antibiotic drugs or determine antibiotic susceptibility of *E. coli* at a high throughput format could improve time compared with traditional tests[203, 216].

CHAPTER 7

CONCLUSIONS

We demonstrate a bacteriophage (phage)-based magnetic separation scheme for the rapid detection of *Escherichia coli* (*E. coli*) in drinking water.T7 phage covalently conjugated to carboxylic acid-modified magnetic beads were used to capture, separate, and purity *E. coli* cells in drinking water. Our scheme was as follows: (1) T7 phage conjugated magnetic beads were used to capture and separate *E. coli* BL21 from drinking water; (2) subsequent phage mediated lysis was used to release endemic β-gal from the bound bacterial cells; (3) the release of β-gal was detected using chlorophenol red-β-D-galactopyranoside (CRPG), a colorimetric substrate which changes from yellow to red in the presence of β-gal. Using this strategy, we were able to detect *E. coli* at a concentration of 1×10^4 CFU·mL^{-1} within 2.5 h. The specificity of the proposed magnetic probes toward *E. coli* was demonstrated against a background of competing bacteria. By incorporating a pre-enrichment step in Luria-Bertani (LB) broth supplemented with isopropyl β-D-thiogalactopyranoside (IPTG), we were able to detect 10 CFU·mL^{-1} in drinking water after 6 hour of pre-enrichment.

The lack of practical methods for bacterial separation remains a hindrance for the low-cost and successful development of rapid detection methods from complex samples. Antibody-tagged magnetic particles are commonly used to pull analytes from a liquid sample. While this method is well-established, improvements in capture efficiencies would result in an increase of the overall detection assay performance. Bacteriophages represent a low-cost and more consistent biorecognition element as compared to antibodies. We have developed nanoscale bacteriophage-tagged magnetic probes, where

T7 bacteriophages were bound to magnetic nanoparticles. The nanoprobe allowed the specific recognition and attachment to *E. coli* cells. The phage magnetic nanprobes were directly compared to antibody-conjugated magnetic nanoprobes. The capture efficiencies of bacteriophages and antibodies on nanoparticles for the separation of *E. coli* K12 at varying concentrations were determined. The results indicated a similar bacteria capture efficiency between the two nanoprobes.

The colorimetric detection of pathogens in a food matrix remains the major disadvantage of poor visible color change. Although significant work has been performed in the area of colorimetric detection, these methods are often expensive and complicated. The field of enzymatic nanostructure-based visual detection of pathogens is still in its early stage and therefore molecule-based visual assays are most used. Here, A novel enzyme-induced metallization colorimetric assay was developed to monitor and measure β-gal activity, and was further employed for colorimetric phage-enabled detection of *E. coli*. This assay relied on enzymatic reaction-induced silver deposition on the surface of gold nanorods (AuNRs). In the presence of β-gal, the substrate p-aminophenyl β-D-galactopyranoside (PAPG) is hydrolyzed to produce p-aminophenol (PAP). Reduction of silver ions by PAP generates a silver shell on the surface of AuNRs, resulting in the blue shift of the longitudinal localized surface plasmon resonance (LSPR) peak and multicolor changes of the detection solution from light green to orange-red. Additionally, this technique was successfully applied to *E. coli* detection in combination with phage infection. Due to the simplicity and short incubation time of this enzyme-induced metallization colorimetric method, the assay is well suited for the detection of bacteria in low-resource settings.

A T7 bacteriophage (phage) has been genetically engineered to carry the *lacZ* operon to enable the overexpression of beta-galactosidase (*β*-gal) during phage infection for colorimetric detection of *Escherichia coli* (*E. coli*) cells. After phage infection, the enzymatic activity of the released *β*-gal was monitored using a colorimetric substrate. Compared with a control T7 phage, our $T7_{lacZ}$ phage resulted in significantly higher levels of *β*-gal expression during phage infection, enabling a lower detection limit of *E. coli* cells. Using this engineered $T7_{lacZ}$ phage, we were able to detect *E. coli* cells at the concentration of 10 $CFU \cdot mL^{-1}$ within 7 hours. Furthermore, we demonstrated the potential for phage-based antibiotic drug sensing by using our $T7_{lacZ}$ phage, and subsequent *β*-gal expression to detect ampicillin resistant *E. coli* cells.

APPENDIX

PUBLICATION

[13] **J. Chen**, S.R. Nugen and V.M. Rotello. An Overview Recognition Element on Nanoscale Probes for the Detection and Sensing of Bacteria Cells. (Preparation)

[12] **J. Chen**, S.D. Alcaine, A.A. Jackson, V.M. Rotello and S.R. Nugen. Colorimetric Detection of *Escherichia coli* with Engineered Enzymatic Bacteriophage. (Preparation)

[11] K. Huang, **J. Chen**, S.R. Nugen and J.M. Goddard. Hybrid Antifouling and Antimicrobial Nanocomposite Coating Prepared by Electroless Plating of Fluoropolymer and Cationic Silica Nanoparticles. ACS Appl. Mater. Interface 2016; 8: 15926-15936. IF = 4.726

[10] **J. Chen**, S. Pang, L. He and S.R. Nugen. Highly Sensitive and Selective Detection of Nitrite Ions Using Fe_3O_4@Au Magnetic Nanoparticles by Surface-Enhanced Raman Spectroscopy. Biosens. Bioelectron 2016; 85: 726-733. IF = 5.636

[9] **J. Chen**, A.A. Jackson, V.M. Rotello and S.R. Nugen. Colorimetric Detection of *Escherichia Coli* Based on the Enzyme-Induced Metallization of Gold Nanorods. Small 2016; 12(18): 2469-2475. IF = 8.368.

[8] P. Wang, S. Pang, **J. Chen**, L. McLandsborough, S.R. Nugen, M. Fan and L. He. Label-free Mapping Bacterial Cells Using Surface-Enhanced Raman Spectroscopy. Analyst 2016; 141(4): 1356-1362. IF = 4.107.

[7] D. Wang, Z. Wang, **J. Chen**, A.J. Kinchla and S.R. Nugen. Rapid Detection of *Salmonella* Using a Redox Cycling-based Electrochemical Method. Food Control 2016; 62: 81-88. IF = 2.806.

[6] Z. Wang, D. Wang, **J. Chen**, D.A. Sela and S.R. Nugen. Development of a Novel Bacteriophage Based Biomagnetic Separation Method as an Aid for Sensitive Detection of Viable *Escherichia coli*. Analyst 2016; 141(3): 1009-1016. IF = 4.107.

[5] **J. Chen**, Y. Li, K. Huang, P. Wang, L. He, K.R. Carter and S.R. Nugen. Nanoimprint Patterned Pillar Substrates for Surface-enhanced Raman Scattering Application. ACS Appl. Mater. Interfaces 2015; 7(39), 22106-22113. IF = 6.723.

[4] **J. Chen**, B. Duncan, Z. Wang, L.-S. Wang, V.M. Rotello and S.R. Nugen. Bacteriophage-based Nanoprobes for Rapid Bacteria Separation. Nanoscale. 2015; 7, 16230-16236. IF = 7.394.

[3] **J. Chen**, S.D. Alcaine, Z. Jiang, V.M. Rotello and S.R. Nugen. Detection of *Escherichia coli* in Drinking Water Using T7 Bacteriophage-conjugated Magnetic Probe. Anal. Chem. 2015; 87: 8977-8984. IF = 5.636.

[2] **J. Chen**, Y. Zhou, D. Wang, F. He, V.M. Rotello, K.R. Carter, J.J. Watkins and S.R. Nugen. UV-nanoimprint lithography as a tool to develop flexible microfluidic devices for electrochemical detection. Lab Chip. 2015;15(14):3086-3094. IF = 6.115.

[1] **J. Chen**, Z. Jiang, J.S. Ackerman, M. Yazdani, S. Hou, S.R. Nugen and V.M. Rotello. Electrochemical nanoparticle-enzyme sensors for screening bacterial contamination in drinking water. Analyst. 2015;140(15):4991-4996. IF = 4.107.

BIBLIOGRAPHY

1. Patel, P. (Bio) sensors for measurement of analytes implicated in food safety: a review. *TrAC, Trends Anal. Chem.* 2002, 21, 96-115.

2. Leonard, P.; Hearty, S.; Brennan, J.; Dunne, L.; Quinn, J.; Chakraborty, T.; O'Kennedy, R. Advances in biosensors for detection of pathogens in food and water. *Enzyme Microb. Technol.* 2003, 32, 3-13.

3. Theron, J.; Cilliers, J.; Du Preez, M.; Brözel, V.; Venter, S. Detection of toxigenic Vibrio cholerae from environmental water samples by an enrichment broth cultivation–pit-stop semi-nested PCR procedure. *J. Appl. Microbiol.* 2000, 89, 539-546.

4. Atlas, R. M. KY 40292, USA. *Environ. Microbiol.* 1999, 1, 283-293.

5. Varmus, H.; Klausner, R.; Zerhouni, E.; Acharya, T.; Daar, A.; Singer, P. Grand challenges in global health. *Science* 2003, 302, 398-399.

6. Whitesides, G. M. The origins and the future of microfluidics. *Nature* 2006, 442, 368-373.

7. Jones, K. E.; Patel, N. G.; Levy, M. A.; Storeygard, A.; Balk, D.; Gittleman, J. L.; Daszak, P. Global trends in emerging infectious diseases. *Nature* 2008, 451, 990-993.

8. Vikesland, P. J.; Wigginton, K. R. Nanomaterial Enabled Biosensors for Pathogen Monitoring - A Review. *Environ. Sci. Technol.* 2010, 44, 3656-3669.

9. Tawil, N.; Sacher, E.; Mandeville, R.; Meunier, M. Surface plasmon resonance detection of E. coli and methicillin-resistant S. aureus using bacteriophages. *Biosens. Bioelectron.* 2012, 37, 24-29.

10. Velusamy, V.; Arshak, K.; Korostynska, O.; Oliwa, K.; Adley, C. An overview of foodborne pathogen detection: In the perspective of biosensors. *Biotechnol. Adv.* 2010, 28, 232-254.

11. Gandhi, M.; Chikindas, M. L. Listeria: a foodborne pathogen that knows how to survive. *Int. J. Food Microbiol.* 2007, 113, 1-15.

12. Park, S.; Worobo, R. W.; Durst, R. A. Escherichia coli O157: H7 as an emerging foodborne pathogen: a literature review. *Crit. Rev. Biotechnol.* 2001, 21, 27-48.

13. Poulsen, L. V. Microbial Biofilm in Food Processing. *LWT - Food Science and Technology* 1999, 32, 321-326.

14. Andersson, D. I.; Hughes, D. Antibiotic resistance and its cost: is it possible to reverse resistance? *Nat. Rev. Microbiol.* 2010, 8, 260-271.

15. Wright, G. D. Molecular mechanisms of antibiotic resistance. *Chem. Commun.* 2011, 47, 4055-4061.

16. Ray, P. C.; Khan, S. A.; Singh, A. K.; Senapati, D.; Fan, Z. Nanomaterials for targeted detection and photothermal killing of bacteria. *Chem. Soc. Rev.* 2012, 41, 3193-3209.

17. Lazcka, O.; Del Campo, F. J.; Munoz, F. X. Pathogen detection: A perspective of traditional methods and biosensors. *Biosensors & Bioelectronics* 2007, 22, 1205-1217.

18. Rompré, A.; Servais, P.; Baudart, J.; de-Roubin, M.-R.; Laurent, P. Detection and enumeration of coliforms in drinking water: current methods and emerging approaches. *J. Microbiol. Methods* 2002, 49, 31-54.

19. Saha, K.; Agasti, S. S.; Kim, C.; Li, X.; Rotello, V. M. Gold nanoparticles in chemical and biological sensing. *Chem. Rev.* 2012, 112, 2739-79.

20. Anker, J. N.; Hall, W. P.; Lyandres, O.; Shah, N. C.; Zhao, J.; Van Duyne, R. P. Biosensing with plasmonic nanosensors. *Nat. Mater.* 2008, 7, 442-453.

21. Shipway, A. N.; Katz, E.; Willner, I. Nanoparticle arrays on surfaces for electronic, optical, and sensor applications. *Chemphyschem* 2000, 1, 18-52.

22. Faraday, M. The Bakerian Lecture: Experimental Relations of Gold (and Other Metals) to Light. *Philosophical Transactions of the Royal Society of London* 1857, 147, 145-181.

23. Sau, T. K.; Murphy, C. J. Self-assembly patterns formed upon solvent evaporation of aqueous cetyltrimethylammonium bromide-coated gold nanoparticles of various shapes. *Langmuir* 2005, 21, 2923-2929.

24. Oldenburg, S.; Averitt, R.; Westcott, S.; Halas, N. Nanoengineering of optical resonances. *Chem. Phys. Lett.* 1998, 288, 243-247.

25. Lu, W.; Singh, A. K.; Khan, S. A.; Senapati, D.; Yu, H.; Ray, P. C. Gold nano-popcorn-based targeted diagnosis, nanotherapy treatment, and in situ monitoring of photothermal therapy response of prostate cancer cells using surface-enhanced Raman spectroscopy. *J. Am. Chem. Soc.* 2010, 132, 18103-18114.

26. Mayer, K. M.; Hafner, J. H. Localized surface plasmon resonance sensors. *Chem. Rev.* 2011, 111, 3828-3857.

27. Fu, J.; Park, B.; Zhao, Y. Limitation of a localized surface plasmon resonance sensor for Salmonella detection. *Sensors Actuators B: Chem.* 2009, 141, 276-283.

28. Jana, N. R.; Gearheart, L.; Murphy, C. J. Wet chemical synthesis of high aspect ratio cylindrical gold nanorods. *J. Phys. Chem. B* 2001, 105, 4065-4067.

29. Wang, C.; Irudayaraj, J. Gold nanorod probes for the detection of multiple pathogens. *Small* 2008, 4, 2204-2208.

30. Wang, C. G.; Irudayaraj, J. Multifunctional Magnetic-Optical Nanoparticle Probes for Simultaneous Detection, Separation, and Thermal Ablation of Multiple Pathogens. *Small* 2010, 6, 283-289.

31. Saha, K.; Agasti, S. S.; Kim, C.; Li, X.; Rotello, V. M. Gold nanoparticles in chemical and biological sensing. *Chem. Rev.* 2012, 112, 2739-2779.

32. Singh, A. K.; Senapati, D.; Wang, S.; Griffin, J.; Neely, A.; Candice, P.; Naylor, K. M.; Varisli, B.; Kalluri, J. R.; Ray, P. C. Gold Nanorod Based Selective Identification of Escherichia coli Bacteria Using Two-Photon Rayleigh Scattering Spectroscopy. *Acs Nano* 2009, 3, 1906-1912.

33. Wang, S.; Singh, A. K.; Senapati, D.; Neely, A.; Yu, H.; Ray, P. C. Rapid Colorimetric Identification and Targeted Photothermal Lysis of Salmonella Bacteria by Using Bioconjugated Oval-Shaped Gold Nanoparticles. *Chemistry-A European Journal* 2010, 16, 5600-5606.

34. Khan, S. A.; Singh, A. K.; Senapati, D.; Fan, Z.; Ray, P. C. Targeted highly sensitive detection of multi-drug resistant Salmonella DT104 using gold nanoparticles. *Chem. Commun.* 2011, 47, 9444-9446.

35. Varshney, M.; Yang, L. J.; Su, X. L.; Li, Y. B. Magnetic nanoparticle-antibody conjugates for the separation of Escherichia coli O157 : H7 in ground beef. *J. Food Prot.* 2005, 68, 1804-1811.

36. Pappert, G.; Rieger, M.; Niessner, R.; Seidel, M. Immunomagnetic nanoparticle-based sandwich chemiluminescence-ELISA for the enrichment and quantification of E. coli. *Microchimica Acta* 2010, 168, 1-8.

37. Yang, H.; Qu, L. W.; Wimbrow, A. N.; Jiang, X. P.; Sun, Y. P. Rapid detection of Listeria monocytogenes by nanoparticle-based immunomagnetic separation and real-time PCR. *Int. J. Food Microbiol.* 2007, 118, 132-138.

38. Gao, J.; Gu, H.; Xu, B. Multifunctional Magnetic Nanoparticles: Design, Synthesis, and Biomedical Applications. *Acc. Chem. Res.* 2009, 42, 1097-1107.

39. Chen, W.-J.; Tsai, P.-J.; Chen, Y.-C. Functional Fe3O4/TiO2 core/shell magnetic nanoparticles as photokilling agents for pathogenic bacteria. *Small* 2008, 4, 485-491.

40. Chen, J.; Duncan, B.; Wang, Z.; Wang, L. S.; Rotello, V. M.; Nugen, S. R. Bacteriophage-based nanoprobes for rapid bacteria separation. *Nanoscale* 2015, 7, 16230-6.

41. Frey, N. A.; Peng, S.; Cheng, K.; Sun, S. H. Magnetic nanoparticles: synthesis, functionalization, and applications in bioimaging and magnetic energy storage. *Chem. Soc. Rev.* 2009, 38, 2532-2542.

42. Schladt, T. D.; Schneider, K.; Schild, H.; Tremel, W. Synthesis and bio-functionalization of magnetic nanoparticles for medical diagnosis and treatment. *Dalton Transactions* 2011, 40, 6315-6343.

43. Jayasena, S. D. Aptamers: an emerging class of molecules that rival antibodies in diagnostics. *Clin. Chem.* 1999, 45, 1628-1650.

44. Cerchia, L.; de Franciscis, V. Targeting cancer cells with nucleic acid aptamers. *Trends Biotechnol.* 2010, 28, 517-525.

45. Cheon, J.; Lee, J.-H. Synergistically integrated nanoparticles as multimodal probes for nanobiotechnology. *Acc. Chem. Res.* 2008, 41, 1630-1640.

46. Jones, M. R.; Osberg, K. D.; Macfarlane, R. J.; Langille, M. R.; Mirkin, C. A. Templated techniques for the synthesis and assembly of plasmonic nanostructures. *Chem. Rev.* 2011, 111, 3736-3827.

47. Nel, A. E.; Mädler, L.; Velegol, D.; Xia, T.; Hoek, E. M.; Somasundaran, P.; Klaessig, F.; Castranova, V.; Thompson, M. Understanding biophysicochemical interactions at the nano–bio interface. *Nat. Mater.* 2009, 8, 543-557.

48. Dreaden, E. C.; Mackey, M. A.; Huang, X.; Kang, B.; El-Sayed, M. A. Beating cancer in multiple ways using nanogold. *Chem. Soc. Rev.* 2011, 40, 3391-3404.

49. Boisselier, E.; Astruc, D. Gold nanoparticles in nanomedicine: preparations, imaging, diagnostics, therapies and toxicity. *Chem. Soc. Rev.* 2009, 38, 1759-1782.

50. Yuan, J.; Xu, Y.; Müller, A. H. One-dimensional magnetic inorganic–organic hybrid nanomaterials. *Chem. Soc. Rev.* 2011, 40, 640-655.

51. Huang, W.-C.; Tsai, P.-J.; Chen, Y.-C. Functional gold nanoparticles as photothermal agents for selective-killing of pathogenic bacteria. 2007.

52. Hamula, C. L. A.; Zhang, H.; Li, F.; Wang, Z.; Chris Le, X.; Li, X.-F. Selection and analytical applications of aptamers binding microbial pathogens. *TrAC, Trends Anal. Chem.* 2011, 30, 1587-1597.

53. Duan, Y. F.; Ning, Y.; Song, Y.; Deng, L. Fluorescent aptasensor for the determination of Salmonella typhimurium based on a graphene oxide platform. *Microchimica Acta* 2014, 181, 647-653.

54. Zuo, P.; Li, X.; Dominguez, D. C.; Ye, B.-C. A PDMS/paper/glass hybrid microfluidic biochip integrated with aptamer-functionalized graphene oxide nano-biosensors for one-step multiplexed pathogen detection. *Lab on a Chip* 2013, 13, 3921-3928.

55. Duan, N.; Wu, S.; Dai, S.; Miao, T.; Chen, J.; Wang, Z. Simultaneous detection of pathogenic bacteria using an aptamer based biosensor and dual fluorescence resonance energy transfer from quantum dots to carbon nanoparticles. *Microchimica Acta* 2014, 182, 917-923.

56. Wang, R.; Xu, Y.; Zhang, T.; Jiang, Y. Rapid and sensitive detection of Salmonella typhimurium using aptamer-conjugated carbon dots as fluorescence probe. *Analytical Methods* 2015, 7, 1701-1706.

57. Kim, Y. S.; Chung, J.; Song, M. Y.; Jurng, J.; Kim, B. C. Aptamer cocktails: Enhancement of sensing signals compared to single use of aptamers for detection of bacteria. *Biosens. Bioelectron.* 2014, 54, 195-198.

58. Duan, N.; Wu, S. J.; Zhu, C. Q.; Ma, X. Y.; Wang, Z. P.; Yu, Y.; Jiang, Y. Dual-color upconversion fluorescence and aptamer-functionalized magnetic nanoparticles-based bioassay for the simultaneous detection of Salmonella Typhimurium and Staphylococcus aureus. *Anal. Chim. Acta* 2012, 723, 1-6.

59. Duan, N.; Wu, S.; Yu, Y.; Ma, X.; Xia, Y.; Chen, X.; Huang, Y.; Wang, Z. A dual-color flow cytometry protocol for the simultaneous detection of Vibrio parahaemolyticus and Salmonella typhimurium using aptamer conjugated quantum dots as labels. *Anal. Chim. Acta* 2013, 804, 151-158.

60. Guerrini, L.; Graham, D. Molecularly-mediated assemblies of plasmonic nanoparticles for Surface-Enhanced Raman Spectroscopy applications. *Chem. Soc. Rev.* 2012, 41, 7085-7107.

61. Fleischmann, M.; Hendra, P. J.; McQuillan, A. J. Raman spectra of pyridine adsorbed at a silver electrode. *Chem. Phys. Lett.* 1974, 26, 163-166.

62. Kambhampati, P.; Foster, M. C.; Campion, A. Two-dimensional localization of adsorbate/substrate charge-transfer excited states of molecules adsorbed on metal surfaces. *The Journal of chemical physics* 1999, 110, 551-558.

63. Alvarez-Puebla, R. A.; Liz-Marzan, L. M. Traps and cages for universal SERS detection. *Chem. Soc. Rev.* 2012, 41, 43-51.

64. Chen, J.; Li, Y.; Huang, K.; Wang, P.; He, L.; Carter, K. R.; Nugen, S. R. Nanoimprinted Patterned Pillar Substrates for Surface-Enhanced Raman Scattering Applications. *ACS Appl. Mater. Interfaces* 2015, 7, 22106-13.

65. Ravindranath, S. P.; Wang, Y.; Irudayaraj, J. SERS driven cross-platform based multiplex pathogen detection. *Sensors Actuators B: Chem.* 2011, 152, 183-190.

66. He, L.; Deen, B. D.; Pagel, A. H.; Diez-Gonzalez, F.; Labuza, T. P. Concentration, detection and discrimination of Bacillus anthracis spores in orange juice using aptamer based surface enhanced Raman spectroscopy. *Analyst* 2013, 138, 1657-1659.

67. Zhang, H.; Ma, X.; Liu, Y.; Duan, N.; Wu, S.; Wang, Z.; Xu, B. Gold nanoparticles enhanced SERS aptasensor for the simultaneous detection of Salmonella typhimurium and Staphylococcus aureus. *Biosens. Bioelectron.* 2015, 74, 872-877.

68. Soper, S. A.; Henry, A. C.; Vaidya, B.; Galloway, M.; Wabuyele, M.; McCarley, R. L. Surface modification of polymer-based microfluidic devices. *Anal. Chim. Acta* 2002, 470, 87-99.

69. Wu, L.; Luan, T.; Yang, X.; Wang, S.; Zheng, Y.; Huang, T.; Zhu, S.; Yan, X. Trace Detection of Specific Viable Bacteria Using Tetracysteine-Tagged Bacteriophages. *Anal. Chem.* 2013, 86, 907-912.

70. Smartt, A. E.; Xu, T.; Jegier, P.; Carswell, J. J.; Blount, S. A.; Sayler, G. S.; Ripp, S. Pathogen detection using engineered bacteriophages. *Anal. Bioanal. Chem.* 2012, 402, 3127-46.

71. van der Merwe, R. G.; van Helden, P. D.; Warren, R. M.; Sampson, S. L.; Gey van Pittius, N. C. Phage-based detection of bacterial pathogens. *Analyst* 2014, 139, 2617-26.

72. Tawil, N.; Sacher, E.; Mandeville, R.; Meunier, M. Bacteriophages: biosensing tools for multi-drug resistant pathogens. *Analyst* 2014, 139, 1224-36.

73. Sergueev, K. V.; He, Y.; Borschel, R. H.; Nikolich, M. P.; Filippov, A. A. Rapid and sensitive detection of Yersinia pestis using amplification of plague diagnostic bacteriophages monitored by real-time PCR. 2010.

74. Símboli, N.; Takiff, H.; McNerney, R.; López, B.; Martin, A.; Palomino, J. C.; Barrera, L.; Ritacco, V. In-house phage amplification assay is a sound alternative for detecting rifampin-resistant Mycobacterium tuberculosis in low-resource settings. *Antimicrob. Agents Chemother.* 2005, 49, 425-427.

75. Pierce, C. L.; Rees, J. C.; Fernández, F. M.; Barr, J. R. Detection of Staphylococcus aureus using 15N-labeled bacteriophage amplification coupled with matrix-assisted laser desorption/ionization-time-of-flight mass spectrometry. *Anal. Chem.* 2011, 83, 2286-2293.

76. Martelet, A.; L'Hostis, G.; Nevers, M.-C.; Volland, H.; Junot, C.; Becher, F.; Muller, B. H. Phage amplification and immunomagnetic separation combined with targeted mass spectrometry for sensitive detection of viable bacteria in complex food matrices. *Anal. Chem.* 2015.

77. Kutin, R. K.; Alvarez, A.; Jenkins, D. M. Detection of Ralstonia solanacearum in natural substrates using phage amplification integrated with real-time PCR assay. *J. Microbiol. Methods* 2009, 76, 241-246.

78. Nakamura, R. M.; Tokunaga, T.; Murohashi, T. Premature Lysis of Bacteriophage-Infected Mycobacteria Induced by Kanamycin 1. *Am. Rev. Respir. Dis.* 1967, 96, 542-544.

79. David, H.; Clavel, S.; Clement, F.; Moniz-Pereira, J. Effects of antituberculosis and antileprosy drugs on mycobacteriophage D29 growth. *Antimicrob. Agents Chemother.* 1980, 18, 357-359.

80. Neufeld, T.; Schwartz-Mittelmann, A.; Biran, D.; Ron, E.; Rishpon, J. Combined phage typing and amperometric detection of released enzymatic activity for the specific identification and quantification of bacteria. *Anal. Chem.* 2003, 75, 580-585.

81. Derda, R.; Lockett, M. R.; Tang, S. K. Y.; Fuller, R. C.; Maxwell, E. J.; Breiten, B.; Cuddemi, C. A.; Ozdogan, A.; Whitesides, G. M. Filter-Based Assay for Escherichia coli in Aqueous Samples Using Bacteriophage-Based Amplification. *Anal. Chem.* 2013, 85, 7213-7220.

82. Laczka, O.; Garcia-Aljaro, C.; del Campo, F. J.; Pascual, F. X. M.; Mas-Gordi, J.; Baldrich, E. Amperometric detection of Enterobacteriaceae in river water by measuring beta-galactosidase activity at interdigitated microelectrode arrays. *Anal. Chim. Acta* 2010, 677, 156-161.

83. Burnham, S.; Hu, J.; Anany, H.; Brovko, L.; Deiss, F.; Derda, R.; Griffiths, M. Towards rapid on-site phage-mediated detection of generic Escherichia coli in water using luminescent and visual readout. *Anal. Bioanal. Chem.* 2014, 406, 5685-5693.

84. Blasco, R.; Murphy, M.; Sanders, M.; Squirrell, D. Specific assays for bacteria using phage mediated release of adenylate kinase. *J. Appl. Microbiol.* 1998, 84, 661-666.

85. Kenzaka, T.; Utrarachkij, F.; Suthienkul, O.; Nasu, M. Rapid monitoring of Escherichia coli in Southeast Asian urban canals by fluorescent-bacteriophage assay. *J. Health Sci.* 2006, 52, 666-671.

86. Callewaert, L.; Walmagh, M.; Michiels, C. W.; Lavigne, R. Food applications of bacterial cell wall hydrolases. *Curr. Opin. Biotechnol.* 2011, 22, 164-171.

87. Oda, M.; Morita, M.; Unno, H.; Tanji, Y. Rapid detection of Escherichia coli O157: H7 by using green fluorescent protein-labeled PP01 bacteriophage. *Appl. Environ. Microbiol.* 2004, 70, 527-534.

88. Tanji, Y.; Furukawa, C.; Na, S.-H.; Hijikata, T.; Miyanaga, K.; Unno, H. Escherichia coli detection by GFP-labeled lysozyme-inactivated T4 bacteriophage. *J. Biotechnol.* 2004, 114, 11-20.

89. Ripp, S.; Jegier, P.; Johnson, C. M.; Brigati, J. R.; Sayler, G. S. Bacteriophage-amplified bioluminescent sensing of Escherichia coli O157: H7. *Anal. Bioanal. Chem.* 2008, 391, 507-514.

90. Schofield, D. A.; Bull, C. T.; Rubio, I.; Wechter, W. P.; Westwater, C.; Molineux, I. J. Development of an engineered bioluminescent reporter phage for detection of bacterial blight of crucifers. *Appl. Environ. Microbiol.* 2012, 78, 3592-3598.

91. Loessner, M. J.; Rees, C.; Stewart, G.; Scherer, S. Construction of luciferase reporter bacteriophage A511:: luxAB for rapid and sensitive detection of viable Listeria cells. *Appl. Environ. Microbiol.* 1996, 62, 1133-1140.

92. Loessner, M. J.; Rudolf, M.; Scherer, S. Evaluation of luciferase reporter bacteriophage A511:: luxAB for detection of Listeria monocytogenes in contaminated foods. *Appl. Environ. Microbiol.* 1997, 63, 2961-2965.

93. Alcaine, S. D.; Tilton, L.; Serrano, M. A. C.; Wang, M.; Vachet, R. W.; Nugen, S. R. Phage-protease-peptide: a novel trifecta enabling multiplex detection of viable bacterial pathogens. *Appl. Microbiol. Biotechnol.* 2015, 99, 8177-8185.

94. Alcaine, S. D.; Pacitto, D.; Sela, D. A.; Nugen, S. R. Phage & phosphatase: a novel phage-based probe for rapid, multi-platform detection of bacteria. *Analyst* 2015.

95. Edgar, R.; McKinstry, M.; Hwang, J.; Oppenheim, A. B.; Fekete, R. A.; Giulian, G.; Merril, C.; Nagashima, K.; Adhya, S. High-sensitivity bacterial detection using biotin-tagged phage and quantum-dot nanocomplexes. *Proc. Natl. Acad. Sci. U. S. A.* 2006, 103, 4841-5.

96. Chen, J.; Alcaine, S. D.; Jiang, Z.; Rotello, V. M.; Nugen, S. R. Detection of Escherichia coli in Drinking Water Using T7 Bacteriophage-Conjugated Magnetic Probe. *Anal. Chem.* 2015, 87, 8977-8984.

97. Liebana, S.; Spricigo, D. A.; Pilar Cortes, M.; Barbe, J.; Llagostera, M.; Alegret, S.; Isabel Pividori, M. Phagomagnetic Separation and Electrochemical Magneto-Genosensing of Pathogenic Bacteria. *Anal. Chem.* 2013, 85, 3079-3086.

98. Naidoo, R.; Singh, A.; Arya, S. K.; Beadle, B.; Glass, N.; Tanha, J.; Szymanski, C. M.; Evoy, S. Surface-immobilization of chromatographically purified bacteriophages for the optimized capture of bacteria. *Bacteriophage* 2012, 2, 15-24.

99. Jiang, Z.; Le, N. D.; Gupta, A.; Rotello, V. M. Cell surface-based sensing with metallic nanoparticles. *Chem. Soc. Rev.* 2015, DOI: 10.1039/C4CS00387J.

100. Zhang, B.; Xing, Y.; Li, Z.; Zhou, H.; Mu, Q.; Yan, B. Functionalized carbon nanotubes specifically bind to α-chymotrypsin's catalytic site and regulate its enzymatic function. *Nano Lett.* 2009, 9, 2280-2284.

101. De, M.; Chou, S. S.; Dravid, V. P. Graphene Oxide as an Enzyme Inhibitor: Modulation of Activity of alpha-Chymotrypsin. *J. Am. Chem. Soc.* 2011, 133, 17524-17527.

102. Yang, X. J.; Zhao, C. Q.; Ju, E. G.; Ren, J. S.; Qu, X. G. Contrasting modulation of enzyme activity exhibited by graphene oxide and reduced graphene. *Chem. Commun.* 2013, 49, 8611-8613.

103. Li, J.; Wu, L. J.; Guo, S. S.; Fu, H. E.; Chen, G. N.; Yang, H. H. Simple colorimetric bacterial detection and high-throughput drug screening based on a graphene-enzyme complex. *Nanoscale* 2013, 5, 619-623.

104. Thiramanas, R.; Laocharoensuk, R. Competitive binding of polyethyleneimine-coated gold nanoparticles to enzymes and bacteria: a key mechanism for low-level colorimetric detection of gram-positive and gram-negative bacteria. *Microchimica Acta* 2015, 1-8.

105. Miranda, O. R.; Li, X.; Garcia-Gonzalez, L.; Zhu, Z.-J.; Yan, B.; Bunz, U. H.; Rotello, V. M. Colorimetric bacteria sensing using a supramolecular enzyme–nanoparticle biosensor. *J. Am. Chem. Soc.* 2011, 133, 9650-9653.

106. Creran, B.; Li, X.; Duncan, B.; Kim, C. S.; Moyano, D. F.; Rotello, V. M. Detection of bacteria using inkjet-printed enzymatic test strips. *ACS Appl. Mater. Interfaces* 2014, 6, 19525-30.

107. Chen, J.; Jiang, Z.; Ackerman, J. D.; Yazdani, M.; Hou, S.; Nugen, S. R.; Rotello, V. M. Electrochemical nanoparticle-enzyme sensors for screening bacterial contamination in drinking water. *Analyst* 2015, 140, 4991-4996.

108. Heo, J.; Hua, S. Z. An Overview of Recent Strategies in Pathogen Sensing. *Sensors* 2009, 9, 4483-4502.

109. Martínez, A. M.; Kak, A. C. Pca versus lda. *Pattern Analysis and Machine Intelligence, IEEE Transactions on* 2001, 23, 228-233.

110. Phillips, R. L.; Miranda, O. R.; You, C.-C.; Rotello, V. M.; Bunz, U. H. F. Rapid and Efficient Identification of Bacteria Using Gold-Nanoparticle–Poly(para-phenyleneethynylene) Constructs. *Angew. Chem. Int. Ed.* 2008, 47, 2590-2594.

111. Li, X.; Kong, H.; Mout, R.; Saha, K.; Moyano, D. F.; Robinson, S. M.; Rana, S.; Zhang, X.; Riley, M. A.; Rotello, V. M. Rapid Identification of Bacterial Biofilms and Biofilm Wound Models Using a Multichannel Nanosensor. *ACS Nano* 2014, 8, 12014-12019.

112. Gupta, S. K.; Suantio, A.; Gray, A.; Widyastuti, E.; Jain, N.; Rolos, R.; Hoekstra, R. M.; Quick, R. Factors associated with E. coli contamination of household drinking water among tsunami and earthquake survivors, Indonesia. *Am. J. Trop. Med. Hyg.* 2007, 76, 1158-1162.

113. Chen, J.; Jiang, Z.; Ackerman, J. D.; Yazdani, M.; Hou, S.; Nugen, S. R.; Rotello, V. M. Electrochemical nanoparticle-enzyme sensors for screening bacterial contamination in drinking water. *Analyst* 2015.

114. Zhang, K.; Fu, L.; Zhang, L.; Cheng, Z. Y.; Huang, T. S. Magnetostrictive particle based biosensors for in situ and real-time detection of pathogens in water. *Biotechnol. Bioeng.* 2014, 111, 2229-38.

115. Chavali, R.; Kumar Gunda, N. S.; Naicker, S.; Mitra, S. K. Detection of Escherichia coli in potable water using personal glucose meters. *Anal. Methods* 2014, 6, 6223-6227.

116. Boyaci, I. H.; Aguilar, Z. P.; Hossain, M.; Halsall, H. B.; Seliskar, C. J.; Heineman, W. R. Amperometric determination of live Escherichia coli using antibody-coated paramagnetic beads. *Anal. Bioanal. Chem.* 2005, 382, 1234-41.

117. Hossain, S. M.; Ozimok, C.; Sicard, C.; Aguirre, S. D.; Ali, M. M.; Li, Y.; Brennan, J. D. Multiplexed paper test strip for quantitative bacterial detection. *Anal. Bioanal. Chem.* 2012, 403, 1567-76.

118. U.S.; Administration, F. D. Standards for the Growing, Harvesting, Packing, and Holding of Produce for Human Consumption. In *Fed. Regist.*, 3646 ed.; 2014; Vol. 78, pp 3503-3646.

119. Gantzer, C.; Maul, A.; Audic, J.; Schwartzbrod, L. Detection of infectious enteroviruses, enterovirus genomes, somatic coliphages, and Bacteroides fragilis phages in treated wastewater. *Appl. Environ. Microbiol.* 1998, 64, 4307-4312.

120. García-Aljaro, C.; Muñoz-Berbel, X.; Jenkins, A. T. A.; Blanch, A. R.; Muñoz, F. X. Surface plasmon resonance assay for real-time monitoring of somatic coliphages in wastewaters. *Appl. Environ. Microbiol.* 2008, 74, 4054-4058.

121. Fu, L.; Zhang, K.; Li, S.; Wang, Y.; Huang, T.-S.; Zhang, A.; Cheng, Z. Y. In situ real-time detection of E. coli in water using antibody-coated magnetostrictive microcantilever. *Sens. Actuator B-Chem.* 2010, 150, 220-225.

122. Foddai, A.; Elliott, C. T.; Grant, I. R. Optimization of a phage amplification assay to permit accurate enumeration of viable Mycobacterium avium subsp. paratuberculosis cells. *Appl. Environ. Microbiol.* 2009, 75, 3896-3902.

123. Chen, J.; Griffiths, M. W. Salmonella detection in eggs using lux+ bacteriophages. *J. Food Prot.* 1996, 59, 908-914.

124. Banaiee, N.; Bobadilla-del-Valle, M.; Riska, P. F.; Bardarov Jr, S.; Small, P. M.; Ponce-de-Leon, A.; Jacobs Jr, W. R.; Hatfull, G. F.; Sifuentes-Osornio, J. Rapid identification and susceptibility testing of Mycobacterium tuberculosis from MGIT cultures with luciferase reporter mycobacteriophages. *J. Med. Microbiol.* 2003, 52, 557-561.

125. Neufeld, T.; Schwartz-Mittelmann, A.; Biran, D.; Ron, E. Z.; Rishpon, J. Combined phage typing and amperometric detection of released enzymatic activity for the specific identification and quantification of bacteria. *Anal. Chem.* 2003, 75, 580-585.

126. Yemini, M.; Levi, Y.; Yagil, E.; Rishpon, J. Specific electrochemical phage sensing for Bacillus cereus and Mycobacterium smegmatis. *Bioelectrochemistry* 2007, 70, 180-184.

127. Chen, G. H.; Chen, W. Y.; Yen, Y. C.; Wang, C. W.; Chang, H. T.; Chen, C. F. Detection of mercury(II) ions using colorimetric gold nanoparticles on paper-based analytical devices. *Anal. Chem.* 2014, 86, 6843-9.

128. Kumar Gunda, N. S.; Naicker, S.; Shinde, S.; Kimbahune, S.; Shrivastava, S.; Mitra, S. Mobile Water Kit (MWK): a smartphone compatible low-cost water monitoring system for rapid detection of total coliform and E. coli. *Anal. Methods* 2014, 6, 6236-6246.

129. Shabani, A.; Marquette, C. A.; Mandeville, R.; Lawrence, M. F. Magnetically-assisted impedimetric detection of bacteria using phage-modified carbon microarrays. *Talanta* 2013, 116, 1047-1053.

130. Chen, J.; Zhou, Y.; Wang, D.; He, F.; Rotello, V. M.; Carter, K. R.; Watkins, J. J.; Nugen, S. R. UV-nanoimprint lithography as a tool to develop flexible microfluidic devices for electrochemical detection. *Lab Chip* 2015, 15, 3086-3094.

131. Jiang, Z.; Le, N. D.; Gupta, A.; Rotello, V. M. Cell surface-based sensing with metallic nanoparticles. *Chem. Soc. Rev.* 2015, 44, 4264-4274.

132. Tamaki, S.; Sato, T.; Matsuhashi, M. Role of lipopolysaccharides in antibiotic resistance and bacteriophage adsorption of Escherichia coli K-12. *J. Bacteriol.* 1971, 105, 968-975.

133. Handa, H.; Gurczynski, S.; Jackson, M. P.; Auner, G.; Walker, J.; Mao, G. Recognition of Salmonella typhimurium by immobilized phage P22 monolayers. *Surf. Sci.* 2008, 602, 1392-1400.

134. Shin, H. D.; Chen, R. R. Extracellular recombinant protein production from an Escherichia coli lpp deletion mutant. *Biotechnol. Bioeng.* 2008, 101, 1288-1296.

135. Mergulhao, F.; Summers, D.; Monteiro, G. Recombinant protein secretion in Escherichia coli. *Biotechnol. Adv.* 2005, 23, 177-202.

136. Zhou, Q. Z.; Chen, X. D. Effects of temperature and pH on the catalytic activity of the immobilized β-galactosidase from Kluyveromyces lactis. *Biochem. Eng. J.* 2001, 9, 33-40.

137. Moldovan, R.; Chapman-McQuiston, E.; Wu, X. On kinetics of phage adsorption. *Biophys. J.* 2007, 93, 303-315.

138. Oncescu, V.; O'Dell, D.; Erickson, D. Smartphone based health accessory for colorimetric detection of biomarkers in sweat and saliva. *Lab Chip* 2013, 13, 3232-3238.

139. Lee, S.; Oncescu, V.; Mancuso, M.; Mehta, S.; Erickson, D. A smartphone platform for the quantification of vitamin D levels. *Lab Chip* 2014, 14, 1437-1442.

140. Hong, J. I.; Chang, B.-Y. Development of the smartphone-based colorimetry for multi-analyte sensing arrays. *Lab Chip* 2014, 14, 1725-1732.

141. Fu, E.; Liang, T.; Spicar-Mihalic, P.; Houghtaling, J.; Ramachandran, S.; Yager, P. Two-dimensional paper network format that enables simple multistep assays for use in low-resource settings in the context of malaria antigen detection. *Anal. Chem.* 2012, 84, 4574-4579.

142. Scallan, E.; Griffin, P. M.; Angulo, F. J.; Tauxe, R. V.; Hoekstra, R. M. Foodborne illness acquired in the United States—unspecified agents. *Emerging Infect. Dis.* 2011, 17, 16-22.

143. Zhu, L.; Yuan, Z.; Simmons, J. T.; Sreenath, K. Zn(ii)-coordination modulated ligand photophysical processes - the development of fluorescent indicators for imaging biological Zn(ii) ions. *RSC Adv* 2014, 4, 20398-20440.

144. Miranda, O. R.; Li, X. N.; Garcia-Gonzalez, L.; Zhu, Z. J.; Yan, B.; Bunz, U. H. F.; Rotello, V. M. Colorimetric bacteria sensing using a supramolecular enzyme-nanoparticle biosensor. *J. Am. Chem. Soc.* 2011, 133, 9650-9653.

145. Tryland, I.; Fiksdal, L. Enzyme Characteristics of β-d-Galactosidase-and β-d-Glucuronidase-Positive Bacteria and Their Interference in Rapid Methods for Detection of Waterborne Coliforms andEscherichia coli. *Appl. Environ. Microbiol.* 1998, 64, 1018-1023.

146. Jacob, F.; Monod, J. Genetic regulatory mechanisms in the synthesis of proteins. *J. Mol. Biol.* 1961, 3, 318-356.

147. Lin, T.-Y.; Lo, Y.-H.; Tseng, P.-W.; Chang, S.-F.; Lin, Y.-T.; Chen, T.-S. A T3 and T7 recombinant phage acquires efficient adsorption and a broader host range. *PloS one* 2012, 7, 30954-30954.

148. Scholl, D.; Adhya, S.; Merril, C. Escherichia coli K1's capsule is a barrier to bacteriophage T7. *Appl. Environ. Microbiol.* 2005, 71, 4872-4874.

149. Garcia, L. R.; Molineux, I. J. Incomplete entry of bacteriophage T7 DNA into F plasmid-containing Escherichia coli. *J. Bacteriol.* 1995, 177, 4077-4083.

150. Fan, C.; Hu, Z. Q.; Mustapha, A.; Lin, M. S. Rapid detection of food- and waterborne bacteria using surface-enhanced Raman spectroscopy coupled with silver nanosubstrates. *Appl. Microbiol. Biotechnol.* 2011, 92, 1053-1061.

151. Akanda, M. R.; Tamilavan, V.; Park, S.; Jo, K.; Hyun, M. H.; Yang, H. Hydroquinone diphosphate as a phosphatase substrate in enzymatic amplification combined with electrochemical–chemical–chemical redox cycling for the detection of E. coli O157: H7. *Anal. Chem.* 2013, 85, 1631-1636.

152. Shen, Z.; Huang, M.; Xiao, C.; Zhang, Y.; Zeng, X.; Wang, P. G. Nonlabeled quartz crystal microbalance biosensor for bacterial detection using carbohydrate and lectin recognitions. *Anal. Chem.* 2007, 79, 2312-9.

153. Stevens, K. A.; Jaykus, L. A. Bacterial separation and concentration from complex sample matrices: A review. *Crit. Rev. Microbiol.* 2004, 30, 7-24.

154. Nash, M. A.; Waitumbi, J. N.; Hoffman, A. S.; Yager, P.; Stayton, P. S. Multiplexed enrichment and detection of malarial biomarkers using a stimuli-responsive iron oxide and gold nanoparticle reagent system. *ACS Nano* 2012, 6, 6776-85.

155. Xie, J.; Xu, C.; Kohler, N.; Hou, Y.; Sun, S. Controlled PEGylation of monodisperse Fe3O4 nanoparticles for reduced non-specific uptake by macrophage cells. *Adv. Mater.* 2007, 19, 3163-3166.

156. Yang, H.; Qu, L.; Wimbrow, A. N.; Jiang, X.; Sun, Y. Rapid detection of Listeria monocytogenes by nanoparticle-based immunomagnetic separation and real-time PCR. *Int. J. Food Microbiol.* 2007, 118, 132-138.

157. Goodridge, L.; Chen, J.; Griffiths, M. Development and characterization of a fluorescent-bacteriophage assay for detection of Escherichia coli O157:H7. *Appl. Environ. Microbiol.* 1999, 65, 1397-404.

158. Singh, A.; Arya, S. K.; Glass, N.; Hanifi-Moghaddam, P.; Naidoo, R.; Szymanski, C. M.; Tanha, J.; Evoy, S. Bacteriophage tailspike proteins as molecular probes for sensitive and selective bacterial detection. *Biosens. Bioelectron.* 2010, 26, 131-138.

159. Lee, S. H.; Onuki, M.; Satoh, H.; Mino, T. Isolation, characterization of bacteriophages specific to Microlunatus phosphovorus and their application for rapid host detection. *Lett. Appl. Microbiol.* 2006, 42, 259-264.

160. Wu, S. J.; Duan, N.; Wang, Z. P.; Wang, H. X. Aptamer-functionalized magnetic nanoparticle-based bioassay for the detection of ochratoxin a using upconversion nanoparticles as labels. *Analyst* 2011, 136, 2306-2314.

161. Wang, S.; Singh, A. K.; Senapati, D.; Neely, A.; Yu, H.; Ray, P. C. Rapid Colorimetric Identification and Targeted Photothermal Lysis of Salmonella Bacteria by Using Bioconjugated Oval-Shaped Gold Nanoparticles. *Chemistry-a European Journal* 2010, 16, 5600-5606.

162. Nanduri, V.; Sorokulova, I. B.; Samoylov, A. M.; Simonian, A. L.; Petrenko, V. A.; Vodyanoy, V. Phage as a molecular recognition element in biosensors immobilized by physical adsorption. *Biosens. Bioelectron.* 2007, 22, 986-992.

163. Bielke, L.; Higgins, S.; Donoghue, A.; Donoghue, D.; Hargis, B. M. Salmonella host range of bactedophages that infect muftiple genera. *Poult. Sci.* 2007, 86, 2536-2540.

164. Minikh, O.; Tolba, M.; Brovko, L.; Griffiths, M. Bacteriophage-based biosorbents coupled with bioluminescent ATP assay for rapid concentration and detection of Escherichia coli. *J. Microbiol. Methods* 2010, 82, 177-183.

165. Hu, L.; de Montferrand, C.; Lalatonne, Y.; Motte, L.; Brioude, A. Effect of Cobalt Doping Concentration on the Crystalline Structure and Magnetic Properties of Monodisperse CoxFe3-xO4 Nanoparticles within Nonpolar and Aqueous Solvents. *J. Phys. Chem. C* 2012, 116, 4349-4355.

166. Chaubey, G. S.; Barcena, C.; Poudyal, N.; Rong, C.; Gao, J.; Sun, S.; Liu, J. P. Synthesis and stabilization of FeCo nanoparticles. *J. Am. Chem. Soc.* 2007, 129, 7214-5.

167. Yi, D. K.; Selvan, S. T.; Lee, S. S.; Papaefthymiou, G. C.; Kundaliya, D.; Ying, J. Y. Silica-coated nanocomposites of magnetic nanoparticles and quantum dots. *J. Am. Chem. Soc.* 2005, 127, 4990-4991.

168. Dai, Q.; Lam, M.; Swanson, S.; Yu, R. H. R.; Milliron, D. J.; Topuria, T.; Jubert, P. O.; Nelson, A. Monodisperse Cobalt Ferrite Nanomagnets with Uniform Silica Coatings. *Langmuir* 2010, 26, 17546-17551.

169. Xu, C.; Wang, B.; Sun, S. Dumbbell-like Au-Fe3O4 nanoparticles for target-specific platin delivery. *J. Am. Chem. Soc.* 2009, 131, 4216-7.

170. Chen, L.; Xu, Z.; Dai, H.; Zhang, S. Facile synthesis and magnetic properties of monodisperse Fe3O4/silica nanocomposite microspheres with embedded structures via a direct solution-based route. *J. Alloys Compd.* 2010, 497, 221-227.

171. Zhang, M.; Cushing, B. L.; O'Connor, C. J. Synthesis and characterization of monodisperse ultra-thin silica-coated magnetic nanoparticles. *Nanotechnology* 2008, 19, 085601-085606.

172. Corr, S. A.; Rakovich, Y. P.; Gun'ko, Y. K. Multifunctional magnetic-fluorescent nanocomposites for biomedical applications. *Nanoscale Research Letters* 2008, 3, 87-104.

173. Can, K.; Ozmen, M.; Ersoz, M. Immobilization of albumin on aminosilane modified superparamagnetic magnetite nanoparticles and its characterization. *Colloids Surf. B. Biointerfaces* 2009, 71, 154-159.

174. Gopinath, S. C. B.; Awazu, K.; Fujimaki, M.; Shimizu, K.; Mizutani, W.; Tsukagoshi, K. Surface functionalization chemistries on highly sensitive silica-based sensor chips. *Analyst* 2012, 137, 3520-3527.

175. Gao, F.; Pan, B. F.; Zheng, W. M.; Ao, L. M.; Gu, H. C. Study of streptavidin coated onto PAMAM dendrimer modified magnetite nanoparticles. *J. Magn. Magn. Mater.* 2005, 293, 48-54.

176. Lu, T. K.; Collins, J. J. Dispersing biofilms with engineered enzymatic bacteriophage. *Proc. Natl. Acad. Sci. U. S. A.* 2007, 104, 11197-202.

177. Schwind, P.; Kramer, H.; Kremser, A.; Ramsberger, U.; Rasched, I. Subtilisin removes the surface layer of the phage fd coat. *Eur. J. Biochem.* 1992, 210, 431-436.

178. Liu, C. M.; Chung, S. H.; Jin, Q. L.; Sutton, A.; Yan, F. N.; Hoffmann, A.; Kay, B. K.; Bader, S. D.; Makowski, L.; Chen, L. H. Magnetic viruses via nano-capsid templates. *J. Magn. Magn. Mater.* 2006, 302, 47-51.

179. Varmus, H.; Klausner, R.; Zerhouni, E.; Acharya, T. Grand challenges in global health. *Science* 2003, 302, 398.

180. Gole, A.; Murphy, C. J. Seed-mediated synthesis of gold nanorods: role of the size and nature of the seed. *Chem. Mater.* 2004, 16, 3633-3640.

181. Jang, H.; Lee, J.; Min, D.-H. Graphene oxide for fluorescence-mediated enzymatic activity assays. *J. Mater. Chem. B* 2014, 2, 2452-2460.

182. Gao, Z.; Deng, K.; Wang, X. D.; Miro, M.; Tang, D. High-resolution colorimetric assay for rapid visual readout of phosphatase activity based on gold/silver core/shell nanorod. *ACS Appl. Mater. Interfaces* 2014, 6, 18243-50.

183. Lee, J.-S.; Lytton-Jean, A. K.; Hurst, S. J.; Mirkin, C. A. Silver nanoparticle-oligonucleotide conjugates based on DNA with triple cyclic disulfide moieties. *Nano Lett.* 2007, 7, 2112-2115.

184. Song, Y.; Wei, W.; Qu, X. Colorimetric biosensing using smart materials. *Adv. Mater.* 2011, 23, 4215-4236.

185. Link, S.; Mohamed, M.; El-Sayed, M. Simulation of the optical absorption spectra of gold nanorods as a function of their aspect ratio and the effect of the medium dielectric constant. *J. Phys. Chem. B* 1999, 103, 3073-3077.

186. Zhang, C.; Yin, A.-X.; Jiang, R.; Rong, J.; Dong, L.; Zhao, T.; Sun, L.-D.; Wang, J.; Chen, X.; Yan, C.-H. Time-Temperature Indicator for Perishable Products Based on Kinetically Programmable Ag Overgrowth on Au Nanorods. *Acs Nano* 2013, 7, 4561-4568.

187. Busbee, B. D.; Obare, S. O.; Murphy, C. J. An Improved Synthesis of High-Aspect-Ratio Gold Nanorods. *Adv. Mater.* 2003, 15, 414-416.

188. Zhou, X.; Zhou, Y.; Ku, J. C.; Zhang, C.; Mirkin, C. A. Capillary Force-Driven, Large-Area Alignment of Multi-segmented Nanowires. *ACS Nano* 2014, 8, 1511-1516.

189. Huang, X.; El-Sayed, I. H.; Qian, W.; El-Sayed, M. A. Cancer Cells Assemble and Align Gold Nanorods Conjugated to Antibodies to Produce Highly Enhanced, Sharp, and Polarized Surface Raman Spectra: A Potential Cancer Diagnostic Marker. *Nano Lett.* 2007, 7, 1591-1597.

190. Jiang, R.; Chen, H.; Shao, L.; Li, Q.; Wang, J. Unraveling the Evolution and Nature of the Plasmons in (Au Core)-(Ag Shell) Nanorods. *Adv. Mater.* 2012, 24, OP200-OP207.

191. Nikoobakht, B.; El-Sayed, M. A. Preparation and growth mechanism of gold nanorods (NRs) using seed-mediated growth method. *Chem. Mater.* 2003, 15, 1957-1962.

192. Liu, J.-M.; Wang, H.-F.; Yan, X.-P. A gold nanorod based colorimetric probe for the rapid and selective detection of Cu2+ ions. *Analyst* 2011, 136, 3904-3910.

193. Yu, C.; Irudayaraj, J. Multiplex biosensor using gold nanorods. *Anal. Chem.* 2007, 79, 572-579.

194. Wang, L.; Zhu, Y.; Xu, L.; Chen, W.; Kuang, H.; Liu, L.; Agarwal, A.; Xu, C.; Kotov, N. A. Side-by-Side and End-to-End Gold Nanorod Assemblies for Environmental Toxin Sensing. *Angew. Chem. Int. Ed.* 2010, 49, 5472-5475.

195. Hauck, T. S.; Ghazani, A. A.; Chan, W. C. W. Assessing the Effect of Surface Chemistry on Gold Nanorod Uptake, Toxicity, and Gene Expression in Mammalian Cells. *Small* 2008, 4, 153-159.

196. Hu, X.; Cheng, W.; Wang, T.; Wang, Y.; Wang, E.; Dong, S. Fabrication, characterization, and application in SERS of self-assembled polyelectrolyte-gold nanorod multilayered films. *The Journal of Physical Chemistry B* 2005, 109, 19385-19389.

197. Jiang, R.; Chen, H.; Shao, L.; Li, Q.; Wang, J. Unraveling the evolution and nature of the plasmons in (Au core)–(Ag shell) nanorods. *Adv. Mater.* 2012, 24, OP200-OP207.

198. Martinez, A. W.; Phillips, S. T.; Carrilho, E.; Thomas III, S. W.; Sindi, H.; Whitesides, G. M. Simple telemedicine for developing regions: camera phones and paper-based microfluidic devices for real-time, off-site diagnosis. *Anal. Chem.* 2008, 80, 3699-3707.

199. Funes-Huacca, M.; Wu, A.; Szepesvari, E.; Rajendran, P.; Kwan-Wong, N.; Razgulin, A.; Shen, Y.; Kagira, J.; Campbell, R.; Derda, R. Portable self-contained cultures for phage and bacteria made of paper and tape. *Lab Chip* 2012, 12, 4269-4278.

200. Chen, J.; Alcaine, S. D.; Jiang, Z.; Rotello, V. M.; Nugen, S. R. Detection of Escherichia coli in Drinking Water Using T7 Bacteriophage-conjugated Magnetic Probe. *Anal. Chem.* 2015.

201. Salwiczek, M.; Qu, Y.; Gardiner, J.; Strugnell, R. A.; Lithgow, T.; McLean, K. M.; Thissen, H. Emerging rules for effective antimicrobial coatings. *Trends Biotechnol.* 2014, 32, 82-90.

202. Mannoor, M. S.; Tao, H.; Clayton, J. D.; Sengupta, A.; Kaplan, D. L.; Naik, R. R.; Verma, N.; Omenetto, F. G.; McAlpine, M. C. Graphene-based wireless bacteria detection on tooth enamel. *Nature communications* 2012, 3, 763.

203. M. B. Coyle, Manual of antimicrobial susceptibility testing, American Society for Microbiology, Washington, DC, 2005.

204. Zhang, M.; Yang, F.; Pasupuleti, S.; Oh, J. K.; Kohli, N.; Lee, I. S.; Perez, K.; Verkhoturov, S. V.; Schweikert, E. A.; Jayaraman, A.; Cisneros-Zevallos, L.; Akbulut, M. Preventing adhesion of Escherichia coli O157:H7 and Salmonella Typhimurium LT2 on tomato surfaces via ultrathin polyethylene glycol film. *Int. J. Food Microbiol.* 2014, 185, 73-81.

205. Wang, P.; Pang, S.; Chen, J.; McLandsborough, L.; Nugen, S. R.; Fan, M.; He, L. Label-free mapping of single bacterial cells using surface-enhanced Raman spectroscopy. *Analyst* 2016.

206. Belgrader, P.; Benett, W.; Hadley, D.; Richards, J. PCR detection of bacteria in seven minutes. *Science* 1999, 284, 449.

207. Maalouf, R.; Fournier-Wirth, C.; Coste, J.; Chebib, H.; Saïkali, Y.; Vittori, O.; Errachid, A.; Cloarec, J.-P.; Martelet, C.; Jaffrezic-Renault, N. Label-free detection of bacteria by electrochemical impedance spectroscopy: comparison to surface plasmon resonance. *Anal. Chem.* 2007, 79, 4879-4886.

208. Alcaine, S. D.; Pacitto, D.; Sela, D. A.; Nugen, S. R. Phage & phosphatase: a novel phage-based probe for rapid, multi-platform detection of bacteria. *Analyst* 2015, 140, 7629-7636.

209. Studier, F. W. Bacteriophage T7. *Science* 1972, 176, 367-376.

210. Yang, H. Enzyme-based ultrasensitive electrochemical biosensors. *Curr. Opin. Chem. Biol.* 2012, 16, 422-428.

211. Wentworth, B. B. Bacteriophage typing of the staphylococci. *Bacteriol. Rev.* 1963, 27, 253.

212. Chan, B. K.; Abedon, S. T.; Loc-Carrillo, C. Phage cocktails and the future of phage therapy. *Future Microbiol.* 2013, 8, 769-783.

213. Hermoso, J. A.; García, J. L.; García, P. Taking aim on bacterial pathogens: from phage therapy to enzybiotics. *Curr. Opin. Microbiol.* 2007, 10, 461-472.

214. Fu, W.; Forster, T.; Mayer, O.; Curtin, J. J.; Lehman, S. M.; Donlan, R. M. Bacteriophage cocktail for the prevention of biofilm formation by Pseudomonas aeruginosa on catheters in an in vitro model system. *Antimicrob. Agents Chemother.* 2010, 54, 397-404.

215. O'Flynn, G.; Ross, R.; Fitzgerald, G.; Coffey, A. Evaluation of a cocktail of three bacteriophages for biocontrol of Escherichia coli O157: H7. *Appl. Environ. Microbiol.* 2004, 70, 3417-3424.

216. Steinkraus, G.; White, R.; Friedrich, L. Vancomycin MIC creep in non-vancomycin-intermediate Staphylococcus aureus (VISA), vancomycin-susceptible clinical methicillin-resistant S. aureus (MRSA) blood isolates from 2001–05. *J. Antimicrob. Chemother.* 2007, 60, 788-794.